IAEA TECDOC SERIES

IAEA-TECDOC-2051

IAEA-TECDOC-2051

Photonuclear Production of Radioisotopes

IAEA
International Atomic Energy Agency

PHOTONUCLEAR PRODUCTION OF RADIOISOTOPES

The following States are Members of the International Atomic Energy Agency:

AFGHANISTAN
ALBANIA
ALGERIA
ANGOLA
ANTIGUA AND BARBUDA
ARGENTINA
ARMENIA
AUSTRALIA
AUSTRIA
AZERBAIJAN
BAHAMAS
BAHRAIN
BANGLADESH
BARBADOS
BELARUS
BELGIUM
BELIZE
BENIN
BOLIVIA, PLURINATIONAL STATE OF
BOSNIA AND HERZEGOVINA
BOTSWANA
BRAZIL
BRUNEI DARUSSALAM
BULGARIA
BURKINA FASO
BURUNDI
CABO VERDE
CAMBODIA
CAMEROON
CANADA
CENTRAL AFRICAN REPUBLIC
CHAD
CHILE
CHINA
COLOMBIA
COMOROS
CONGO
COSTA RICA
CÔTE D'IVOIRE
CROATIA
CUBA
CYPRUS
CZECH REPUBLIC
DEMOCRATIC REPUBLIC OF THE CONGO
DENMARK
DJIBOUTI
DOMINICA
DOMINICAN REPUBLIC
ECUADOR
EGYPT
EL SALVADOR
ERITREA
ESTONIA
ESWATINI
ETHIOPIA
FIJI
FINLAND
FRANCE
GABON
GAMBIA
GEORGIA
GERMANY
GHANA
GREECE
GRENADA
GUATEMALA
GUINEA
GUYANA
HAITI
HOLY SEE
HONDURAS
HUNGARY
ICELAND
INDIA
INDONESIA
IRAN, ISLAMIC REPUBLIC OF
IRAQ
IRELAND
ISRAEL
ITALY
JAMAICA
JAPAN
JORDAN
KAZAKHSTAN
KENYA
KOREA, REPUBLIC OF
KUWAIT
KYRGYZSTAN
LAO PEOPLE'S DEMOCRATIC REPUBLIC
LATVIA
LEBANON
LESOTHO
LIBERIA
LIBYA
LIECHTENSTEIN
LITHUANIA
LUXEMBOURG
MADAGASCAR
MALAWI
MALAYSIA
MALI
MALTA
MARSHALL ISLANDS
MAURITANIA
MAURITIUS
MEXICO
MONACO
MONGOLIA
MONTENEGRO
MOROCCO
MOZAMBIQUE
MYANMAR
NAMIBIA
NEPAL
NETHERLANDS, KINGDOM OF THE
NEW ZEALAND
NICARAGUA
NIGER
NIGERIA
NORTH MACEDONIA
NORWAY
OMAN
PAKISTAN
PALAU
PANAMA
PAPUA NEW GUINEA
PARAGUAY
PERU
PHILIPPINES
POLAND
PORTUGAL
QATAR
REPUBLIC OF MOLDOVA
ROMANIA
RUSSIAN FEDERATION
RWANDA
SAINT KITTS AND NEVIS
SAINT LUCIA
SAINT VINCENT AND THE GRENADINES
SAMOA
SAN MARINO
SAUDI ARABIA
SENEGAL
SERBIA
SEYCHELLES
SIERRA LEONE
SINGAPORE
SLOVAKIA
SLOVENIA
SOUTH AFRICA
SPAIN
SRI LANKA
SUDAN
SWEDEN
SWITZERLAND
SYRIAN ARAB REPUBLIC
TAJIKISTAN
THAILAND
TOGO
TONGA
TRINIDAD AND TOBAGO
TUNISIA
TÜRKİYE
TURKMENISTAN
UGANDA
UKRAINE
UNITED ARAB EMIRATES
UNITED KINGDOM OF GREAT BRITAIN AND NORTHERN IRELAND
UNITED REPUBLIC OF TANZANIA
UNITED STATES OF AMERICA
URUGUAY
UZBEKISTAN
VANUATU
VENEZUELA, BOLIVARIAN REPUBLIC OF
VIET NAM
YEMEN
ZAMBIA
ZIMBABWE

The Agency's Statute was approved on 23 October 1956 by the Conference on the Statute of the IAEA held at United Nations Headquarters, New York; it entered into force on 29 July 1957. The Headquarters of the Agency are situated in Vienna. Its principal objective is "to accelerate and enlarge the contribution of atomic energy to peace, health and prosperity throughout the world''.

IAEA-TECDOC-2051

PHOTONUCLEAR PRODUCTION OF RADIOISOTOPES

INTERNATIONAL ATOMIC ENERGY AGENCY
VIENNA, 2024

COPYRIGHT NOTICE

For further information on this publication, please contact:

Radiochemistry and Radiation Technology Section
International Atomic Energy Agency
Vienna International Centre
PO Box 100
1400 Vienna, Austria
Email: Official.Mail@iaea.org

Printed by the IAEA in Austria
April 2024

IAEA Library Cataloguing in Publication Data

Names: International Atomic Energy Agency.
Title: Photonuclear production of radioisotopes / International Atomic Energy Agency.
Description: Vienna : International Atomic Energy Agency, 2024. | Series: IAEA TECDOC series, ISSN 1011-4289 ; no. 2051 | Includes bibliographical references.
Identifiers: IAEAL 24-01672 | ISBN 978-92-0-116424-7 (paperback : alk. paper) | ISBN 978-92-0-116524-4 (pdf)
Subjects: LCSH: Photonuclear reactions. | Electron accelerators. | Radioisotopes.

FOREWORD

The use of radioisotopes in medicine is witnessing steady growth in all parts of the world. Among the radioisotopes used in medicine, technetium-99m (^{99m}Tc) is currently the most widely applied in clinics. The supply of molybdenum-99 (^{99}Mo) for ^{99}Mo/^{99m}Tc generators is hence vital for the functioning of nuclear medicine departments. Since the worldwide supply crisis of ^{99}Mo in 2007–2009, many countries have begun investigating alternative routes for the production of ^{99}Mo and ^{99m}Tc. These efforts have proved useful, opening up new production avenues. In 2017 the IAEA initiated a coordinated research project entitled New Ways of Producing Technetium-99m (Tc-99m) and Tc-99m Generators to identify technical aspects, in particular the use of a high power electron linear accelerator for the production of ^{99}Mo.

The use of dedicated accelerators capable of producing photons with sufficient energy and flux for radionuclide production is attractive for multiple reasons. This route eliminates the use of uranium and the handling of the associated nuclear waste, and the facilities used can be modular with the feasibility of independent operation of each module. As the list of radionuclides with potential diagnostic and/or therapeutic applications continues to grow, the interest in exploring alternative ways to produce radioisotopes is also increasing. This includes the photonuclear route for routine production of radioisotopes.

This publication is the outcome of a meeting of an international team of experts that discussed various technical and scientific details applicable to the production of important radionuclides such as ^{99}Mo, copper-67 (^{67}Cu), scandium-47 (^{47}Sc) and actinium-225 (^{225}Ac) using the photonuclear route. It compiles the available information and recent developments in using electron accelerators for the production of medical radioisotopes and is expected to be of interest to scientists and technical professionals in the fields of electron accelerators and radioisotope production.

The IAEA thanks the experts who contributed to this publication, in particular W. Diamond (Canada). The IAEA officer responsible for this publication was A. Korde of the Division of Physical and Chemical Sciences.

EDITORIAL NOTE

This publication has been prepared from the original material as submitted by the contributors and has not been edited by the editorial staff of the IAEA. The views expressed remain the responsibility of the contributors and do not necessarily represent the views of the IAEA or its Member States.

Guidance and recommendations provided here in relation to identified good practices represent expert opinion but are not made on the basis of a consensus of all Member States.

Neither the IAEA nor its Member States assume any responsibility for consequences which may arise from the use of this publication. This publication does not address questions of responsibility, legal or otherwise, for acts or omissions on the part of any person.

The use of particular designations of countries or territories does not imply any judgement by the publisher, the IAEA, as to the legal status of such countries or territories, of their authorities and institutions or of the delimitation of their boundaries.

The mention of names of specific companies or products (whether or not indicated as registered) does not imply any intention to infringe proprietary rights, nor should it be construed as an endorsement or recommendation on the part of the IAEA.

The authors are responsible for having obtained the necessary permission for the IAEA to reproduce, translate or use material from sources already protected by copyrights.

The IAEA has no responsibility for the persistence or accuracy of URLs for external or third party Internet web sites referred to in this publication and does not guarantee that any content on such web sites is, or will remain, accurate or appropriate.

CONTENTS

1. INTRODUCTION

1.1. BACKGROUND

Radioisotopes are used in nuclear medicine to provide information about the functionality of specific organs or to diagnose and treat diseases. The thyroid, bones, heart, liver, and many other organs can be easily imaged, and disorders in their function can be revealed aiding the diagnosis of a patient's illness. In some cases, radioisotopes can also be used to treat tumours.

Radiopharmaceuticals are broadly categorized into two segments: diagnostic and therapeutic. Diagnostic methods include Single Photon Emitting Tomography (SPECT) and Positron Emission Tomography (PET). Particulate emitters such as alpha, beta, or Auger electron emitting radioisotopes are used for therapeutic applications. Suitable organic carrier molecules are labelled with the radionuclides of choice for designing target specific radiopharmaceuticals which are useful for molecular imaging and radionuclide therapy. Brachytherapy is another modality that uses radioactivity for therapy, where radioisotopes are implanted as a sealed source directly near or in the affected organ.

Over 10 000 hospitals worldwide use medical radioisotopes, and about 90% of the procedures are performed for diagnosis in cardiology, oncology and neurology. The most common radioisotope used in diagnosis is ^{99m}Tc, with some 40 million procedures per year, accounting for over 80% of all nuclear medicine procedures worldwide [2]. Although radionuclide therapy is less common than diagnostic uses of radioisotopes in medicine, it is nevertheless widespread, important, and growing. Several isotopes are already in use, such as ^{90}Y, ^{131}I, ^{177}Lu, and ^{223}Ra. There remains much interest in other isotopes such as ^{47}Sc, ^{67}Cu, and ^{225}Ac and interest would increase if they were to become readily available.

Most radioisotopes used in nuclear medicine are currently produced with either research reactors or cyclotrons, depending upon the desired isotope. Several of the most commonly used isotopes (^{99}Mo/^{99m}Tc, ^{131}I, ^{90}Y and others) are derived from the fission of uranium in reactors, although some of these isotopes can also be formed by neutron irradiation of stable nuclei in a reactor.

In recent years, the supply of reactor based isotopes has been threatened globally because of reliability problems caused by the age of research reactors and processing facilities. For example, nearly all the world's supply of ^{99}Mo is met by six nuclear research reactors, all but one being over 45 years old. Many of these have suffered reliability problems, presenting a continuing threat to the security of supply. Thus, the global supply of radioisotopes, in particular ^{99}Mo, has not been steady over the last ten years due to reactor shutdowns, both scheduled and unscheduled, and failures in supply chains and logistics. Furthermore, the reactors are coming under increasing pressure to switch from Highly Enriched Uranium (HEU) to Low Enriched Uranium (LEU) fuel, which is not compatible with established processes for radioisotope extraction. This requires the development of alternative processes to assure a similarly reliable supply of ^{99}Mo after switching to LEU. Australia's OPAL reactor, South Africa's SAFARI reactor and the MARIA research reactor in Poland have already converted to LEU targets. The ^{99}Mo supply problem threatens nuclear medicine globally and is the subject of an intense industry wide effort to find technically feasible long term solutions.

New radiopharmaceutical development (academic and commercial) depends directly on isotope availability. In the early stages of development, an isotope can be supplied intermittently. However, for clinical trials or commercial use, the isotope supply needs to be reliable and of high pharmaceutical quality grade (i.e., compliant with Good Manufacturing Practice GMP).

Some medical isotopes cannot be produced in sufficient radiochemical or radionuclidic purity via cyclotron or reactor irradiation. Thus, despite their highly desirable characteristics for medical applications, their availability in limited purity dictates the usage in pre-clinical research. For example, ^{67}Cu is an isotope that researchers have identified as having suitable characteristics for cancer therapy and for diagnostic applications in combination with ^{64}Cu. However, attempts to produce it with reactors or high energy proton accelerators (proton linacs or cyclotrons) have resulted in a product that has low specific activity and radionuclidic purity. This hinders careful evaluations of the efficacy of ^{67}Cu labelled radiopharmaceuticals due to necessary interference correction in dose estimations arising from isotope mixtures.

Photonuclear reactions have been studied from the beginning of nuclear physics. Several facilities were constructed to investigate the fundamental aspects of the interaction of photons with matter. However, as research interests have evolved, many of these facilities have been shut down or been redirected to other research activities. The severe shortage of ^{99}Mo for medical applications from 2007–2009 stimulated renewed interest in photonuclear reactions with the practical goal of finding an alternative production method for useful quantities of ^{99}Mo. Photonuclear production of ^{99}Mo via the ^{100}Mo(γ, n) reaction for medical use was initially described in a patent [3] and later explored in more detail in a series of electron linac based experiments at Idaho National Laboratory [4]. An economic analysis based on these results indicated that the cost of delivering a dose of ^{99m}Tc for clinical diagnosis of a patient via this photonuclear route could be competitive with ^{99m}Tc derived from fission generators.

In response to the ^{99}Mo shortage, major initiatives to explore commercial photonuclear medical isotope production began in both Canada and the USA. Since 2008, technical developments have demonstrated successful pilot production facilities capable of producing TBq ^{99}Mo quantities. Over the course of these developments, opportunities for producing medically significant quantities of other isotopes have also evolved. In addition, the advantages and challenges associated with photonuclear radioisotope production have been understood in more detail.

1.2. OBJECTIVE

The objective of this publication is to provide an overview of the current state of methods for the photonuclear production of isotopes with a particular focus on those medical radioisotopes that could be produced in sufficient quantities for clinical use in nuclear medicine.

1.3. SCOPE

This publication is intended to serve as a guide describing the photonuclear production of medical isotopes. The publication includes the basic principles of photonuclear reactions. The equipment and methods discussed herein should provide reference to the state of the art facilities, in using electron accelerators for the production of radioisotopes via the photonuclear route. This information is targeted to scientists and technologists engaged in the production of radioisotopes and electron accelerator applications.

1.4. STRUCTURE

The publication gives a stepwise overview of the topics related to the production of radioisotopes using electron accelerators. Section 2 covers principles applicable to photonuclear reactions, details on reaction models and suitable tools to perform nuclear transport calculations. The photonuclear reactions used for production of medically relevant radioisotopes and cross-section measurements are also given in detail in this section. The

technical details and methods applicable for producing intense multi-MeV photon beams, including different types of electron accelerators, the design of targets, converters and cooling techniques are discussed in Section 3. This section also provides production details of specific radioisotopes (^{99}Mo, ^{67}Cu, ^{47}Sc, ^{225}Ac) that are under active development for the production of clinically relevant quantities. The associated radiochemistry aspects related to the separation and purification of the desired radioisotopes are covered in Section 4. The conclusion section highlights the current applications of electron accelerators for medical radioisotope productions and challenges for widespread use of this route for routine production of medical radioisotopes.

2. PRINCIPLES OF PHOTONUCLEAR REACTIONS

A photonuclear reaction is a nuclear reaction induced by photon. Photonuclear reactions occur when atomic nuclei are excited via the capture of incident photons and relax by emitting one or several elementary particles or nuclei fragments. The process of photon capture is called photo absorption. De-excitation occurs through emission of one or several nucleons or through fission. The latter is called photofission and usually occurs for elements with fissile isotopes, such as uranium or plutonium.

2.1. COMMON FEATURES OF PHOTONUCLEAR REACTIONS

Photo-absorption is a purely electromagnetic process and generally has a considerably lower cross-section compared to hadronic processes involving neutrons and protons. For photon energies below approximately 30 MeV, that are generally used for photonuclear production of radioisotopes, photo-absorption induces the excitation of nucleons resulting in a collective oscillation, where the neutron subsystem oscillates against the proton subsystem. The energy of the maximum excitation of this type is called the Giant Dipole Resonance (GDR). As an example, Fig. 1 shows the photo-absorption cross-section of the ^{100}Mo isotope as function of photon energy. The GDR is seen as the broad maximum of the photonuclear reaction cross-section for the photon energies around 15–18 MeV.

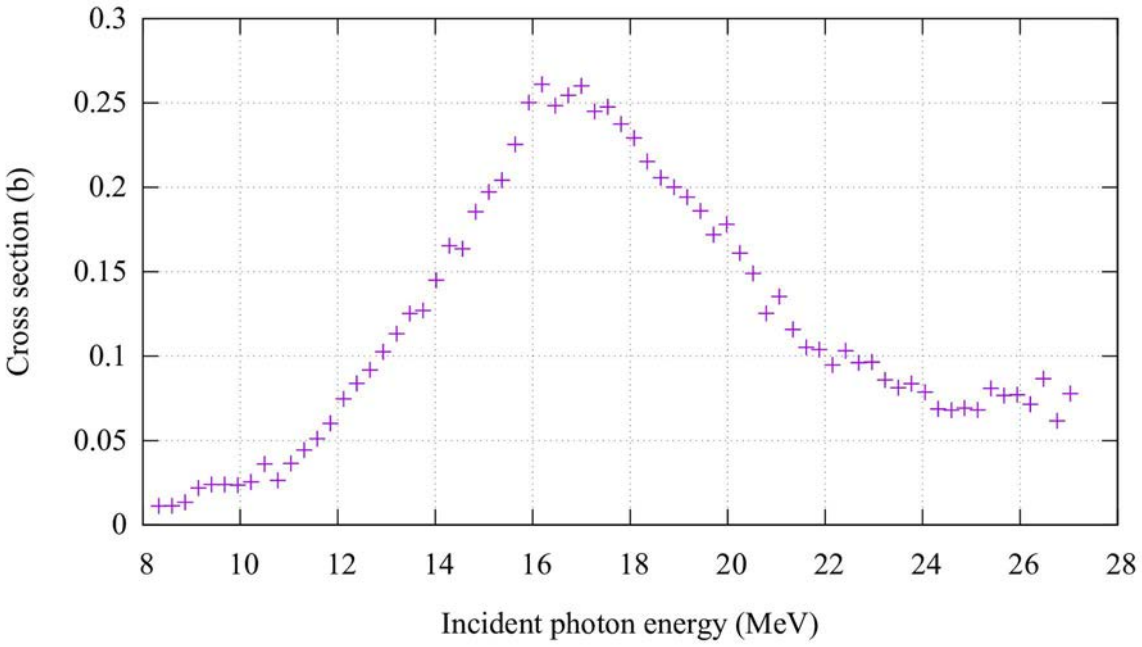

FIG. 1. Photo-absorption cross-section for ^{100}Mo (reproduced from Ref. [8]).

The GDR is of crucial importance for the photonuclear production of radioisotopes because this resonance region is used in almost all applications involving photonuclear reactions.

For medium and heavy nuclei (mass number A > 40), photo absorption cross-sections in the GDR region can be approximated by a Lorentzian resonance curve in Eq. (1):

$$\sigma_{GDR}(E) = \sum_i \sigma_i \frac{(E\Gamma_i)^2}{(E^2 - E_i^2)^2 + (E\Gamma_i)^2} \quad (1)$$

where σ_i is the cross-section at GDR peak, E the energy of the GDR peak and Γ_i the peak width. For the incident photon energies above 40 MeV, another photo-absorption mechanism, the quasi-deuteron regime, becomes important and an additional term is added to account for this effect [5]. For spherically symmetric nuclei below the quasi-deuteron regime, there is a single GDR peak as in Fig. 1, and the sum in equation (1) contains only one term (i = 1). For asymmetric nuclei, Eq. (1) contains two terms, describing two resonance peaks (i = 2). An example of such a case is the photo absorption cross-section of ^{181}Ta as a function of photon energy shown in Fig. 2. Equation (1) is often used in cross-section evaluation procedures, where the parameters σ_i, E_i and Γ_i are determined to fit available experimental data (see Section 2.3).

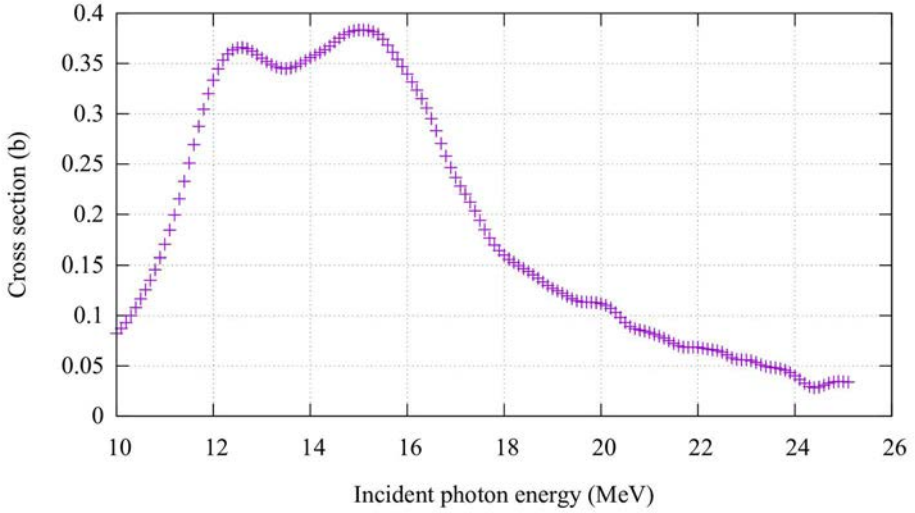

FIG. 2. Photo absorption cross-section for ^{181}Ta (reproduced from Ref. [8]).

The photon interaction with light nuclei (A < 40) is more complex than for medium and heavy nuclei. In this case, photon interaction with individual nucleons is much more significant and Eq. (1), which describes collective excitation modes, is generally inapplicable. The energy dependence of the photo absorption cross-section for light nuclei becomes more complex, as shown in FIG. 3.

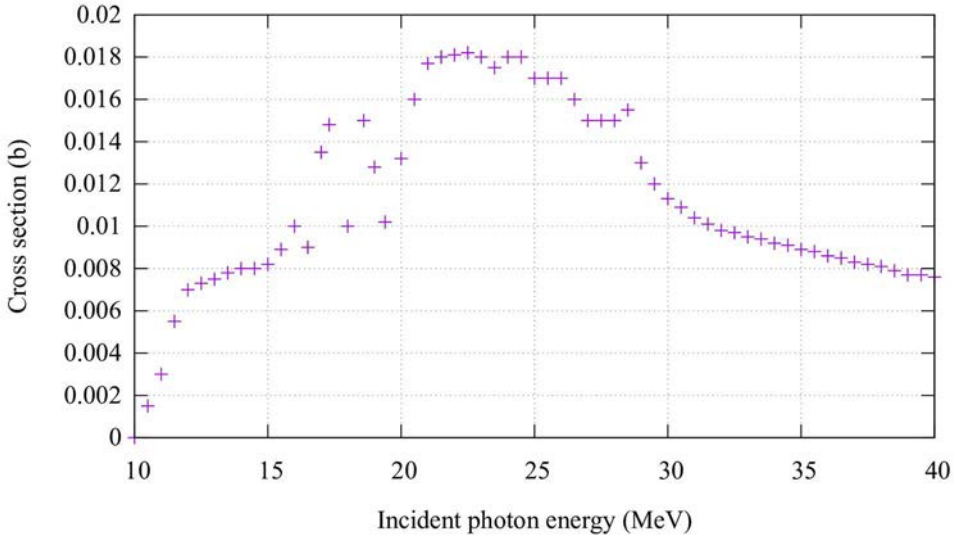

FIG. 3. Photo absorption cross-section for ^{19}F (reproduced from Ref. [8]).

Photonuclear production of medical radioisotopes (RI) generally uses bremsstrahlung photons from a metal converter, typically tungsten or tantalum, irradiated by an electron beam from an electron accelerator. The bremsstrahlung photon spectrum contains a continuum of photons with energies from near zero up to the incident beam energy which is typically 35–40 MeV. While the primary RI production usually takes place for photon energies within the GDR resonance area, photons with energy higher than the separation energy of two nucleons (typically above 16 MeV) can initiate (γ, 2n), (γ, pn) or (γ, 2p) reactions. For incident photon energy above 24 MeV, photonuclear reaction channels with three output particles open up: (γ, 3n), (γ, 2np), etc. Such reactions might also be used for RI production, the ^{70}Ge (γ,2n)^{68}Ge reaction can serve as example. However, photonuclear reactions above these thresholds result in the production of isotopes that are not desirable, impacting the radioisotopic purity of the desired product and inducing more pronounced activation. Figure 4 shows experimental cross-sections of (γ, n), (γ, 2n), (γ, 3n) reactions for ^{100}Mo. It can be seen that for incident photon energies above 16 MeV the (γ, 2n) reaction will dominate over the (γ, n) reaction.

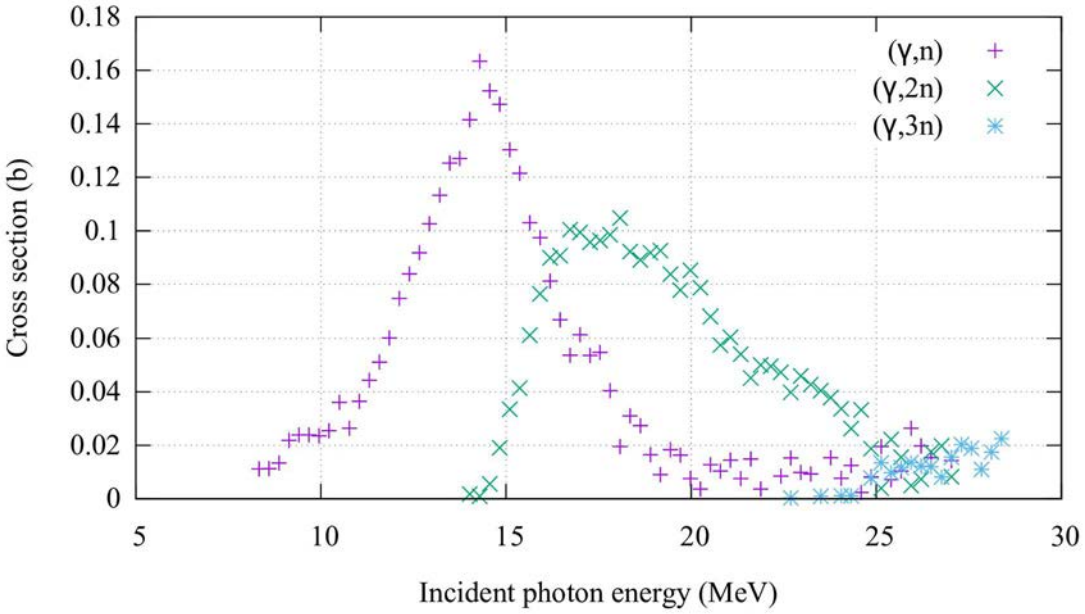

FIG. 4. Experimentally determined cross-sections of (γ, n), (γ, 2n) and (γ, 3n) reactions for ^{100}Mo (reproduced from Ref. [8]).

2.2. PHOTONEUTRON AND PHOTOPROTON REACTIONS

The type of particle emitted from the excited nucleus after photo absorption greatly depends on the mass number. As discussed above, for A < 40 direct photon nucleon interactions can also contribute to photonuclear reactions [6]. This interaction results in relatively high energies and angular anisotropy of the emitted particles when compared to heavier nuclei. There is a general trend for many light nuclei that proton binding energies are lower than those for neutrons and hence proton emission dominates.

For the medium to heavy nuclei, the situation changes drastically. For such nuclei, proton emission is suppressed by a Coulomb barrier and de-excitation occurs through the emission of neutrons. The emitted neutrons have an isotropic angular distribution and an evaporation energy spectrum with an emission probability proportional to $E_n exp(-E_n/T)$, where E_n is neutron energy and T is nuclear temperature. Protons are primarily emitted as a result of direct nuclear reactions and have a higher energy and anisotropic angular distribution.

For medium nuclei, a gradual dominance transition from the (γ, p) reaction channel towards the (γ, n) channel is observed. The ratio of the integral cross-sections for both reactions, shown in FIG. 5, illustrates the overall tendency. However, for medium weight nuclei the relative magnitude of (γ, n) and (γ, p) processes is rather sensitive to the details of nuclear structure. For example, for ^{24}Mg the ratio of the integral cross-sections is an order of magnitude larger than that for ^{26}Mg as shown in Fig. 6. The physical reason for this phenomenon is the alpha cluster structure of ^{24}Mg nuclei (expected in 4n nuclei) suppressing neutron emission [7].

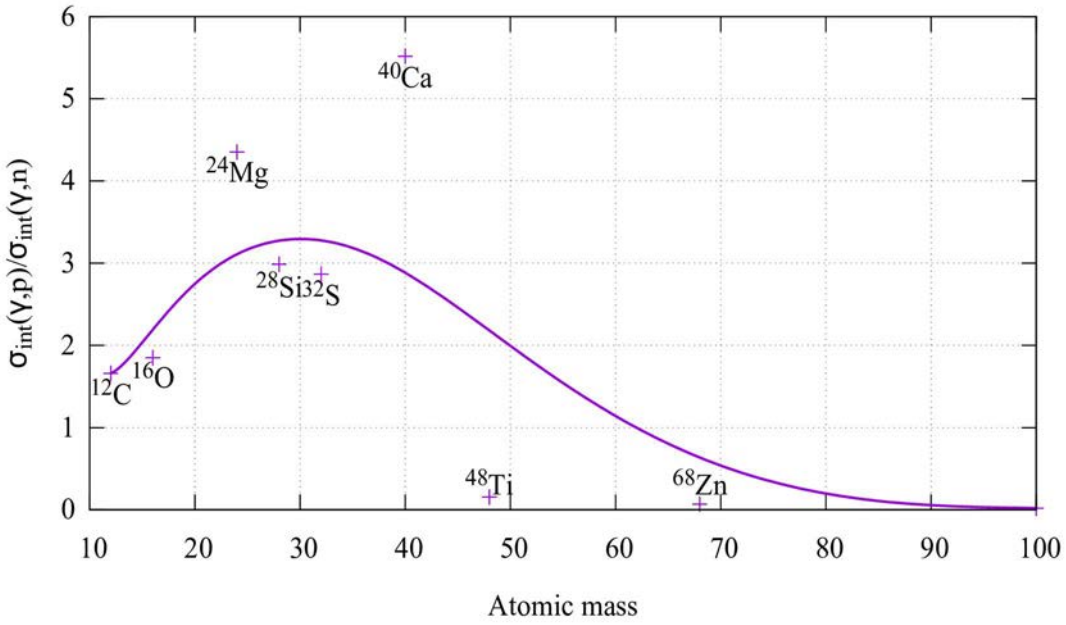

FIG. 5. Ratio of the integral cross-sections of (γ, p) and (γ, n) reactions for 10 < A < 100 (reproduced from Ref. [8]).

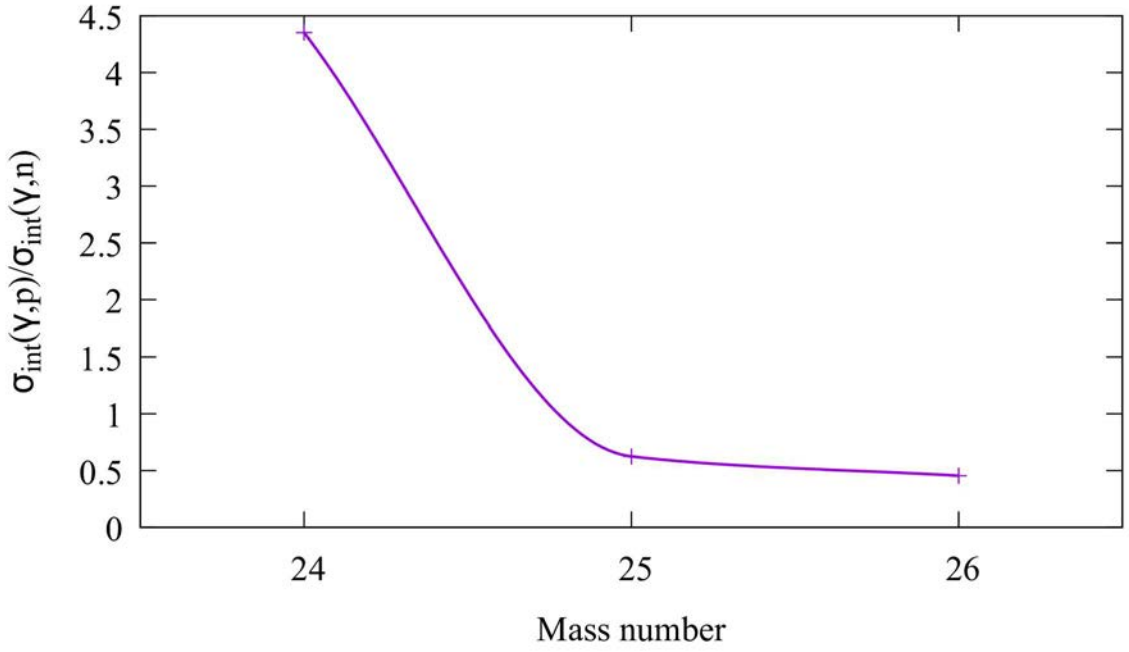

FIG. 6. Ratio of the integral cross-sections of (γ, p) and (γ, n) reactions for magnesium isotopes ^{24}Mg, ^{25}Mg, ^{26}Mg (reproduced from Ref. [8]).

2.3. MODELS OF PHOTONUCLEAR REACTIONS AND REACTION CODES

According to modern theoretical approaches, for an incident photon energy below 30 MeV, almost all photonuclear reactions pass through the following stages:

— Photo-absorption;
— Pre-equilibrium stage;
— Compound nucleus stage.

There is also some contribution from direct photonuclear reactions that do not pass through the compound nucleus stage, but such reactions are rather seldom for this photon energy range.

In most cases the incident photon causes collective excitation of the nuclei where neutrons are shifted against photons. Following Chadwick et al. [5], the photo absorption cross-section is written in the following form Eq. (2):

$$\sigma(E) = \sigma_{GDR}(E) + \sigma_{QD}(E) \tag{2}$$

where σ_{GDR} is GDR photo-absorption cross-section given by equation (1) and σ_{QD} describes the contribution from the quasi-deuteron excitation. Parameters of the GDR cross-sections are obtained by fits of experimental data to equation 1 and some model parameterization is used for the quasi-deuteron component. The most common approach uses a model representation for σ_{QD} from Eq. (3) [8]:

$$\sigma_{QD}(E) = L\frac{NZ}{A}\sigma_d(E)f(E) \tag{3}$$

where L=6.5 is the Levinger parameter, $\sigma_d(E)$ is the deuteron disintegration cross-section and $f(E)$ is the Pauli-blocking function. For $\sigma_d(E)$ and $f(E)$ the following parametrizations are suggested in Eq. (4–5) [9]:

$$\sigma_d(E) = 61.2\frac{(E-2.224)^{\frac{3}{2}}}{E^3} \tag{4}$$

$$f(E) = 8.3714 \cdot 10^2 - 9.8343 \cdot 10^{-3}E + 4.1222 \cdot 10^{-4}E^2 - 3.4762 \cdot 10^{-6}E^3 + 9.3537 \cdot 10^{-9}E^4 \tag{5}$$

This model for calculating photo absorption cross-section is implemented in a number of reaction and transport codes such as EMPIRE [10], TALYS [11], FLUKA [12].

The pre-equilibrium state immediately follows photo-absorption and corresponds to the transition from an excited state to the compound nucleus state. The common approach adopted by most of the reaction codes for photonuclear reactions uses a particle hole representation of the excitations from the incident photons. Such calculations are often performed in the frameworks of the exciton and hybrid semi-classical models [5].

The exciton model implies solving the corresponding balance equations for the nuclear system evolution and the calculation of particle emission probabilities [13]. Hybrid models use Monte Carlo methods for simulation of the nuclear system evolution [14]. EMPIRE and GNASH [15] reaction codes implement both models, while TALYS implements only the exciton model.

After the pre-equilibrium state, the nucleus enters the compound nucleus state. The compound nucleus decays to the ground state through particle or photon emission, or fission. This process

is commonly described using statistical models based on the Hauser-Feshbach theory [16]. Within this approach, the cross-section of a nuclear reaction with initial state *i* and final state j is expressed as in Eq. (6)

$$\sigma_{ij}(E) = \sum_{I\pi} \sigma_i^C(E, I, \pi) P_j(E, I, \pi) \quad (6)$$

where $\sigma_i^C(E, I, \pi)$ is cross-section of compound nucleus formation with spin I and parity π *and* $P_j(E, I, \pi)$ is the probability of the compound nucleus decay to the j channel. This probability is expressed through the transmission coefficients $T_j(E, J, \pi)$ as in Eq. (7)

$$P_j(E, I, \pi) = \frac{T_j(E,I,\pi)}{\sum_c T_c(E,I,\pi)} \quad (7)$$

Transmission coefficients T_j can be calculated using data on nuclear level densities, gamma-ray strength functions, etc. Such calculations are usually implemented by the reaction codes, but the necessary parameters are also stored in IAEA RIPL [17].

2.4. PHOTOFISSION

Photo fission reactions at incident photon energy below 30 MeV share the initial photo absorption stage with ordinary photonuclear reactions, but the final fission process is much more complex. The similarity to photo absorption processes leads to similar energy dependence of the photon fission cross-sections. Namely, the GDR effect causes the photo absorption cross-section of the photofission reaction to have a broad peak ranging from 10 to 20 MeV. An example of such a dependency for ^{235}U photofission is shown in FIG. 7.

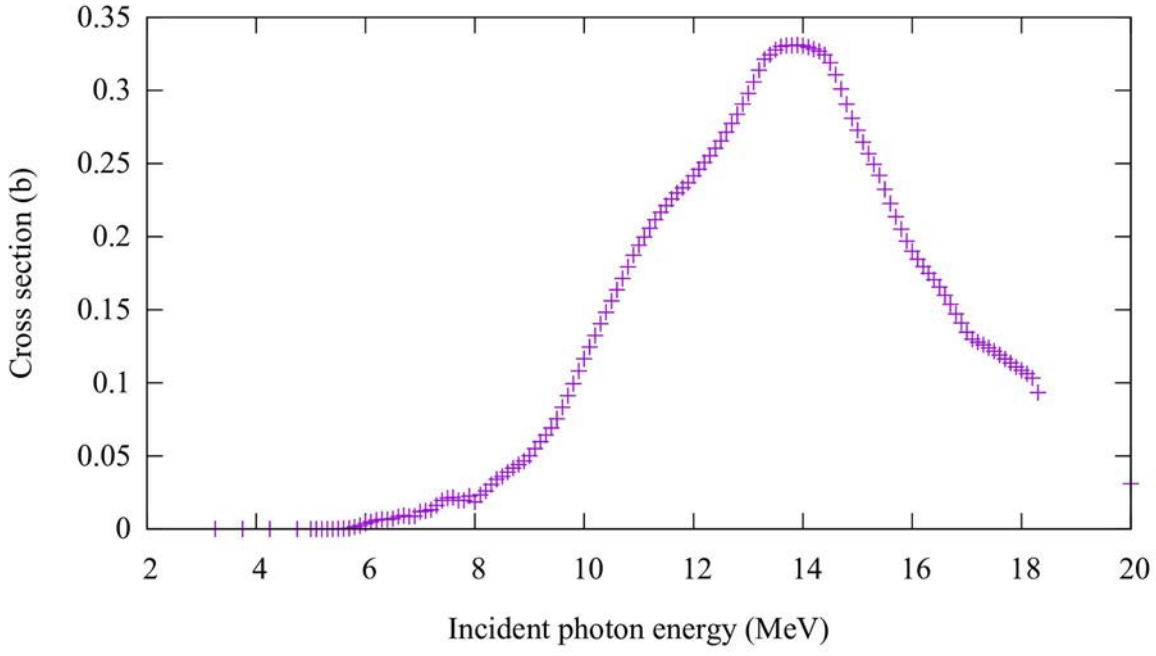

FIG. 7. Cross-section of ^{235}U photofission reaction (reproduced from Ref. [8]).

The energy of the absorbed photon excites collective vibration modes. As a result, the nucleus experiences considerable deformation that eventually results in breakup into two or more fragments. The emerging fragments are usually in highly excited states and emit photons and neutrons during the subsequent de-excitation process. Such emission processes are called

'prompt', while the radiation from the decay of the fission products is called 'delayed'. For the photon energy between 10 and 100 MeV, the distribution of fission product masses has two pronounced maxima. This is quite different from neutron or proton induced fission, where for high excitation energies the distribution exhibits one single maximum.

The modern theoretical description of the photofission process implies that fission goes through a set of definite transition states characterized by quantum numbers I (spin), π (parity), and K (projection of spin I on the nucleus symmetry axis). As a result of photon absorption, a compound nucleus is formed that decays by fission, neutron, or photon emission. The corresponding cross-section is given by the expression, in Eq. 8, similar to Eq. (5):

$$\sigma_f(E) = \sum_{I\pi K} \sigma_{\text{abs},\gamma}(E, I, \pi) P_f(E, I, \pi, K) \quad (8)$$

where $\sigma_{\text{abs},\gamma}$ is photoabsorption cross-section and P_f is fission probability of the transition state defined by I, π, and K quantum numbers. The fission probability, P_f, can be calculated using statistical models.

2.5. NUCLEAR REACTION CODES

Nuclear data for photonuclear reactions obtained from experimental measurements is generally incomplete or non-existent. Not only is there insufficient cross-section data, but also the energy and angular distributions of the reaction products are very rarely measured in the experiments. Consequently, nuclear reaction codes are used to obtain comprehensive information on photonuclear reactions. These codes implement theoretical models to calculate all three stages of the photonuclear reaction: photo-absorption, pre-equilibrium stage, and decay of the compound nuclei. These nuclear reaction codes are commonly used for the evaluation of nuclear data and production of nuclear data libraries.

The modern reaction codes used for the calculation of photonuclear reactions include EMPIRE [10], TALYS [11], CCONE [18], and MEND-G [19]. These codes were used for the production of the recent IAEA Photonuclear Data Library 2019 [20]. All these codes implement a similar set of modern theoretical models, but the details of the implementation are quite different. As a result, there is often ambiguity in the computed values [20]. In some cases, the peculiarities of the implemented models can produce results that deviate considerably. An example is the discrepancy in the cross-section magnitude predicted by TALYS for titanium and copper isotopes [21, 22].

2.6. TRANSPORT CODES

Practical implementation of photonuclear isotope production often requires calculation of the isotope yields in the production target, photon fluxes, and energy depositions for the design of components in the isotope production facility. Transport codes are used for this analysis.

Transport codes simulate the transport of elementary particles and ions through matter. Generally, there are two types of transport codes: deterministic and Monte Carlo. Deterministic codes solve the integro-differential transport equation to calculate characteristics of the particle transport, while Monte Carlo methods simulate the process of particle interaction with matter using statistical sampling. Deterministic codes are primarily used in nuclear reactor physics. Simulations of photonuclear isotope production use Monte Carlo transport codes almost exclusively.

A Monte Carlo simulation is a kind of computer experiment. During simulation, a particle trajectory is sampled at repeated time intervals using the probability distributions of the relevant physical processes: scattering, absorption, emission, etc. To obtain consistent results a large number of statistical trials are necessary. In general, an estimation of the relative error of a Monte Carlo simulation is approximately $1/\sqrt{N}$, where N is a number of trials.

Simulation of actual isotope production facilities usually requires significant computer resources. Photonuclear isotope production is especially demanding because the typical cross-sections of photonuclear reactions are low compared to the cross-sections of electromagnetic processes for photons (Compton scattering and pair production). For example, ^{100}Mo cross-sections for Compton scattering, pair production, and photo absorption at 15 MeV are 1.59, 4.59 and 0.197 barns, respectively, while the peak cross-section for the (γ, n) reaction is 0.16 barns. Consequently, the sampling ratio for photonuclear interactions is low and, to ensure statistical validity of the calculated results, a large number of trials is necessary.

Simulation of the particle interactions during transport requires comprehensive information about the corresponding physical processes: cross-sections, angular distributions, emission spectra, etc. Depending upon the implementation, the corresponding nuclear data is either stored in a database supplied with the code system or obtained from analytical models during calculations. Most modern Monte Carlo codes use a combined approach: some data, particularly cross-sections, are stored in databases, and some is calculated using approaches similar to those used by nuclear reaction codes. However, not all codes implement models for photonuclear reactions and the available models are often inaccurate. The essential discrepancies of calculations using built-in models with experimental data for the GDR energies were reported for GEANT4 [23, 24] and PHITS [25]. Generally, Monte Carlo codes that use evaluated nuclear data libraries such as MCNP [26] provide more accurate results, but this also depends on the quality of the nuclear data. It should be noted that available photonuclear data is often incomplete, and usage of analytical models is unavoidable.

Universal Monte Carlo transport codes, such as MCNP [26], FLUKA [12], GEANT4 [27], PHITS [28], PENELOPE [29] and EGS-nrc [30] are the most frequently used codes for simulation of isotope production. The first four are capable of simulating photonuclear reactions (in the case of MCNP the photonuclear data libraries are necessary), and the last two support simulations of electromagnetic processes only.

The MCNP transport code has been developed and maintained by Los Alamos National laboratory since 1957. It is considered as one of the most stable and verified codes for Monte Carlo simulations. Using nuclear data libraries in the ENDF format, MCNP is highly configurable for simulation of various physical processes including photonuclear. The drawbacks of the MCNP code system includes the complicated syntax of the input file and poor geometry visualization support. Also, there is no built-in capability to calculate isotope yield from the nuclear reactions.

The Monte Carlo transport code FLUKA is maintained by the INFN-CERN Collaboration. The modern versions of this code implement an advanced model of the photonuclear interactions using the FLUKA Giant Resonance total cross-section database that contains evaluations for 190 nuclides. There is also an option to calculate the production of residual nuclei from the nuclear reactions in certain regions of the model geometry.

The PHITS (Particle and Heavy Ion Transport code System) code base has been developed and maintained by the collaboration between JAEA, RIST, KEK, JAXA, Kyushu University, TU Vienna (Austria) and CEA (France). The physical models implemented in the code system

include support for calculations of photonuclear reactions. One can obtain distribution of the residual nuclei per selected model regions or spatial distribution over the rectangular or cylindrical mesh. PHITS uses an input file syntax similar to that of MCNP, simplifying the usage of already developed models in PHITS simulations.

The GEANT4 simulation toolkit has been developed and maintained by CERN. GEANT4 is actually a collection of C++ classes intended for microscopic simulation of particle transport in various media. Such an approach provides great flexibility in the selection of various physical models at the cost of laborious C++ programming. While GEANT4 includes support for simulation of photonuclear reactions, the models implemented are inaccurate for GDR energies. At the same time, the open architecture of GEANT4 allows extending the set of physical models using a more accurate approach [23].

2.7. DATABASES OF PHOTONUCLEAR REACTIONS

There are two main types of databases containing data on photonuclear reactions. The first type are nuclear data libraries of experimental nuclear reaction data. The most reliable library of this type is EXFOR [1], maintained by the Network of Nuclear Reaction Data Centers. EXFOR is not a specialized library for photonuclear reactions; it contains data on nuclear reactions induced by other elementary particles and light nuclei as well. References to the corresponding bibliographic sources and additional information important for data analysis and interpretation are also stored in the library, along with cross-section data.

The other main type of databases are evaluated nuclear data libraries containing specially processed experimental data and results of evaluations using nuclear reaction codes. Usually, the evaluation procedure includes analysis of the available experimental data for possible discrepancies and inconsistencies. This analysis is complemented by calculations using nuclear reaction codes. The parameters of reaction codes are adjusted to achieve the agreement with available experimental data.

When there is no experimental data for the nuclide being considered, the results of the model calculations are stored in the evaluated library. Sometimes the model parameters used during calculations are extracted from the experimental data for the neighboring nuclides. In either case, nuclear data obtained from pure model calculations can contain significant discrepancies from true values and should be used with considerable caution.

Evaluated photonuclear data is stored in general purpose evaluated nuclear data libraries such as ENDF/B-VIII.0 [31] or TENDL-2017 [32], and also in specialized photonuclear libraries such as JENDL/PD-2016 [33] or the 1999 IAEA Photonuclear Data Library [8]:

- ENDF/B-VIII.0 [31] was released by the Cross-Section Evaluation Working Group (CSEWG) of Brookhaven National Laboratory National Nuclear Data Center in 2018. It contains photonuclear data for 163 elements and isotopes;
- TENDL-2017 [32] contains reaction data evaluated using the TALYS reaction code [11]. The evaluated library contains photonuclear data for 283 stable isotopes;
- JENDL/PD-2016 [33] was developed by Nuclear Data Center of Japan Atomic Energy Agency. Two versions of the library are available: standard, containing photonuclear data for 181 nuclides, and expanded, containing data for 2681 nuclides;
- The 1999 IAEA Photonuclear Data Library [8] contains evaluated data for 164 nuclides, obtained after evaluation of nuclear data from six photonuclear data libraries. An additional 37 nuclides were included in the recent 2019 IAEA Photonuclear Data Library [34], among them 9 isotopes are considered relevant for medical applications.

2.8. PRODUCTION OF MEDICAL RADIOISOTOPES

A wide range of radioisotopes for diagnostics and therapy can be produced via different photonuclear reactions. The application area of the isotope depends on the type of emitted particles: γ emitters are used for SPECT, positron emitters are used for PET, and β^- and α emitters are used for cancer therapy. Isotopes of the same element are used in pairs, where one has therapeutic and another imaging capabilities. These matched pairs are referred to as theranostics and examples of such pairs of radionuclides are ^{44g}Sc/^{47}Sc, ^{64}Cu/^{67}Cu, ^{68}Ga/^{67}Ga, ^{86}Y/^{90}Y.

An important characteristic in the production of medically relevant radioisotopes is the presence of stable (or long lived) isotopes of the same element in the target. When no stable isotopes are present, the produced radioisotope is called carrier free. In reality, it is almost impossible to obtain radioisotopes with 100% isotopic abundance. In this case, the term no carrier added (n.c.a.) is used to describe radioisotopes with minimal concentration of stable or long lived isotopes. The opposite case is called carrier added (c.a.).

Concerning the photonuclear production route, radioisotopes obtained from (γ, p) reactions are usually no carrier added because a different chemical element is produced. Photo neutron reactions always result in carrier added radioisotopes as the product is isotopic with the element in the target.

Table 1 gives a non-exhaustive summary of medical radioisotopes that can be produced by photonuclear reactions. The table contains references describing possible medical applications of each radioisotope (column 7), as well as references dedicated to the production method, or the cross-section measurements if the production has not been studied yet (column 4). The table is sorted according to the periodic number of the radioisotope.

A recent review on the photonuclear production of radiometals for medical applications was given by Kazakov et al. [35], focusing on experimental studies with ^{99}Mo/^{99m}Tc, ^{47}Sc, ^{67}Cu, ^{225}Ac, ^{177}Lu, ^{44}Ti/^{44}Sc, ^{111}In, ^{105}Rh, ^{68}Ge/^{68}Ga and ^{188}Re.

TABLE 1. EXAMPLES OF PHOTONUCLEAR REACTIONS FOR MEDICAL RADIOISOTOPE PRODUCTION

Radio-Nuclide	$T_{1/2}$	Production Route	Reference Production	Decay Mode	Possible Applications	Reference Applications
^{15}O	122 s	^{16}O(γ,n)^{15}O	[36]	ec β^+	PET imaging neurology, cardiology, oncology to evaluate oxygen consumption, lung and myocardial perfusion, blood distribution and flow	[37, 38]
^{18}F	110 min	^{nat}Ne(γ,pn)^{18}F ^{20}Ne(γ,2n)^{18}Ne →^{18}F ^{19}F(γ,n)^{18}F ^{23}Na(γ,αn)^{18}F	[39, 40] [41, 42] [43]	ec β^+	PET imaging with ^{18}F-FDG and other radiopharmaceuticals for oncology, visualization of inflammations	[44-46]
^{43}K	22.2 h	^{44}Ca (γ,p)^{43}K	[47]	β^-	Myocardium imaging	[48-50]

TABLE 1. EXAMPLES OF PHOTONUCLEAR REACTIONS FOR MEDICAL RADIOISOTOPE PRODUCTION

Radio-Nuclide	$T_{1/2}$	Production Route	Reference Production	Decay Mode	Possible Applications	Reference Applications
^{43}K	22.2 h	^{44}Ca (γ,p)^{43}K	[47]	β^-	Myocardium imaging	[48-50]
^{47}Sc	3.35 d	^{48}Ca(γ,n)^{47}Ca ^{47}Ca(β-)^{47}Sc ^{48}Ti(γ,p)^{47}Sc	[51, 52] [53, 54]	β^-	Palliative care of metastatic bone pain, cancer radioimmunotherapy, SPECT theranostic application	[55-57]
^{57}Co	271 d	^{58}Ni (γ,p)^{57}Co	[58-60]	ec	Mössbauer spectroscopy for microbiological and biochemical applications. hypothetic source for brachytherapy, gamma-chamber calibration	[61-63]
^{64}Cu	12.7 h	^{66}Zn(γ,pn)^{64}Cu ^{65}Cu(γ,n)^{64}Cu	[64] [65-67]	ec β^+, β^-	PET imaging and radiotherapy cancer treatment, theranostic application	[68-71]
^{67}Cu	61.83 h	^{68}Zn(γ,p)^{67}Cu ^{nat}Zn(γ,p)^{67}Cu	[22, 51, 60, 72-74]	β^-, IT	Radiotherapy, radioimmunotherapy, theranostic application	[75, 76]
^{67}Ga	78.3 h	^{69}Ga(γ,2n)^{67}Ga	[77]	ec	SPECT imaging for lymphoma, lung cancer, melanoma and multiple myeloma detection, potential as therapeutic radionuclide	[78-80]
^{68}Ge/ ^{68}Ga	271 d / 61.7 min	^{70}Ge(γ,2n)^{68}Ge ^{68}Ge→^{68}Ga	[81, 82]	ec/ec β^+	^{68}Ga generator, PET imaging, diagnosis neuroendocrine tumors, theranostic pair for ^{90}Y or ^{177}Lu	[83-85]
^{75}Se	120 d	^{76}Se(γ,n)^{75}Se	[86, 87]	ec	SPECT imaging, Brachytherapy	[88, 89]
^{77}Br	57 h	^{79}Br(γ,2n)^{77}Br ^{78}Kr(γ,n)^{77}Kr ^{77}Kr→^{77}Br	[64] [90]	ec β^+	PET imaging, labelling anti-tumor monoclonal antibodies, potential interest in internal radiotherapy	[91]
^{90}Y	64 h	^{91}Zr(γ,p)^{90}Y	[92]	β^-	Microspheres therapy, Implants, radioembolization	[93-95]
^{99}Mo/ ^{99m}Tc	65.9 h / 6 h	^{100}Mo(γ,n)^{99}Mo	[59, 96-100]	β^- / IT	^{99m}Tc generator, SPECT imaging of brain, liver, lungs, heart, etc.	[101]
^{103}Pd	16.99 d	^{nat,104}Pd(γ,n) ^{103}Pd	[102, 103]	ec	Brachytherapy	[104]
^{105}Rh	1.5 d	^{106}Pd(γ,p)^{105}Rh	[102, 103]	β^-	Monoclonal antibodies and peptides labelling, Palliative care of metastatic bone pain	[105-107]
^{111}In	2.8 d	^{112}Sn(γ,p)^{111}In	[108-110]	ec	SPECT, Auger therapy radiolabeling leukocytes, peptides, antibodies, blood scans	[111, 112]

TABLE 1. EXAMPLES OF PHOTONUCLEAR REACTIONS FOR MEDICAL RADIOISOTOPE PRODUCTION

Radio-Nuclide	$T_{1/2}$	**Production Route**	**Reference Production**	**Decay Mode**	**Possible Applications**	**Reference Applications**
^{117m}Sn	14 d	^{118}Sn(γ,n)^{117m}Sn	[110, 113, 114]	IT	Bone pain palliation, Targeted alpha therapy (TAT)	[115-118]
^{125}I	59.49 d	^{126}Xe (γ, n)^{125}Xe→^{125}I	-	ec	Brachytherapy, Auger therapy	[9, 120]
^{131}Ba/ ^{131}Cs	11.5 d /9.7 d	^{132}Ba(γ,n)^{131}Ba ^{131}Ba(ε,β$^+$)^{131}Cs	[121]	ec β$^+$/ ec	Brachytherapy for treating cancers in prostate, breast, head and neck, lung, and pancreas	[122, 123]
^{149}Pm	53.08 h	^{150}Nd(γ,n)^{149}Nd ^{149}Nd→^{149}Pm	[124-126]	β-	Potential agent for radiotherapy and theranostic application	[127]
^{153}Sm	1.93 d	^{154}Sm(γ,n)^{153}Sm	[128]	β$^-$	Bone pain palliation	[129, 130]
^{155}Dy/ ^{155}Tb	9.9 h/ 5.32 d	^{156}Dy (γ, n)^{155}Dy→^{155}Tb	[131]	ec β$^+$/ec	SPECT imaging	[132, 133]
^{166}Ho	26.8 h	^{167}Er(γ,p)^{166}Ho	[134, 135]	β$^-$	SPECT, CT, MRI imaging tumor treatment, brachytherapy, labelled nanoparticles therapy, bone marrow ablation, cancer radioimmunotherapy	[136]
^{175}Yb	4.2 d	^{176}Yb(γ,n)^{175}Yb	[137, 138]	β$^-$	Palliative care of metastatic bone pain, potential therapeutic application Auger therapy	[139, 140]
^{177}Lu	6.71 d	^{178}Hf(γ,p)^{177}Lu	[34, 141]	β$^-$	TAT, peptide receptor radionuclide therapy, bone pain palliation, theranostic application, radio-immunotherapy	[142, 143]
^{188}Re	0.71 d	^{189}Os(γ,p)^{188}Re	[144, 145]	β$^-$	Bone pain palliation, therapeutic application	[146, 147]
^{186}Re	3.7 d	^{187}Re(γ,n)^{186}Re	[102, 148]	β$^-$,ec	Bone pain palliation, synovectomy, nanoparticles labelling for brachytherapy, Treatment of some forms of brain tumors	[149, 150]
^{195m}Pt	4.01 d	^{195}Pt (γ, γ') ^{195m}Pt	[151-154]	IT	SPECT imaging, tumor cell uptake control during chemotherapy, possible therapeutic agent	[151-154]
^{224}Ra/ ^{212}Pb/ ^{212}Bi	3.7 d/ 10.64 h /60.6 m	^{226}Ra(γ,2n) ^{224}Ra	[124, 154]	α/ β$^-$, IT/α, β$^-$	Potential TAT agents	[155, 156]

TABLE 2. EXAMPLES OF PHOTONUCLEAR REACTIONS FOR MEDICAL RADIOISOTOPE PRODUCTION

Radio-Nuclide	$T_{1/2}$	Production Route	Reference Production	Decay Mode	Possible Applications	Reference Applications
^{225}Ra/ ^{225}Ac/ ^{213}Bi	15 d / 10 d /43 min	^{226}Ra(γ,n)^{225}Ra ^{225}Ra(β$^-$)^{225}Ac	[154, 157-161]	β$^-$ / α	TAT, metastatic cancer treatment antibodies labelling, generator of ^{213}Bi	[158, 162, 163]

2.8.1. ^{99}Mo/^{99m}Tc

With a half-life of $T_{1/2}$ = 6 h, ^{99m}Tc is the primary radioisotope used for SPECT imaging, typically obtained as the daughter of ^{99}Mo having a half-life of 65.9 h. The photonuclear route for ^{99}Mo production proceeds via the ^{100}Mo(γ,n)^{99}Mo reaction having a maximum cross-section of about 0.16 barns between 14–15 MeV. Figure 8 depicts cross-sections for (γ, n), (γ, 2n), (γ, 3n) and (γ, p) reactions for ^{100}Mo that are recommended by the IAEA based on evaluations of experimental data and theoretical calculations.

Recalling the discussion from Section 2.1, the photonuclear production route typically uses bremsstrahlung photons with a maximum energy of 35–40 MeV. Thus, the production of ^{99}Mo is accompanied by the generation of stable molybdenum isotopes ^{98}Mo, ^{97}Mo, and β$^-$ radioactive ^{99}Nb, that decays to ^{99}Mo with a half-life of 15 secs.

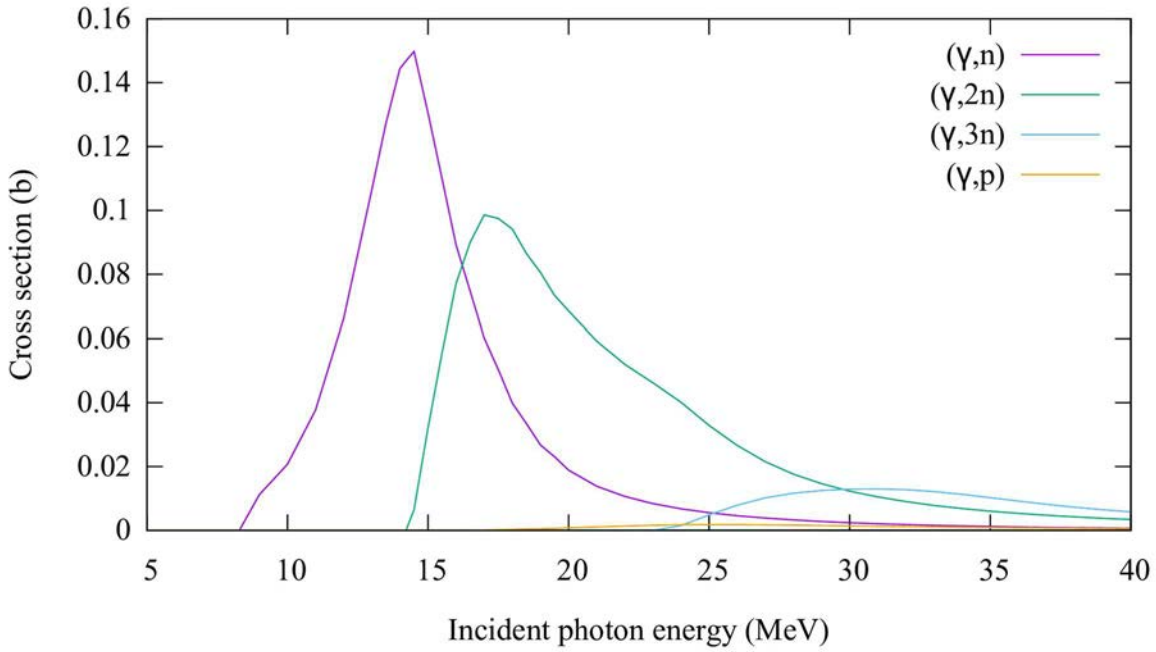

FIG. 8. Recommended cross-sections for the photonuclear reactions on ^{100}Mo (reproduced from Ref. [8]).

2.8.2. Copper-67

Copper-67 ($T_{1/2}$ = 61.83 h) is a β$^-$ emitter with average electron energy of 141 keV. The ^{67}Cu nuclide also has γ emissions at 91.3, 93.3 and 184.6 keV that can be used for SPECT imaging. The emission probabilities for these γ rays are 6.3%, 14.8% and 44.2%, respectively [164].

Photonuclear production of ^{67}Cu is based on the ^{68}Zn(γ, p)^{67}Cu reaction. Experimental data for this reaction in the EXFOR library [1] contains only five points based on measurements from 1957 [165]. Cross-sections from evaluated nuclear data libraries TENDL-2017 [32] and JENDL/PD-2016 [33] deviate significantly from the experimental data (FIG. 9). A recently developed combined model of photonuclear reactions CMPR [22] provides better agreement in energy but predicts higher values for the cross-section values at the GDR peak. Very recently, new measurements on the cross-section of the ^{68}Zn(γ, p)^{67}Cu reaction have been reported with largely deviating results [166]. It can be concluded that additional determinations of the photonuclear cross section for this reaction are required in the future.

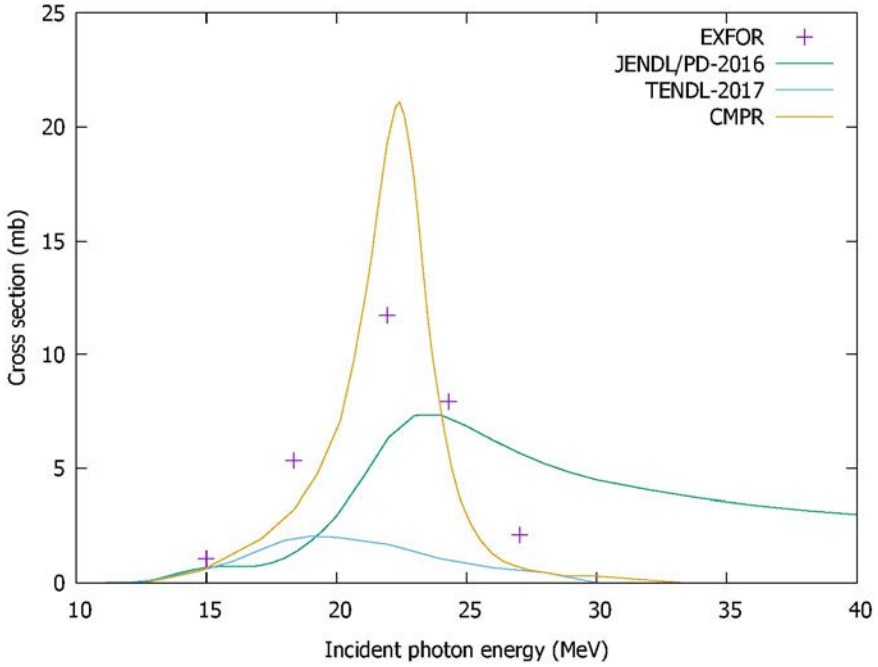

FIG. 9. Measured and theoretical data for the cross-section of the ^{68}Zn (γ, p)^{67}Cu reaction (reproduced from Ref. [8]).

2.8.3. Scandium-47

Scandium-47 ($T_{1/2}$ = 3.35 days) is a β^- emitter with an average electron energy of 162 keV and γ emission line at 159 keV (abundance 68.3%) [167]. The direct method for ^{47}Sc production uses the photo proton reaction ^{48}Ti(γ, p)^{47}Sc. The experimental cross-section for this reaction has a GDR peak centred at 22.5 MeV with a maximum at 28.7 mbarn (see FIG. 10). At the same time, evaluated cross-sections from TENDL-2017 [32] and JENDL/PD-2016 [33] libraries are two times smaller than experimental data from the EXFOR database [168]. The CMPR model provides significantly better agreement with experimental data.

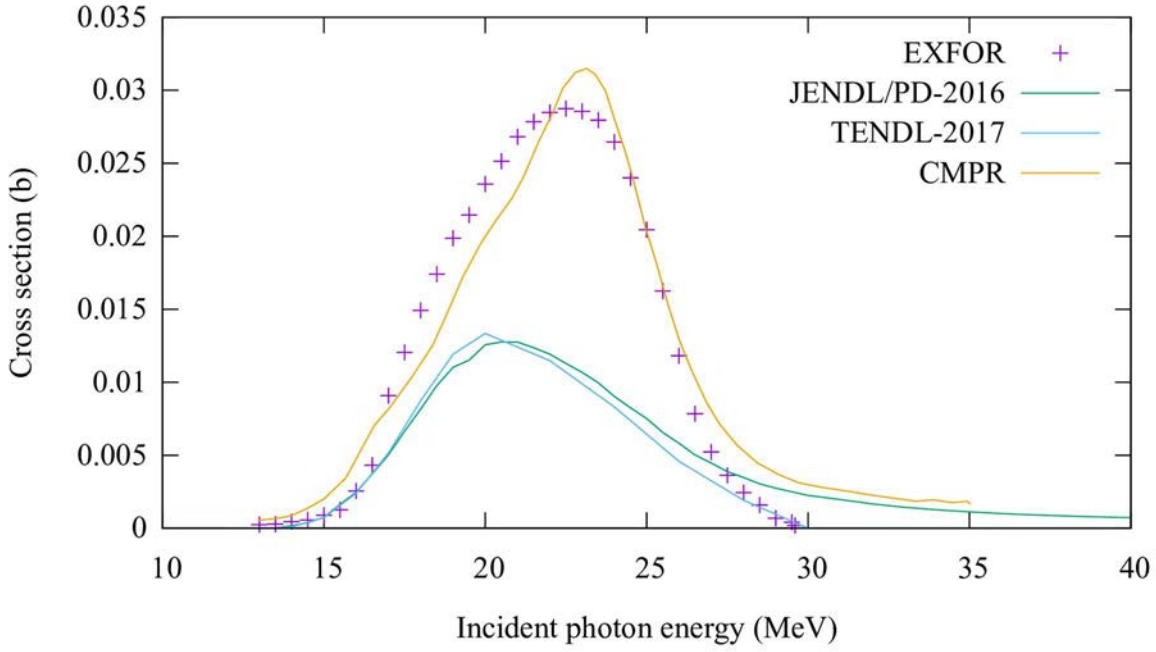

FIG. 10. Cross-section for $^{48}Ti(\gamma,p)^{47}Sc$ reaction (reproduced from Ref. [8]).

Another possible route for photonuclear ^{47}Sc production is the $^{48}Ca(\gamma, n)^{47}Ca$ reaction, where ^{47}Ca could be used as ^{47}Sc generator [169]. The cross-section of this reaction extracted from various nuclear data libraries is shown in FIG. 11 11. One can see that evaluated libraries TENDL-2017 [32] and JENDL/PD-2016 [33] essentially underestimate the cross-section magnitude compared to experimental EXFOR [1] data.

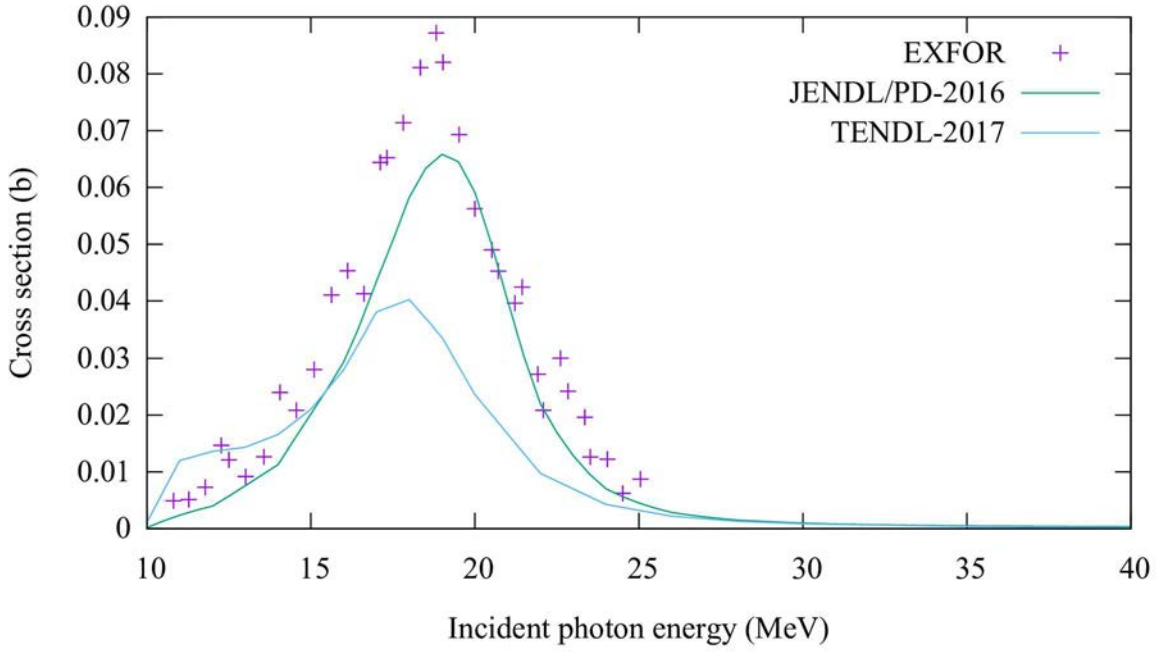

FIG. 11. Cross-section for the $^{48}Ca(\gamma,n)^{47}Ca$ reaction (reproduced from Ref. [8]).

2.8.4. Actinium-225

Actinium-225 ($T_{1/2}$ = 10 days) is a nuclide for α therapy that has shown promising results in cancer treatment. Being an α emitter (E_α = 5.8 MeV) with weak γ emission (100 and 150 keV with 1.7% and 0.6%, respectively), it is accompanied with a complex decay chain of short lived α and β decaying isotopes, of which ^{213}Bi is also considered for therapy purposes.

Production of carrier free ^{225}Ac can be achieved via ^{225}Ra/^{225}Ac generators where ^{225}Ra is produced via the reaction ^{226}Ra(γ, n)^{225}Ra. Experimental data on the cross-section for this reaction are unavailable, and evaluated nuclear data libraries TENDL-2017 [32] and JENDL/PD-2016 [33] (FIG. 12) solely rely on theoretical calculations. Comparison of TENDL predictions with available experimental data on integral ^{225}Ra production yields [160, 170] indicate that theoretical calculations might underestimate the true cross-section. Dedicated experimental efforts to measure this quantity at various photon energies are urgently required to enable reliable predictions on ^{225}Ra yields in future ^{225}Ac production facilities. It is interesting to note that in contrary to the (γ, n) reaction, cross section data for ^{226}Ra photofission do exist [171, 172].

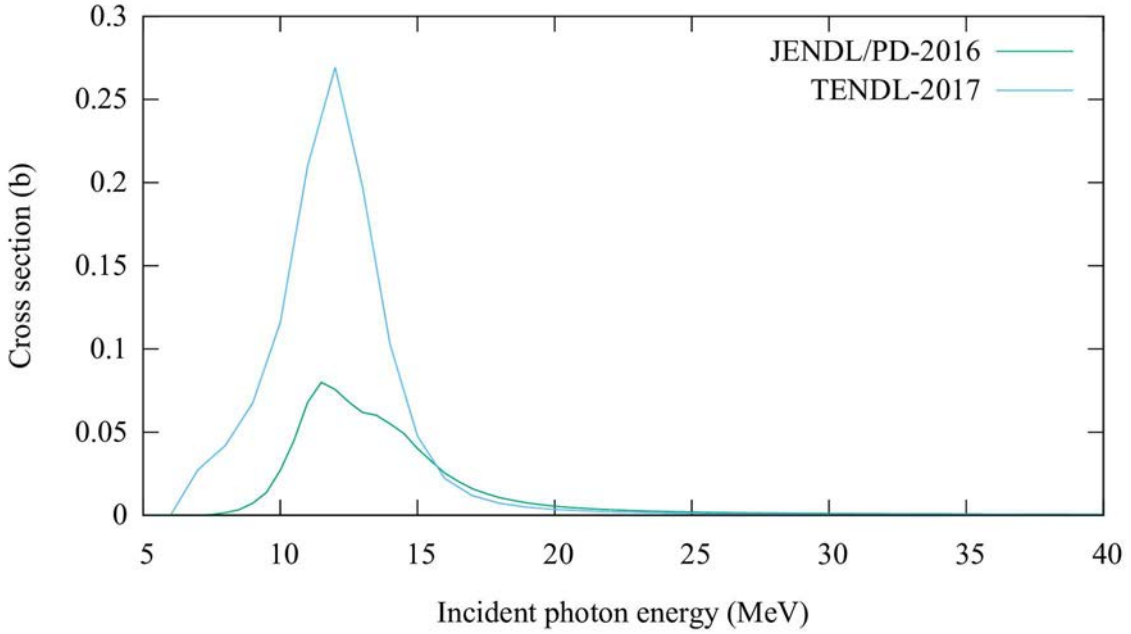

FIG. 12. Cross-section for the ^{226}Ra (γ, n)^{225}Ra reaction (reproduced from Ref. [8]).

2.9. EXPERIMENTAL MEASUREMENTS OF PHOTONUCLEAR REACTION DATA

It was noted in Section 2.5 that the nuclear data for photonuclear reactions obtained from experimental measurements is generally incomplete or non-existent. There is insufficient cross-section data, and the energy and angular distributions of the reaction products are rarely measured in experiments. Most of the experimental photonuclear reaction data was obtained by a few facilities during the 1960's, 1970's and into the 1980's. Many of these facilities have been closed for many years. There were significant challenges in obtaining precise measurement data and several different techniques were developed to overcome various obstacles.

2.9.1. Bremsstrahlung method

The earliest method used can be described as the bremsstrahlung method. Electron bremsstrahlung produces a continuous spectrum of photons with the upper energy limit at the electron energy and the yield of photons increases as the energy decreases until, at low energies, self-absorption in the target reduces the yield [173]. The bremsstrahlung spectrum is produced as an electron beam strikes a high Z target, and the measurement involves recording a yield curve while incrementally changing the incident electron energy in small increments and subtracting the two results to obtain a differential curve. The data is deconvoluted to produce a curve of the cross-section as a function of the incident photon energy. These measurements required good stability and reproducibility of the accelerator parameters, good counting statistics and knowledge of the bremsstrahlung flux and spectrum [174]. There may be systematic differences in data measured at different facilities because of the challenges of the measurement.

2.9.2. Positron annihilation in flight

There are several methods to produce beams of mono-energetic photons which can be used for photonuclear cross-section determinations. Two of these methods are the annihilation in flight of fast positrons considered in this section and tagged bremsstrahlung considered in the next. Berman and Fultz described the technique in several publications [8, 175]. The method consists of producing a beam of fast positrons of a defined energy E_{e+} and directing them to strike a thin, low Z target to produce, in the forward direction, a mono-energetic beam of annihilation photons having an energy $E_\gamma = E_{e+} + 0.76$ MeV (the latter term being ¾ of the rest mass of the annihilating pair) [175]. The photonuclear measurement determines the number of counts (N_i) produced by the positron beam of energy E_{+o}, $N^+(E_o)$, and a second step of measuring the number of counts from an electron beam of energy E_{-o}, $N^-(E_o)$. The process is repeated at the next energy, E_{+1}, etc. The photonuclear cross-section is given by the difference of the two measurements $N^+(E_o)$ - $N^-(E_o)$ divided by the number of photons that irradiated the target [8]. The measurement does not require deconvolution, as is needed by the bremsstrahlung method, and is hence more accurate. It does have the challenge of significantly poorer statistics because of the low intensity of the photon beam that depends on both the positron production and then the conversion to photons; both processes have small cross-sections.

2.9.3. Bremsstrahlung tagging

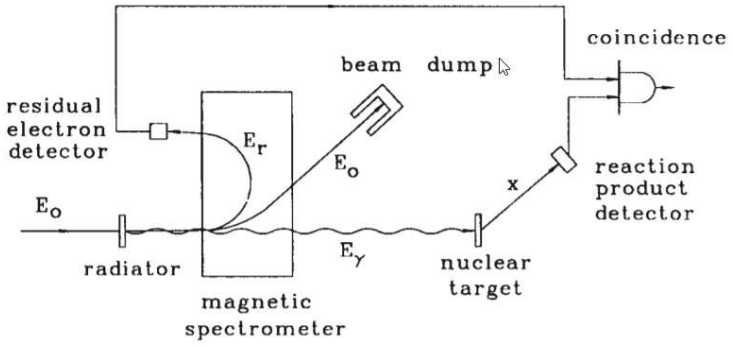

FIG. 13. Illustration of the bremsstrahlung tagging process (reproduced from Ref. [8]).

Photonuclear cross-section measurement is possible using ‘tagged photons’, i.e., photons with defined energies and time arrivals. When a mono-energetic beam of electrons of energy E_o hits

a very thin radiator (typically a thin foil), it produces a continuous spectrum of bremsstrahlung. Most of the electrons do not interact with the thin radiator and are directed to a beam dump to stop them. The path of scattered electrons of residual energy E_r is then bent in the spectrometer magnet towards the focal plane of an appropriate spatially resolved electron detector (the tagger, FIG. 13), which measures E_r from the position and scattered electron flux (proportional to number of photons). The difference between E_o and E_r is the energy of the radiated photon (neglecting any nucleus recoil) in Eq. (9):

$$E_\gamma = E_o - E_r \tag{9}$$

With tagged photons, it is possible to determine the correlation in time of the scattered electron and the reaction product of the bremsstrahlung photon impinging on a target by coincidence measurement. This provides one of the better measurements of photonuclear cross-section. The major limitation is the maximum counting rate limited to about 10^6 events per second by the coincidence counting requirements.

2.9.4. Laser Compton backscattering

Compton backscattering of laser light from relativistic electrons is a promising method of producing useful yields of high energy monochromatic polarized photons. The head on collision of relativistic electrons and laser photons creates a pencil like beam of γ rays that depends on the properties of the electron beam and the laser beam [176]. The energy of the produced γ ray depends on the backscattering angle (θ) of the laser photon and is given by the well known formula in Eq. (10) [176]:

$$E_\gamma = \frac{E_L(1-cos\theta_L)}{1-\beta cos\theta+E_L(1-cos(\theta_L-\theta))/E_e} \tag{10}$$

where E_L is the energy of the laser photon, E_e is the electron beam energy, θ_L is the incident angle of the laser photon, and $\beta = v_e/c$. For a head-on collision, $\theta_L = \pi$, θ is much less than unity and $\gamma = E_e/mc^2$, the gamma energy is given approximately by:

$$E_\gamma = \frac{4\gamma^2 E_L}{1+(\gamma\theta)^2+4\gamma E_L/mc^2} \tag{11}$$

Production of high energy photons requires high energy electrons leading to the requirement of storage rings of high luminosity. Aoki et al. [176] describes how these requirements lead to brightness requirements of both the laser and electron sources and Li et al. describes some early measurements using the technique [177]. Ejiri et al. reported on measurements of photonuclear cross-sections of gold and molybdenum using photons produced by laser Compton backscattering [178]. The photon intensity of around 10^8 to 10^{12} per second was possible with intense lasers and intense electron beams. In future, dedicated facilities should be capable of producing high intensity photon sources with the intensity of the order of 10^{14} per second or higher [178]. These should enable new measurements with better statistics than some of the present measurements.

3. PRODUCTION OF INTENSE MULTI-MEV PHOTON BEAMS

Particle accelerators produce and accelerate beams of charged particles, such as electrons, protons, and ions. A source which produces charged particles and a device that provides energy to the particle to speed them up by applying a static or oscillating electrical field are the two main basic components of any accelerator. Particle accelerators vary in design and size. Photon beams of varying energies find numerous applications, electron accelerators are hence the most used types of particle accelerators.

3.1. ELECTRON ACCELERATORS

Electron accelerators are widely used for a great variety of applications that include medical therapy, industrial irradiation processing, sterilization, etc., in addition to being parts of major research facility infrastructure for synchrotron light sources, free electron lasers or fundamental physics. These accelerators cover a very large range of beam energy from a few MeV to many GeV, as well as large range of average beam power from 10^{-3} to 10^{6} W. The IAEA database [179] of industrial irradiation facilities and interactive map give an overview about the distribution of linear accelerators all over the world. However, photo production of isotopes typically requires a narrower range of beam energy, typically 25–50 MeV, and high average power, typically 5 kW to more than 100 kW. There are several different electron accelerator types that meet these requirements: room temperature electron linear accelerators, super conducting linacs, microtrons, and the high energy rhodotron recently developed by the Belgian company Industrial Beam Applications, S.A. (IBA).

3.1.1. Room temperature electron linac

The most widely used type of electron accelerators for energies greater than 10 MeV is the room temperature Radiofrequency (RF) electron linac [180]. A typical linac consists of a high voltage electron gun which injects a beam of electrons into a copper accelerator structure. High power excites the structure to provide an axial accelerating gradient resulting in an energy gain of around 7–10 MeV/m. The frequency of the RF is either around 1.3 GHz (L-Band) or 3 GHz (S-Band) as those are the two main frequencies where high power klystron amplifiers are readily available. Since the output power of a single klystron is often insufficient to power the entire accelerator, the accelerating structure is separated into several sections, each powered by a single klystron amplifier.

Since the power to achieve the designed accelerating gradient of several megawatts cannot be supplied continuously, the klystrons are pulsed to provide short (4–20 μs) pulses with megawatts of peak power. This results in the acceleration of a short pulse of electrons to full energy. The number of pulses per second then determines the average power of the linac.

Electrons are produced by an electron gun at the entrance and accelerated to a final energy that is dependent on the beam power and design of the accelerator. Typically, a room temperature RF electron linac will have a modest (few percent) energy spread in the electron beam and beam losses near the end of the accelerator of one or two percent, producing a significant radiation source during operation and potentially high residual radiation fields in the copper for a short time after the accelerator is turned off. This type of accelerator can provide a cost effective source in a new facility designed to produce high yields of isotopes. The same technology used for this accelerator type has been applied in low energy (less than 10 MeV) industrial and medical applications for many years and has proven to be very robust. The linacs used to produce radioisotopes can generate up to 150 kW at 40 MeV and have the additional feature of the ability to change electron beam energy on a pulse by pulse basis. This is achieved with solid

state modulators and a smart control system that enables the production of several beams of modest energy difference, separated by a single deflection magnet. This is a useful feature to produce two different isotopes or two target areas for the same isotope at lower power and phased to remove the isotopes at different times to meet a better schedule. The limitation for the maximum beam power is due to commercial availability of suitable high power RF sources.

3.1.2. Superconducting electron linacs

In the past 35 years, designers of a growing number of accelerators have chosen superconducting technology over normal conducting copper. The motivation for using superconducting cavities for photonuclear isotope production is related to RF losses in the cavities (RF to beam power conversion efficiency). In comparison to room temperature linacs, where roughly half of the RF power is going into the cavities, superconducting accelerators have an advantage because most of the RF power is coupled to the beam and is not taken up by the cavities. There is a price associated with the operation of superconducting accelerators - one has to keep the RF niobium cavities at very low temperatures of less than 4.5 K. This type of cooling requires a cryoplant, which is often expensive and complex in operation. Ostroumov et al. [181] provided an in-depth analysis of the advantages and cost of the superconducting linac in comparison with normally conducted (copper) linacs. The conclusion of the publication is that a superconducting linac for isotope production will be quite expensive and take several years, even when standard components are used. This can change if superconducting linac technology becomes more common. The maximum power achievable with a superconducting linac is ~200 kW. The limitations for the superconducting technology stem from the capacity of the cryoplant and ability to dissipate heat.

3.1.3. Microtron

A microtron is a cyclic electron accelerator developed in the Soviet Union. The electrons are accelerated by an RF electric field of constant amplitude and frequency in a static homogeneous magnetic field. In the vacuum chamber, electrons follow circular paths with a common tangent point, at which the accelerating cavity is located supplying the RF field. The path of electrons differs for each pass due to increasing momentum [182, 183]. A racetrack microtron is a larger scale microtron, which uses two electromagnets oriented in two semicircles. The path of electrons between these semicircles remains straight, creating a geometry similar to a racetrack.

Standard microtrons such as the MT-25 provide electron beam energies between 6 to 25 MeV with currents up to several tens of μA. However, their power output is too low to be considered as useful for efficient production of radioisotopes. Larger scale facilities do exist that enable electron energies beyond 1 GeV, such as the Mainzer Mikrotron (MAMI) in Mainz, Germany. Microtrons have been used for a number of studies, involving photon activation analysis, photonuclear cross section measurements and fundamental research.

3.1.4. IBA rhodotron

A rhodotron is a compact electron accelerator based on the recirculation of a beam through successive diameters of a single coaxial cavity resonating in metric waves [184]. The name comes from the fact that the particle path looks like a rosette. Rhodotrons are commonly used for sterilization applications in industry providing up to 800 kW of beam power at maximum 10 MeV.

Recently IBA announced the development of the TT300-HE rhodotron electron beam accelerator [185]. In this concept the acceleration of electrons occurs in a radiofrequency driven

polarized circular cavity by multiple passes of the electron pulse using bending dipole magnets. The maximum electron energy that can be reached with 12 passes is 40 MeV at a beam current of 3.125 mA, yielding a maximum beam power of 125 kW. At this beam power, the overall consumption of the accelerator is 450 kW, which translates into an overall efficiency above 20%, superior to typical for room temperature linacs. The machine is capable of providing electron energies down to 1 MeV. The radiofrequency system is operating in pulsed mode (10–70 Hz) with a duty cycle between 1% and 12.5% and is supplied by three separate tetrodes that can be operated in continuous and pulsed mode. The beam transport system consists of one vacuum beam line and optical elements to reach the specified beam properties on target.

Another advantage of the rhodotron is the compact size of installation. It comes with a mass of 22 tons and requires a minimum space of 4 x 4 x 4 m. As such, it represents a rather compact design of an electron accelerator if compared to standard linacs. Apart from the accelerator vault, a dedicated power supply, control and cooling rooms with active water cooling are required to operate the machine. A graphical representation of the IBA high energy rhodotron is given in Fig. 14.

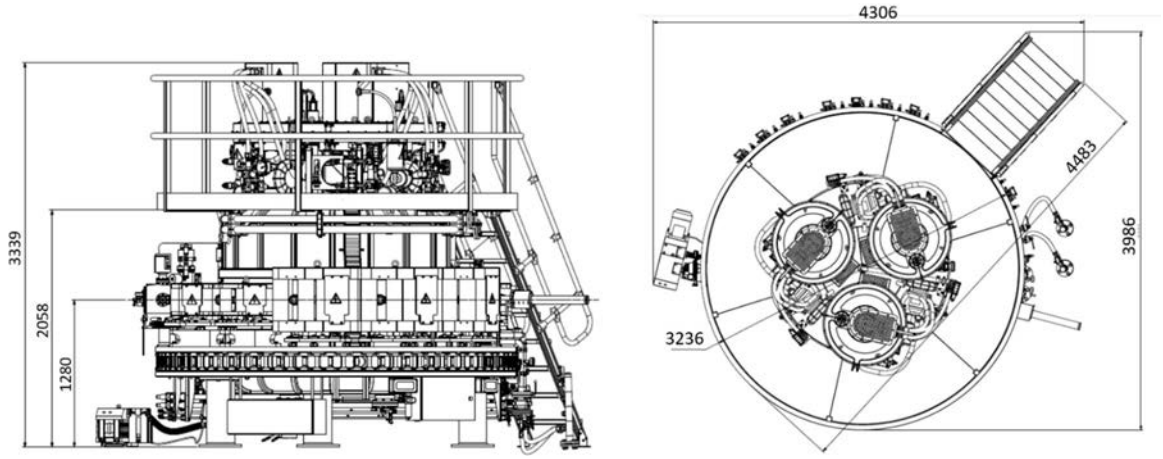

FIG. 14. Front and top view of the IBA high energy TT-300HE rhodotron. Dimensions are given in mm (courtesy of S. Heinitz, Belgian Nuclear Research Centre).

In March 2019, NorthStar Medical Radioisotopes, LLC announced the signing of a contract with IBA for delivery of eight rhodotrons to expand US production of non-uranium based ^{99}Mo. In May 2021 IBA announced that two TT-300 HE rhodotrons were installed at the NorthStar facility in Beloit, Wisconsin [186].

3.2. ACCELERATOR FACILITY DESIGN AND SAFETY

Currently there are no dedicated facilities for photonuclear isotope production existing in the world. This situation is changing as two commercial companies are planning to build facilities for isotope production in the near future, NorthStar Medical Technologies and Niowave. NorthStar Medical Technologies is building a dedicated facility in Beloit, Wisconsin, USA which is planned to start production of ^{99}Mo from enriched ^{100}Mo at the end of 2022. Niowave is building a facility in Lansing, Michigan, USA. The starting date for its commercial production of isotopes has not been announced yet.

There are several accelerator facilities that are used for photonuclear isotope R&D and the production of small quantities of radioisotopes. Some examples of such facilities include the Canadian Isotope Innovations linac located at the Canadian Light Source, Saskatoon, Saskatchewan, Canada; the Low Energy Accelerator Facility at Argonne National Laboratory,

Lemont, Illinois, USA; the Idaho Accelerator Center in Pocatello, Idaho, USA; Institute of Nuclear Physics of Lomonosov Moscow State University, Moscow, Russia; and Kharkiv Institute of Physics and Technology, Kharkiv, Ukraine and others. These facilities operate electron accelerators in the 20–50 MeV energy range suitable for photonuclear isotope production. However, these laboratories are not optimized for radioisotope production in terms of beam energy and power and axillary equipment.

3.2.1. Facility design considerations

The basic requirements for a new facility are given by the physical size of the accelerator and target assembly, the shielding requirements and the space for personnel to operate and maintain. The electron beam produces a very intense photon field from the bremsstrahlung process and a neutron field resulting from the photo neutron reactions. The neutron field is typically comparable to that produced by a high powered medical isotope cyclotron, while the photon field is much more intense. The IAEA provides a guidebook dedicated to the design and operation of a new accelerator facility including the shielding requirements [187]. Equations 17 and 18 from that document provide a 'rule of thumb' for the thick target bremsstrahlung yield at 0 and 90 degrees with respect to the electron beam. These are reproduced below as equations below:

The absorbed dose rate at 0 degrees $((\text{Gy/h})\ (\text{kW-m}^{-2})^{-1}) \sim 300\ E_0$.

The absorbed dose rate at 90 degrees $((\text{Gy/h})\ (\text{kW-m}^{-2})^{-1}) \sim 50$.

where E_0 is the energy of the electrons in MeV. The unit m^{-2} is included to suggest an inverse square dependence on distance from the target for this type of radiation. Note that at the approximation for the 90° was derived for energies higher than 100MeV. However, Mao,X et al [188] simulated bremsstrahlung spectra from thick targets at 90° for electron energies ranging from 50 MeV to 10 GeV and concluded the following:

(a) The incident electron energy does not affect the shape of the bremsstrahlung spectra significantly;
(b) The majority of the photons are low energy (less than 10 MeV);
(c) Among them 1.5–10 MeV photons are produced by the small angle bremsstrahlung from secondary electrons and, 1.5 MeV photons are produced by Crompton scattering: These results imply that the source term for bremsstrahlung at 90° is relatively independent of energy and hence the approximation of 50 Gy/h/kW can be considered. However, Monte Carlo radiation transport codes, such as MNCP or similar [189] should be used to estimate the absorbed dose rate, while designing the actual facility.
As an example, the absorbed dose rate for a 30 MeV electron beam is about:
D ~ 9000 Gy/h/kW at one metre and 0°;
D ~ 50 Gy/h/kW at 1 m and 90°.

Electron beam powers typically encountered for isotope production in existing facilities are between 20–40 kW. For a position of the accelerator at a distance of 5–10 m from the target, a reduction of the bremsstrahlung field between seven to ten orders of magnitude is required, depending on the location and occupancy requirements. The Tenth Value Layers (TVL) for bremsstrahlung produced by 30 MeV electrons is about 50 cm of ordinary concrete [190]. It would require in excess of 3 m of ordinary concrete at 90° and over 4 m at 0 degrees to attenuate the bremsstrahlung beam to levels that would permit occupancy outside the walls.

The use of local high density shielding around the isotope target can reduce those requirements significantly and also reduce the production of ozone and radioactive oxygen and nitrogen in the facility [187]. The TVL's for attenuation of bremsstrahlung from 30 MeV electrons for steel and lead are 11 and 5.7 cm [190]. A local shield around the target with at least six TVL's in the forward direction and four TVL's from 90° back to 180° will reduce the bremsstrahlung to levels such that the facility shielding will be mostly determined by the neutron fields and the thickness of concrete required would be comparable to the shielding requirements of a medium energy cyclotron facility. The local shielding will also reduce levels of residual radiation in the room to levels that enable entry to the facility soon after the beam is shut down.

A room temperature electron linac is about 3 m long and ½ m wide and would require around 1 m of free space on both sides and at the low energy end, in order to allow personnel passage and for maintenance requirements. The shielded isotope production target should be placed at least 2 to 4 meters from the linac to enable the use of some optical elements to produce an electron beam of the desired shape. The local target shielding will extend another 1.5 m beyond the target. This would produce an enclosure with an interior dimension of at least 3 m wide by 8–10 m long with a wall thickness of about 2 m. The shielded target assembly can be in the same enclosure with the linac or in a separate target room that would add additional length. If the target assembly is in the same room as the linac, it will be necessary to provide some local shielding around the end of the linac because of a few percent beam spill near the exit of the accelerator. In [191] a conceptual drawing is provided of a dedicated facility to produce ^{225}Ac with a room temperature electron linac. It proposes using a 90° bending magnet with a partial wall separating the high energy end of the linac and the bending magnet from the isotope target region.

An Argonne National Laboratory (ANL) technical report on a high power (250 kW) superconducting electron accelerator at 50 MeV for production of ^{99}Mo [181] concluded that the minimum floor space for such a facility would be about 120 m^2, somewhat smaller than required for an equivalent room temperature linac.

Safe operation of the facility is ensured by a design that conforms with the local regulatory framework of the sitting location. The shielding will be required to reduce the exterior radiation fields to levels consistent with those regulations. Part of the requirements will be a safety interlock system that, as a minimum requirement, shall ensure that the facility is searched before the shielded door is secured and that it is impossible to enter while the accelerator is in operation. Appropriate accelerator and beamline interlocks will also be incorporated into the safety interlock system. If water is used for target cooling, there will be radiolysis products produced in the water that may produce hydrogen and oxygen [187]. If local shielding is not used around the isotope target, then radioactive ^{15}O ($T_{1/2}$ =122 s) and ^{13}N ($T_{1/2}$ = 10 m) will be produced by air activation [187] and needs to be taken into account to respect release limits. Ozone will also be produced by the passage of either electrons or high intensity bremsstrahlung through air. The ozone needs to be managed or it will damage most cable insulations and any other polymer used inside the shielded facility.

3.2.2. NorthStar accelerator facility design (Practical example)

NorthStar Medical Technologies has designed and is now building an accelerator based facility for ^{99}Mo isotope production. The general layout of the facility is shown in Fig. 15. This design is optimized for ^{99}Mo production and incorporates all the important features of the production facility.

The Rhodotron accelerator designed by IBA is used as an electron beam source. The Rhodotron is an efficient recirculating accelerator, generating a low energy dispersion and a low emittance electron beam. The operating parameters for the accelerators are assumed to be 120 kW at 40 MeV. Choice of the accelerator is dictated by commercial availability, cost, and accelerator efficiency in beam production. 40 MeV energy was chosen for optimal production of the isotope while keeping production of the byproducts to a minimum. Because of the high cost of enriched ^{100}Mo, a high beam power is desired. The helium gas cooling system of the target is compatible with the beam power provided from both accelerators.

The design incorporates two accelerators for increased reliability; irradiations can be conducted using a single accelerator if one of the machines is not available. Additionally, irradiation of the same target with two beams allows doubling of the isotope production yield for the same target mass, which increases specific activity and reduces consumption of enriched ^{100}Mo. Local shielding surrounding the target is applied as discussed above, thus reducing the shielding requirements for other parts of the facility. Iron and high density concrete is used for local target shielding.

The facility utilizes a horizontal target retrieval system and irradiated targets are transported into an adjacent hot cell. It allows target manipulations without exposure of the personnel to high radiation fields. It also allows timely maintenance and replacement work on irradiated target holders and associated equipment. After target extraction, the irradiated ^{100}Mo is transferred to a chemical processing facility for dissolution and purification.

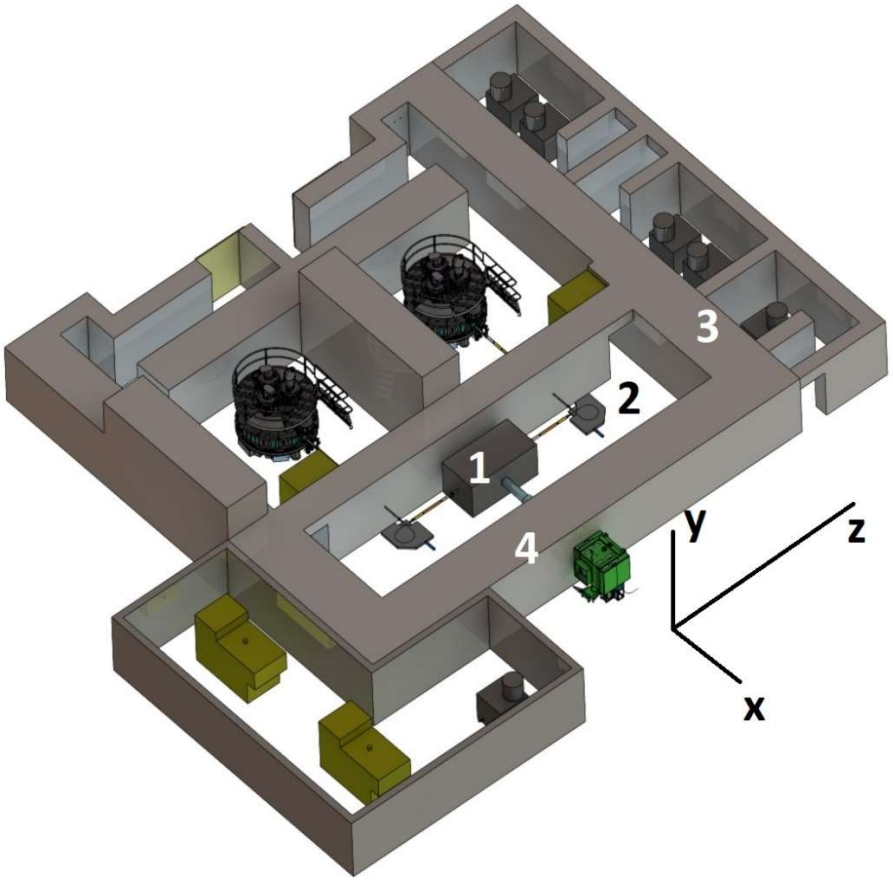

FIG. 15. Conceptual design of the NorthStar facility layout. 1 – local shielding, 2 – irradiation room, 3 – wall perpendicular to the beam's axis, 4 – the wall close to the "hot cell" (in green) (Courtesy of S. Chemerisov, Argonne National Laboratory).

3.3. TARGETS

The interaction of high energy photons with nuclei may induce a variety of photonuclear reactions including (γ, xn), (γ, xp) and (γ, f). Depending on the mass of the nucleus and the reaction type involved, the cross-sections for those reactions differ largely from 10–500 mbarn. [8]. The electron energy range of 15–40 MeV is typical for accelerators described in Section 3.1. Photons are created as bremsstrahlung radiation from electron stopping in a high Z material. Commercial radionuclide production requires beams of high intensity and several types of electron accelerators do exist to meet this demand. Compared to radioisotope production via cyclotrons, however, the photonuclear method has not yet found wider popularity. Radionuclide production via photonuclear reactions comes with the advantage of larger targets and lower thermal load per target volume if compared to proton induced methods. The photonuclear pathway also leads to fewer reaction products than from hadronic interactions with matter and may thus lead to higher radiopurity of the desired product. Depending on the impact of beam related costs, this radioisotope production method may be more competitive than other routes. Nevertheless, all aspects of the production need to be considered for an evaluation of its economic viability.

The technology for electron based or photonuclear production of several medical radioisotopes has been developed by public institutions, private companies or in collaborations between them mainly in the last 10 years. The highest technology readiness level is currently characterized by the ^{99}Mo production technology using photo neutron reactions on a ^{100}Mo target. NorthStar Medical Technologies developed the ^{99}Mo production in collaboration with ANL (Argonne National Laboratories), LANL (Los Alamos National Laboratories) and ORNL (Oak Ridge National Laboratory) [97, 192-194]. SHINE Technologies, LLC proposed ^{99}Mo production by photofission of low enriched uranium and developed the method in collaboration with ANL [72, 195, 196]. Similar technology for ^{99}Mo production was also implemented at Niowave Inc. [197-207].

The routine based production of ^{67}Cu through the photo proton reaction from ^{68}Zn [51, 198, 199, 208, 209] is already successfully performed at ANL and Canadian Light Source, Inc. Dedicated feasibility studies for ^{67}Cu photonuclear production using available linear accelerators were performed at the National Science Center, Kharkov Institute of Physics and Technology, Ukraine (KIPT) [73, 210] and the Society for Applied Microwave Electronics Engineering and Research (SAMEER), India [211].

The technology for ^{47}Sc production starting from ^{48}Ti targets is under development, however, several feasibly studies have already taken place [51, 53, 208]. The method for production of ^{57}Co calibration sources for gamma cameras was developed by KIPT [58].

Tests on ^{225}Ra production through high energy photon irradiation of old brachytherapy ^{226}Ra sources were performed by Melville et al. [161]. Maslov et al. [158] reported on ^{225}Ac production yields from irradiated planar ^{226}Ra targets averaging up to 550 Bq/μA/h/mg at 24 MeV. In 2019 Niovawe Inc. has reported about the technology for ^{225}Ac photonuclear production from a liquid ^{226}Ra target [201], simultaneously to ^{99}Mo photofission production in an already existing and licensed facility. Examples of other radionuclides that were experimentally produced via photonuclear reactions are given in Table 1 of Section 2.8.

The system for photonuclear radioisotope production contains the following functional components depicted in Fig. 16:

— Electron accelerator;

— Bremsstrahlung converter;
— Isotope target;
— Target station;
— Target transfer system.

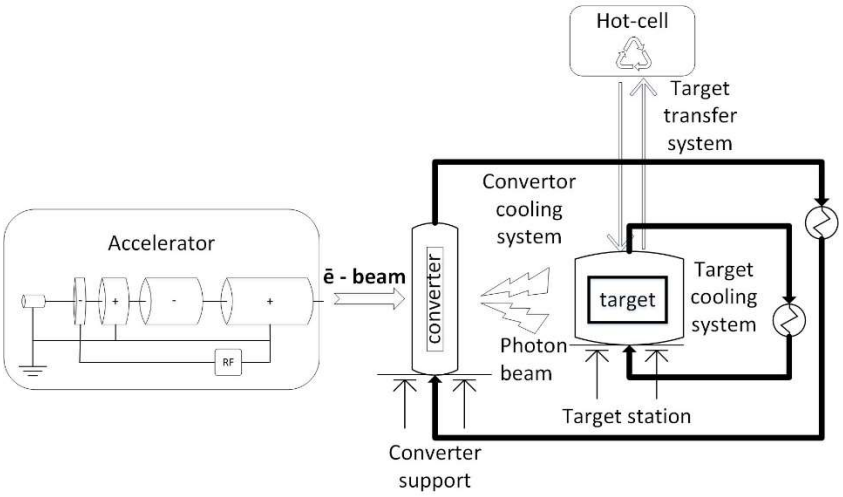

FIG. 16. Scheme for photonuclear radioisotope production (Courtesy of H. Skliarova, Belgian Nuclear Research Centre).

The accelerator provides an electron beam of the desired characteristics such as energy, intensity, profile etc. The bremsstrahlung converter (or radiator) is responsible for stopping the electron beam and thus creating a source of bremsstrahlung of high energy photons. A considerable portion of beam energy is deposited in the converter and one of the critical aspects of the system is an efficient cooling of this component. The target station is used to support the target containing the precursor material during the irradiation. It also guarantees an appropriate cooling of the target during irradiation and its loading and unloading from the irradiation position and provides an interface with an appropriate transfer system. The latter ensures safe transportation of irradiated target to a shielded hot cell for further processing. This transportation system could also be used for loading of new (or recovered) target material into the target station for new irradiations. The following review includes parts dedicated to the converter and the target with their respective cooling systems, as well as the target station with the target loading/unloading transport system.

3.3.1. Converter and Target Geometry Optimization

3.3.1.1. *One stage setup (without converter) vs two-stage setup (with converter)*

For given beam parameters that are usually determined by the electron accelerator, the yield of a medical radioisotope produced by a photonuclear reaction essentially depends on the design of the isotope target and the converter (if used). The typical design of a converter target generally includes several disks of a high Z material such as tantalum or tungsten. The coolant (usually water) flowing through the gaps between the disks removes the heat deposited in the converter. The very similar design is often used for the production target, with a series of disks made of the corresponding (mostly isotopically enriched) target material. The peculiarities of the converter and target design have great influence on the medical radioisotope yield. Thus, the design stage of the isotope production facility relies heavily on the detailed Monte Carlo calculations.

Selection of the appropriate material for the converter target is not straightforward. Studies on bremsstrahlung production [212, 213] showed that the yield in the forward direction is nearly independent of the Z value of the converter material, a fact that is initially counterintuitive. The high Z material produces higher yields of bremsstrahlung but also increases scattering out of the narrow cone in the forward direction that is used for isotope production and increases absorption of the high energy photons compared to a low Z material. The increased absorption of high Z material also leads to an optimum thickness of the converter targets. Sherman et al. [212] showed the bremsstrahlung yield increases in the forward direction of a tantalum converter with thickness until about 2.05 g/cm^2 and decreases with increasing converter thickness. During the design of the photonuclear radioisotope production facility, the converter thickness should be optimized for each considered material to maximize the electron gamma conversion efficiency [214]. Various efficiency criteria are presented in [215-217].

The above considerations show that the choice of directly irradiating the isotope target with electrons (one stage) or using a converter (two stage) essentially influences the production yield majorly depending on the heat deposition in the converter and target and thus on the performance of the cooling system.

Both setups were thoroughly studied for the case of photonuclear ^{99}Mo production. However, the calculated estimations of ^{99}Mo yield exhibit strong dependency on the details of the model being considered. For example, Chemerisov et al. [193] reported a two stage approach with a tantalum converter having a 6% higher yield than a similar setup without converter. At the same time this increase is achieved only for thin tantalum foils (0.2–0.3 mm) that could hardly be considered as a true bremsstrahlung converter because a substantial part of the incident electrons pass through and produce high energy photons directly in the target.

Studies with targets composed of multiple metal disks showed a clear advantage over the two stage setup. In the report [218] Chemerisov et al. showed results of irradiating a stack of 25 one mm thick by 12 mm diameter discs of either natural or 98% enriched ^{100}Mo targets with a 42 MeV beam of electrons for 6.5 days at 8 kW. The yield per target increased by more than a factor of three in the first four target discs before reaching the maximum yield for the next six disks. FIG. 17 shows results of FLUKA simulations [219] of ^{99}Mo production yields obtained in these studies [218]. The calculated yield estimations exhibit the same trend as experimental data, while absolute values are about 20% lower. From the calculations it also follows that substantial increase of molybdenum yield occurs in the first six molybdenum disks.

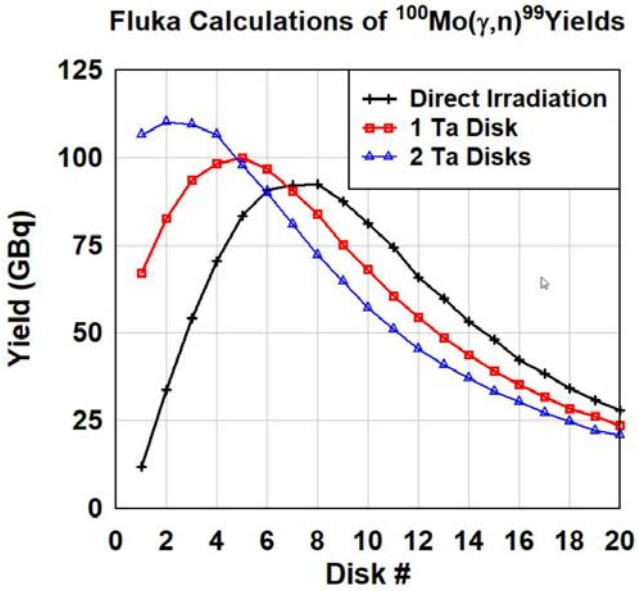

FIG. 17. FLUKA calculations of the yield of ^{99}Mo from direct irradiation of twenty ^{100}Mo disks and irradiation of the same stack with a one-mm and two one-mm disks of tantalum at the beginning of the stack (Courtesy of W. Diamond, Atomic Energy of Canada).

Table 2 shows the integral ^{99}Mo production yields in five disk increments. The one stage configuration with no converter (0 mm Ta) resulted in lower yields for the first five disks compared to the configuration with converter, whereas for disks deeper in the target the opposite is observed. As the thickness of the isotope target increases, the effect becomes less pronounced and for 20 disks the total integral yield differs by less than 10% for all configurations, in agreement with the Monte Carlo simulation results shown by Chemerisov et al. [193].

TABLE 2. CALCULATED YIELD OF ^{99}Mo FROM GROUPS OF FIVE DISKS SUMMED TOGETHER

	Yield [GBq]	**Yield (Σ yield) [GBq]**	**Yield (Σ yield) [GBq]**	**Yield (Σ yield) [GBq]**
Disk #	1-5	6-10	11-15	16-20
0 mm Ta	253.8	444.4 (698.2)	301.6 (999.8)	174.3 (1174.1)
1 mm Ta	441.8	414.8 (856.6)	246.4 (1103.0)	121.7 (1224.7)
2 mm Ta	530.2	365.2 (895.4)	207.9 (1103.3)	125.8 (1229.1)

The values given in brackets are yield summations from first to last disk given in the respective column.

Another possible way of increasing radioisotopes yield is the optimization of the target geometry. An example of such optimization procedure can be found in the paper [220]. The aim is a more efficient utilization of the target volume to achieve higher specific activities given the economic value and availability of the isotope target. Figure 18 depicts calculated spatial distributions of the ^{99}Mo yield in optimized targets for both, the one stage and two stage setups. It is shown that the optimized shape in fact provides an approximation of the target area with a high photonuclear reaction rate thus considerably increasing specific activity of the produced radioisotope.

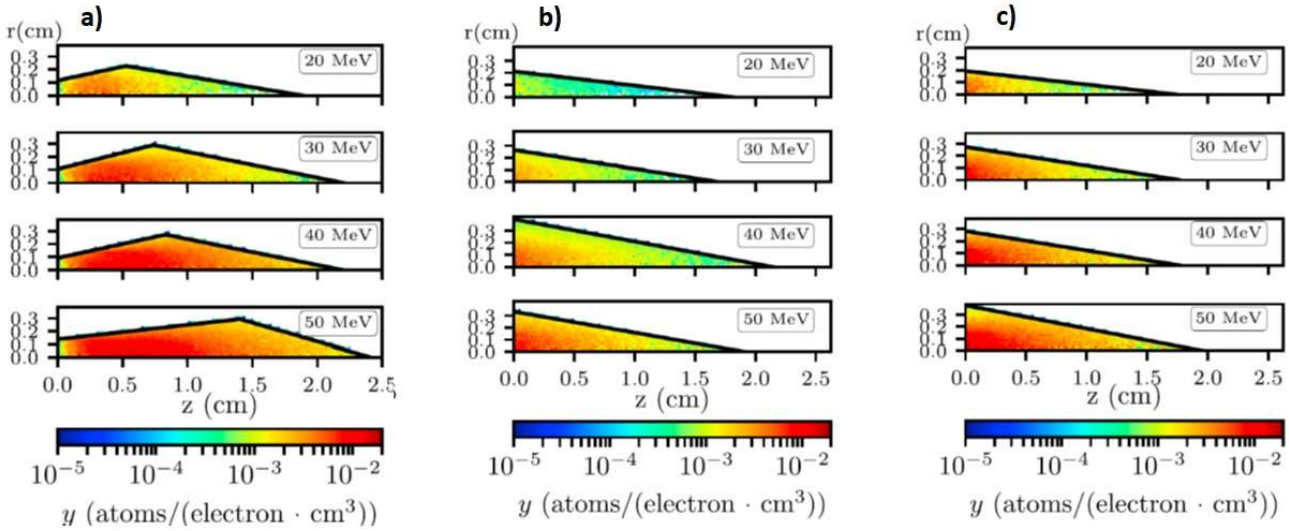

FIG. 18. Spatial distribution of ^{99}Mo specific yield for optimized targets: (a) one-stage setup; (b) two-stage thick W converter; (c) two-stage optimized thickness W converter (reproduced from Ref.[220], with permission courtesy of [Elsevier]).

3.3.1.2. Converter Target Distance

The use of a converter generally requires a more complex design of the target cooling system than required for direct irradiation of the isotope target. The converter can be mounted in a water cooled envelope that is separated from the target cooling envelope. De Jong et al. illustrates such a system in reference [221]. This design introduces a significant distance between the converter and the isotope target and reduces the yield by a large amount compared to direct irradiation [222]. Diamond et al. [191] have proposed a design that combines the tantalum converter in the same envelope as the radium isotope targets to reduce the spacing to a minimum. This should be possible for the production of ^{225}Ra that decays to ^{225}Ac with a half-life of 14.9 days. The decay period allows the intense radiation from the short half-life products such as ^{180}Ta and ^{178}Ta to decay before the target is processed. An alternate approach is to build a target chamber that includes a converter installed from below or from a side of the chamber while the isotope target is installed into the same target chamber from above. Both converter and target will be cooled with a common water circuit and the return can be through a third line from the chamber or co-axially within one of the lines as shown in Diamond et al. [191]. This can reduce the distance between the two targets without requiring the removal of the converter together with the isotope targets.

Jang et al. [223] have done a detailed study with Monte Carlo calculations and experimental verification of the optimal thickness of a tungsten converter target versus electron energy and the effects of spacing between the converter and isotope target. This work was done for a number of electron beam diameters from 0.1–15 mm FWHM. It is clearly a multidimensional problem and the authors have done the work of optimizing the converter thickness and target distance for a MoO_3 target of 10 mm diameter and 5 mm thickness. Figure 19 shows one interpretation of Jang's work. At a typical irradiation energy to produce ^{99}Mo of 35 MeV, there is a loss in yield of about 12% at a distance of 2 mm between the converter and isotope target in going from a very small diameter electron beam to 5 mm FWHM. Increasing the beam diameter to 7.5 mm produces a significantly larger loss of yield (about 30% compared to 2.5 mm diameter electron beam). Small beam diameters will lead to challenges of heat dissipation in the centre of the converter and isotope targets. Practical values will generally lay in the range from about 4–6 mm (FWHM) for facilities using between 10–40 kW of electron beam power.

In Fig. 19, the primary y-axis shows the yield of ^{99}Mo in the 10 mm diameter by 5 mm thick target at the 2 mm position as a function of beam width. The three curves of $Y_{x\text{-mm}}/Y_{2\text{-mm}}$, referenced to the secondary y axis, show the change in yield of ^{99}Mo at x mm from the converter target compared to the yield at a spacing of 2 mm, as a function of the beam diameter. At a distance of 5 mm, there is already a 20% loss in yield compared to 2 mm and by 10 15-mm the loss increases to about 40% (50%). These results will change significantly for an increase in the target diameter, but the mass of the target increases as the square of the radius and linear with thickness, an important consideration if a high value enriched isotope is used as target material.

These calculations show the value of the overall design of the target geometry. There also needs to be careful considerations of the thermal design of the various target components.

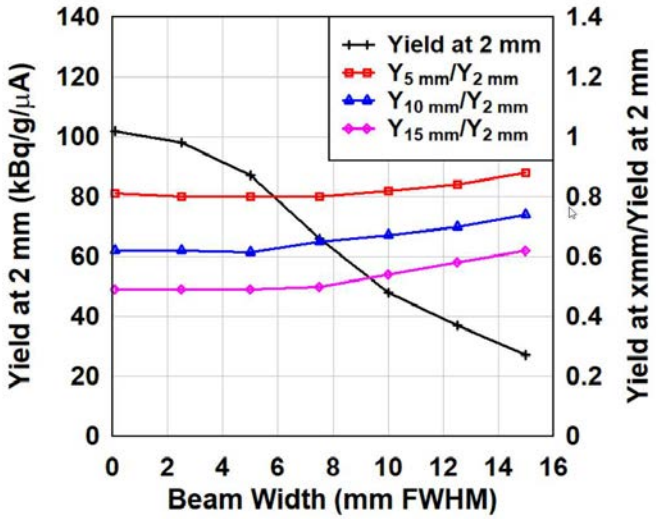

FIG. 19. Effects of beam diameter and converter to isotope target spacing (reproduced from Ref. [223]).

3.3.2. Converter Target Materials

3.3.2.1. *High-Z materials: Ta and W*

One of the main challenges of photonuclear technology is the conversion of a high intensity electron beam (>10 kW/cm^2) into a flux of mixed electron and gamma radiation, which is irradiating the target. High Z materials provide maximum efficiency of the conversion. The simplest and probably the most used converter configuration includes disc/plate or several parallel disks/plates of a high Z material, cooled by forced water flow. The most popular materials for this application are tungsten and tantalum. Some examples of such configurations are presented below.

Tantalum or tungsten [191, 223] water cooled disks can be used as an electron gamma converter at low and medium production power level. Tantalum was used for many years as a thick neutron production target for the ORELA (Oak Ridge Electron Linear Accelerator) linac [224]. Seven tantalum plates of increasing thicknesses from 1.5–7.5 mm and water cooled on both sides of each plate were used as the target. The beam energy was 150 MeV and the beam power was 50 kW with a full width at half maximum (FWHM) of about one cm. Both aluminium and beryllium were used as the housing material and served as the window separating the water cooling and the vacuum system. The combination of water cooled tungsten plates in an aluminium housing was used at the Rensselaer Polytechnic Institute (RPI) linac [225] at beam

powers up to 50 kW at 50 MeV. There were early reports of flaking of radioactive tungsten pieces during high power operation that were cleaned up with a water filtration system [225].

The amount of energy deposited in thin plates of a converter material is largely determined by the collision stopping power of the electrons in the material. For tantalum, this only changes by about 16% from 10 MeV (1.21 MeV/g/cm^2) to 100 MeV (1.43 MeV/g/cm^2) [226]. Most of the energy produced by the increasing radiative stopping power at higher electron energies leaves a thin target although some of the photons will be absorbed by the second and third converter foils if used as part of the converter. Diamond et al.[191] shows that the energy deposited in three one-mm thick tantalum plates, as calculated by FLUKA with a 20 kW electron beam of 25 MeV, is 2.12, 2.77 and 2.45 kW for plates 1 to 3, respectively.

The collision stopping power in tantalum at 25 MeV is 1.31 MeV/g/cm^2 [226]. The product of this and the thickness of the tantalum piece of 0.1 cm times the density of 16.6 g/cm^3 is 2.2 MeV, or nearly 9% of the 25 MeV total beam energy compared to the calculated energy loss of just over 10% of the electron beam power. As the beam energy increases, the amount of MeV deposited in the tantalum increases slowly while the energy of the electron beam increases at a faster rate. This enables higher beam powers to be used as the energy increases. If the power deposited in the pieces of tantalum are found to be limiting, then thinner pieces can be used at a small loss in yield because of the longer spacing. It should be possible to design a water cooled converter target with tantalum plates that covers most practical irradiation conditions in the range of 10 to 40 kW at energies from 25–50 MeV.

3.3.2.2. *Composite material*

The converters can be made not only of a single high Z material. The use of composite converters made of several layers of different materials can provide better thermal and mechanical performance. Gao and collaborators [215] have studied both a single high Z material and a composite of a high Z material (tungsten) and a low Z material (aluminium, copper, silver gold) converter for a 6 MeV 100 μA linac irradiation. To find the optimized thickness and material with biggest conversion efficiency, the authors have performed a Monte Carlo simulation for the irradiation process in order to maximize the photon dose while keeping the energy leakage rate lower than 0.05 %.

The Canadian particle accelerator centre, TRIUMF, experimentally studied several composite target configurations consisting of high Z materials, like gold or tantalum, deposited onto aluminium by electroplating or explosion bonding [227]. Tantalum on aluminium prepared by explosion bonding (100 μm, 1000 μm) has shown better resistance to 500 h irradiation with the power equivalent to 100 kW. Explosion bonded gold on aluminium (100 μm), or gold with thin nickel or nickel and zinc under layers prepared by selective brush plating (500 μm) and by electrodeposition (10 μm) on aluminium samples showed to change both morphology and composition under the beam irradiation already after 50 h, thus having an inferior performance.

3.3.2.3. *Liquid metal converter*

Niowave Inc. has reported to use of an eutectic mixture of lead and bismuth (LBE) for the gamma photon, gamma neutron converter for the photofission production of ^{99}Mo from LEU (in solid form) and simultaneous photonuclear production of ^{225}Ra from ^{226}Ra (liquid form) [195, 199, 226]. The geometry of the LBE converter developed by Niowave will be discussed in section 3.3.3.4.

3.3.3. Converter cooling geometries

3.3.3.1. *Water as a coolant*

Water cooling of materials irradiated by a high intensity beam of electrons produces substantial amounts of radiolysis products that are corrosive to many materials. Argonne reported that water cooled molybdenum targets dissolved some of the molybdenum material during irradiation. The heating of the discs due to the interaction with the beam should be estimated and controlled, since under elevated temperature an oxidation of the metal occurs and can cause target losses. Thus, in the experiment performed at ANL, when using a water cooled target it was observed that after irradiations the disks were black in appearance due to a thin layer of molybdenum oxide on the surface. The losses in weight for the samples were in the range of 0.3–0.7%, which could have been due to a partial dissolution of the target in the cooling water during irradiation [229]. Based on the negative experience with direct water cooling of Mo targets, ANL and LANL changed to pressurized helium cooling [97, 230].

Materials such as aluminium, beryllium and titanium have tenacious oxides that are resistant to the radiolysis products and are used for electron beam windows and target chambers. Tantalum is also resistant to radiolysis products and is a good choice for a conversion target.

Lillard et al. [231] studied the corrosion of downstream components in a loop irradiated with 800 MeV protons to determine the corrosion rates of typical materials that might be used in the construction of a proton spallation target. He found that the corrosion rates were highly dependent on the materials used in the loop, the cleanliness and the corrosion chemistry used to control the buildup of products such as hydrogen peroxide. Lillard et al. notes that the water radiolysis models for both fission reactors and accelerators predict that similar species are formed in both environments, so his measurements are likely relevant for an electron accelerator. The conclusions of this study were that the cooling loop should be made entirely with type 304 stainless steel, thoroughly cleaned before use with a periodic flush and refill with de-ionized water and treated with the addition of small amounts of hydrogen gas that reduces the buildup of hydrogen peroxide, referred to as hydrogen water chemistry control [231]. Aluminium alloys (AL6061 and AL5052), tantalum and alloy 718 had very low corrosion rates while tungsten was nearly 50 times higher than tantalum. Measurements made with a loop using copper components and no chemistry control demonstrated one to three orders of magnitude higher corrosion rates [231]. It may be concluded that a carefully constructed cooling loop with hydrogen water chemistry control is sufficient to reduce the degradation of molybdenum during irradiation, but this remains to be experimentally verified.

3.3.3.2. *Helium cooling*

Due to problems associated with radiolysis and corrosion in water based cooling systems, gas cooled accelerator systems using He offer a suitable alternative. Although technologically more challenging to realize, they come with the advantage of having much less complex coolant chemistry and significant less activation. A helium gas cooling for an electron accelerator target was developed by ANL and LANL [97, 191, 232-234]. It was successfully demonstrated that it is possible to dissipate up to 1 kW per 12 x 1 mm disk using such a system [97]. It operates in a closed loop design and was tested with up to 10 kW on target. Details on the He loop design are given in Section 3.3.6.1 below. The scale up to handle up to 120 kW beam power will still require further testing and optimizations.

3.3.3.3. Geometry with increased heat exchange surface

The ARIEL electron gamma converter of TRIUMF is designed for up to 100 kW of beam power corresponding to a heat flux of 6.0×10^6 W/m^2. To dissipate this heat, the low Z high thermal conductivity (Al) substrate is machined into a fin array.

Various fin geometries were investigated, but a simple vertical fin array was preferred due to higher manufacturability [235, 236]. The actual concept is a trench type converter. The converter prototype corresponding to an optimized geometry was 4 mm tall and had 1.2 mm thick fins, with 1.2 mm thick channels between them. A bench test corresponding to the described geometry for a converter prototype was performed using a tungsten inert gas welder. The measured temperatures were compared with ANSYS [237] simulations showing an average error of less than 10%.

Other ways to improve the thermal stability of the converter, target and beam window can be beam sweeping over the target and the target movement in respect to the beam. Another alternative is the rotation of the converter with respect to the target and beam as is proposed in a recent study [238].

3.3.3.4. *Liquid metal cooling*

The idea of liquid metal cooling of an accelerator target is not new. Having a higher density and considerably higher boiling points than water, heavy liquid metal cooling technology is applied in several research centres around the globe. It was extensively studied as an option for the high power target of the European Spallation Source ESS with Hg, Pb or LBE as cooling medium. Hg cooling is successfully applied for the rotating uranium target at the GELINA facility, Joint Research Centre Geel, for beam powers up to 10 kW [239, 240] and for ion linear accelerator targets for radioisotope production [241, 242]. However, for radioisotope production, liquid metal cooling of targets has not been really considered, due to the complexity of the system and issues of safety in routine operation.

Although designed and tested for a different purpose, the windowless target electron beam experimental irradiation (WEBEXPIR) represents a pioneering example of a liquid metal loop reliably operating under intense electron beams [243]. The tests were conducted with an industrial rhodotron TT-1000 that provided a 7 MeV electron beam with currents up to 10 mA. It was concluded that the LBE free surface flow was not disturbed by the interaction with the electron beam and that vacuum conditions stayed well within the design specifications.

Independently, Niowave Inc. designed an LBE converter cooling system, where the flow is generated by differences in the density of the coolant at different temperatures. The feasibility study of an LBE converter [198, 199] for low beam power was performed. The tubes are kept above the LBE melting temperature of 124°C using resistance heating tapes. The cooling performance of this converter was tested at Idaho Accelerator Center by irradiating a Zn target attached to the back of the converter. It was reported that the Zn target temperature did not exceed 150ºC even at 1 kW [198].

Additionally, a forced flow LBE converter was developed at Niowave Inc. to withstand higher beam powers. Due to limitations incurred by a conventional window based design, a windowless approach was considered for high power applications. This converter design used a ‘waterfall’ feature where the LBE is driven in a closed loop via an electromagnetic pump. The system is designed to be operational at electron beam powers of 100 kW at 40 MeV [206].

Liquid sodium is yet another coolant medium that is currently foreseen for target cooling within the SMART project undertaken at IRE, Belgium, for ^{99}Mo production using a high power superconducting electron linac provided by ASML, Netherlands.

It is important to note that the usage of liquid metals for cooling applications in nuclear installations comes with its own challenges. During operation, coolant chemistry control is crucial to keep corrosion at an acceptable level. Activation and suitable strategies for disposal need to be foreseen. Experience with liquid metal coolants in accelerator facilities is generally very limited despite their promising potential for high power applications.

3.3.4. Target material form

3.3.4.1. *Pressed and sintered discs*

Pressed and sintered discs of ^{100}Mo are used for ^{99}Mo photonuclear production at NorthStar Medical Technologies [244] and Canadian Light Source Inc. [221, 245]. The method for production of the molybdenum discs for NorthStar Inc. was developed by Oak Ridge National Laboratories (ORNL) [246] and validated with the support of ANL [247]. Originally, powder metallurgy fabrication of ^{100}Mo targets was used for the development of the ^{99}Mo production. The main advantages of powder metallurgy are small material losses and the production of dense, high quality parts using elemental molybdenum powder. One of the critical aspects was the development of a controlled production method, which is a combination of powder morphology, lubricants, pressing technique and sintering conditions. This enabled the production of target disks with controlled densities, minimal variations in dimensions and little or no distortion [248].

In addition to the standard pressing and sintering approach, additive manufacturing was also studied for the fabrication of complete target assemblies [249]. In order to guarantee the reproducibility, ORNL developed a method of preliminary treatment of Mo powders suitable for use by an AM250 Renishaw AM machine [250].

3.3.4.2. *Container based target and encapsulated solid material*

Metallic ^{68}Zn inside an alumina crucible is used at ANL for the production of ^{67}Cu. After irradiation, the zinc is sublimated in vacuum, and the copper and byproducts are then dissolved from the alumina crucible and chemically separated [72]. Canadian Light Source Inc. is using mechanically encapsulated targets of ^{68}ZnO for the production of ^{67}Cu.

Loosely packed or pressed titanium dioxide targets contained within two aluminium foil envelopes were used to study linear accelerator based ^{47}Sc production at ANL [53]. The ANL group has reported difficulties with the titanium dioxide sintering and their dissolution after irradiation [251].

During the feasibility study for the photonuclear production of ^{99}Mo at KIPT (Ukraine), Dikiy et al. [100] considered both, metallic Mo and MoO_3 as a precursor material. Two versions of truncated cone shaped target were made: one consisting of 30 g of elemental ^{nat}Mo and an aluminium capsule with external cooling fins, which contained two foils of Mo and 50 g of MoO_3. Both targets contained nearly the same amount of natural Mo. A thermocouple was placed inside each target to measure the temperature during irradiation. During 30 min of irradiation at the KUT-20 accelerator with an average current of 7 μA at 30 MeV, the steady state temperature at the centre of the MoO_3 target increased to 75ºC at a cooling water

temperature of 36ºC. The produced activity of ^{99}Mo was about 8.2 MBq for the metallic target and 5.9 MBq for the combined oxide and foil target.

The same group [73] reported on comparisons of metallic molybdenum to MoO_3 with regard to ^{99}Mo production efficiency for a constant cylindrical target volume. It was found that for the same irradiation parameters, the measured activity of ^{99}Mo was about ten times lower for the oxide target compared to Mo metal. During irradiation with the KUT-30 accelerator at an average current of 260 μA (9.2 kW beam power), a sintering of the MoO_3 powder was observed, which indicated inefficient cooling. Based on those results, oxide targets were considered of little use for photonuclear production of ^{99}Mo with regard to both the production yield and thermal performance of the target.

3.3.4.3. *Liquid form*

Niowave Inc. has reported [201] the use of a closed stainless steel container hosting an aqueous solution of $^{226}RaNO_3$ as the target for photonuclear production of ^{225}Ra simultaneous to the photo fission production of ^{99}Mo from LEU. It was declared that the commercial scale system of Niowave is designed to produce 370 GBq per week of ^{225}Ac from a nitrate based solution of ^{226}Ra. At the beginning of 2019, it was also reported that the demonstration scale production of 370 MBq batches of ^{225}Ac at Niowave had begun and should have been completed in April 2019.

3.3.5. Target mounting/dismounting system

During the initial stages of the photonuclear isotope production technology development, manual target mounting and dismounting methods were and are commonly applied. However, facilities aimed to produce commercially relevant activities will require the handling of targets at much higher degrees of activation. This will result in the necessity of remote handling techniques until the target assembly is inserted into a shielded flask. The target discs are typically held in an enclosure that enables high throughput of coolant, usually either water or helium [218]. The operational procedures after irradiation will depend upon the design of the target and the cooling system used. Some examples are described below.

Chemerisov et al. [234] reported using a mechanical lift driven by a linear screw drive to lower the target assembly from the irradiation site inside of a high density local shield to a location below the shield where the target assembly is transferred to a shielded flask on a cart for transport to a hot cell.

DeJong et al. [222] showed a photograph of the remote handling components to remove the irradiated discs to a location above the local shielding for transfer to a shielded flask. The shielded flask then is transported to a hot cell by a trolley.

3.3.6. Examples of linac based technologies for radioisotopes production

3.3.6.1. *^{99}Mo Production*

NorthStar Medical Technologies with the support of the National Nuclear Security Administration (NNSA) and US National Laboratories ANL, LANL and ORNL, are developing the accelerator based production of ^{99}Mo by using the photonuclear reaction ^{100}Mo(γ, n)^{99}Mo in an enriched ^{100}Mo target, using a high power electron accelerator to produce an intense flux of bremsstrahlung photons to efficiently drive the nuclear reaction. Because of the high cost of enriched ^{100}Mo targets, the material has to be recycled and losses during the recycling process

and size of the target have to be minimized to make the production process commercially viable. Minimization of the enriched material inventory leads to a desire to use targets as small as possible and to use the highest possible beam power. Those requirements make the cooling of the target challenging. Initial experiments at ANL were conducted by using a water cooling system where the water coolant was in direct contact with molybdenum targets [229]. While those experiments demonstrated photonuclear approach capabilities, some dissolution of molybdenum was observed. After this observation, LANL designed a helium cooling system that was built and tested at ANL Low Energy Accelerator Facility (LEAF) [247].

- *Design of the target*

The initial design on the target was optimized for available power and energy of the electron accelerator at Argonne. This design was based on 6 mm Full Width Half Maximum (FWHM) beam size and 100 g/s mass flow rate of the helium through the target. The target was designed to accommodate up to 20 kW of beam power on the target. Later, a production facility scale target was developed capable of handling up to 120 kW of beam power [252]. This target consists of 81, 0.5 mm thick 29 mm diameter disks. The scaled-up version of the helium cooling system was designed and tested at LANL [252]. For scaled down tests at Argonne, a shorter target was utilized because of the helium flow limitations of the installed gas cooling system.

The target holder contains the disks with flow channels between each disk. The holder is inserted into the target housing that provides the pressure boundary for the helium coolant. The beam window is integral with the housing and is shaped to minimize beam attenuation and still provide adequate containment of the pressurized helium. The helium flow is directed into the target holder from the roots blower located inside the pressure vessel and then returned to the pressure vessel.

- *Gaseous Helium Cooling System*

The helium cooling system diagram is shown in Fig. 20. The maximum mass flow rate achievable with this cooling system is 136 g/s at 20.7 bar pressure. The vessel maintains the static pressure in the system. A motor and blower are located inside the vessel and are used to circulate the helium through the closed system. An after cooler heat exchanger is located outside the vessel at the discharge of the blower. This heat exchanger removes the heat from compression and from the motor. An oil filter is located downstream of the after cooler and upstream of the target assembly to prevent particle blockage in the target coolant channels and protect the target from oil contamination in case of seal failure in the root's blower. There is a bypass around the target assembly for system recirculation when the target is not in place. A heat exchanger located in the return from the target removes the heat generated in the target from electron beam bombardment. The flow is returned to the vessel at the discharge from the heat exchanger.

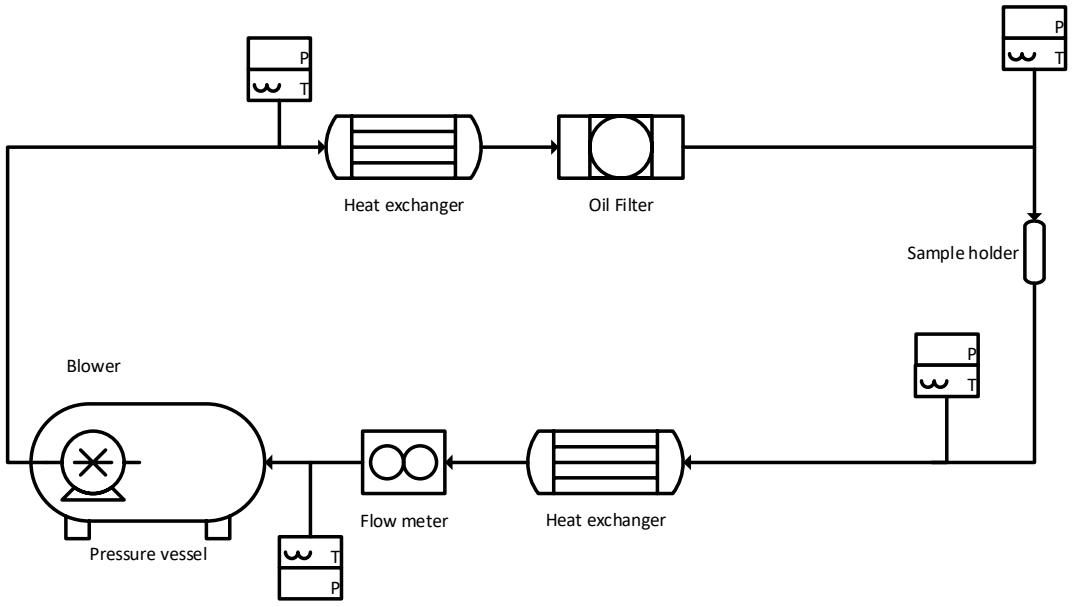

FIG. 20. Helium cooling system diagram (Courtesy of S. Chemerisov, Argonne National Laboratory).

3.3.6.2. ^{67}Cu Production

There have been a number of experimental studies of ^{67}Cu production using an electron accelerator [253-255] using natural zinc as a target material. Copper-67 ($T_{1/2}$ = 2.58 d) is formed via (γ, p) reactions on ^{68}Zn having a natural abundance of 18.5%. Table 3 shows all the competing reactions for a ^{nat}Zn target including the threshold energies for reactions with a significant cross-section. The main competing reaction for a photonuclear reaction on natural zinc is ^{64}Cu from the (γ, pn) reaction on ^{66}Zn. The (γ, pn) has a smaller cross-section compared to the (γ, p) reaction of interest and has a threshold energy that is 10 MeV higher so it can be avoided or minimized by choice of proper electron energy. If an isotopically enriched target is used, then there is a very low production of competing reactions, ^{68}Cu has a short half-life of 5.1 min and the other products are stable. The enriched isotope is available in large quantities because there is a demand for ZnO depleted in ^{64}Zn (natural abundance of 49.2%) as an anti-corrosion additive to water systems in some models of BWR reactors.

TABLE 3. POTENTIAL COMPETING PHOTONUCLEAR REACTIONS OCCURRING WITH ^{NAT}ZN

Reactions: **Threshold [MeV]:**	**(γ, n)** **10.2**	**(γ,2n)** **17.3**	**(γ, p)** **10.0**	**(γ, pn)** **19.1**	**(γ,α)** **5.3**
^{64}Zn(γ,x) (49.2%)	^{63}Zn	^{62}Zn	stable	short $T_{1/2}$	stable
^{66}Zn(γ,x) (27.7%)	^{65}Zn	stable	stable	^{64}Cu	stable
^{68}Zn(γ,x) (18.5%)	stable	stable	^{67}Cu	short $T_{1/2}$	stable
^{67}Zn(γ,x) (4.0%)	stable	^{65}Zn	short $T_{1/2}$	stable	^{63}Ni
^{70}Zn(γ,x) (0.6%)	stable	stable	short $T_{1/2}$	short $T_{1/2}$	^{66}Ni

From all generated radionuclides isotopic with the target material, ^{65}Zn constitutes a challenge in terms of gradual buildup of residual activity that cannot be separated chemically. Having a half-life of 244 d and a γ line at 1115 keV, it needs to be considered when handling target material recycled multiple times.

Copper-67 can be used for both diagnostic and therapeutic purposes (theranostic application). Johnsen et al. [255] shows the approximate requirements for each use and for therapeutic applications the range is from 1.6 to 15.6 GBq with an average of 3.9 GBq. This leads to the requirement to optimize the production of ^{67}Cu using large zinc targets enriched in ^{68}Zn at the maximum electron beam power that can be safely used in routine production and the subsequent efficient separation. Johnsen [255] also compared some of the advantages and disadvantages of both reactor produced and cyclotron produced ^{67}Cu that are equally relevant to production by the photonuclear route. A major advantage is that the enriched isotope ^{67}Zn required for the reactor (n, p) reaction was quoted (in 2015) as $17 000 per gram compared to $2 000 per gram for enriched ^{68}Zn and the reaction cross-section of about 10 mb for the fast neutron reaction is similar to the (γ, p) cross-section. The fast neutron flux in a nuclear reactor is typically about 3–10 times lower than the thermal flux, so fast neutron fluxes would be about the same as the relevant photon flux for a high-power irradiation leading, to specific activities that are about the same for a high flux reactor and lower for most research reactors.

Copper-67 is produced at Argonne National Laboratory via a photonuclear reaction at its Low Energy Accelerator Facility (LEAF). The team at Argonne has developed a patented process that provides approximately 37 GBq to customers per batch, with radionuclidic purity of >99% and a specific activity exceeding 1.85 TBq/mg (^{67}Cu/total Cu at end of irradiation). The National Isotope Development Centre is accepting orders for ^{67}Cu, and batches are produced on a monthly basis.

3.3.6.3. Scandium-47 Production

Scandium-47 is a promising β^- emitter for the preparation of radiolabelled antibodies due to its favourable average beta energy of 162 keV and convenient half-life of 3.35 days. It also decays with a 159.4 keV γ line which allows in vivo imaging with a SPECT scanner. Currently, its clinical application is inhibited by the lack of regular availability of sufficient quantities. It can be produced by several methods such as ^{48}Ti(p, 2p)^{47}Sc, with high energy protons with an energy above about 40 MeV and a low cross-section of 10–15 mb. It can also be produced by high energy neutrons via the ^{47}Ti(n, p)^{47}Sc reaction. This reaction requires a reactor such as the high flux reactor at Oak Ridge National Laboratories to produce reasonable quantities. Aliev et al. [256] provides a table of the cyclotron and reactor reactions used to produce ^{47}Sc, including references to the original research. That work also shows some of the contaminant reactions. Some of the preferred routes require costly enriched isotopes such as ^{46}Ca with a natural abundance of only 0.004%. Inagaki et al. [257] shows the typical requirements for a therapeutic treatment using ^{47}Sc to be from 5.5 to 7.4 GBq. This high activity per treatment leads to the requirement of the production of high activity per irradiation by any method used to produce it.

Despite cyclotron or reactor routes, ^{47}Sc can also be produced using the photonuclear reaction ^{47}Ti(γ, p)^{47}Sc with either a natural titanium or enriched ^{48}Ti target. There are a number of experimental investigations of the ^{48}Ti(γ, p)^{47}Sc reaction using both TiO_2 and metal titanium targets [255, 257, 258]. Titanium metal should be an excellent target material. It has been used as an electron beam window in contact with water on one side and vacuum on the other side. The radiolysis products in the water did not produce corrosion during long periods of use at high beam power. Metallic titanium targets of one to two mm thickness and water cooled on both sides, should be able to operate at electron beam powers of 20–30 kW at a beam profile of five to seven mm (FWHM), in close proximity to a water cooled converter target. This will require recycling the target material to a metal rather than an oxide, which may be more challenging. If it can be done, there is significant value during the irradiation process.

Natural titanium consists of five isotopes from ^{46}Ti to ^{50}Ti and the (γ, p) reaction on all but ^{46}Ti leads to a radioactive scandium isotope. Table 4 shows all the competing reactions for a ^{nat}Ti target including the threshold energies for reactions with a significant cross-section. The threshold energies for the ^{nat}Ti(γ, pn) reactions are near 23 MeV, significantly higher than for the ^{nat}Ti(γ, p) reactions. Attention needs to be paid to ^{44}Ti ($T_{1/2}$ = 58.9 y), as it will build up in recycled target material. Table 5 shows the four scandium isotopes produced by the ^{nat}Ti(γ, p) reaction with their basic decay properties.

TABLE 4. POTENTIAL COMPETING PHOTONUCLEAR REACTIONS OCCURRING WITH ^{NAT}TI

Reactions: **Threshold [MeV]:**	**(γ, n)** **11.6**	**(γ,2n)** **20.5**	**(γ, p)** **11.4**	**(γ, pn)** **23**	**(γ,α)** **9.4**
^{46}Ti(γ,x) (8.3%)	^{45}Ti	^{44}Ti	stable	$^{44g/m}$Sc	stable
^{47}Ti(γ,x) (7.4%)	stable	^{45}Ti	^{46}Sc	stable	stable
^{48}Ti(γ,x) (73.7%)	stable	stable	^{47}Sc	^{46}Sc	stable
^{49}Ti(γ,x) (5.4%)	stable	stable	^{48}Sc	^{47}Sc	^{45}Ca
^{50}Ti(γ,x) (5.2%)	stable	stable	^{49}Sc	^{48}Sc	stable

TABLE 5. NUCLEAR PROPERTIES OF SCANDIUM RADIOISOTOPES PRODUCED BY THE ^{NAT}TI(Γ, P) REACTION

0	**Half-life**	**Decay Mode**	**E_γ keV (%)**	**E_β keV (%)**
^{46}Sc	83.9 d	β^- (100)	889 (100) 1120 (100)	111 (100)
^{47}Sc	3.3 d	β^- (100)	159 (68)	142 (68) 203 (32)
^{48}Sc	43.7 h	β^- (100)	158 (10) 227 (90)	983 (100) 1037 (98) 1312 (100)
^{49}Sc	57.2 m	β^- (100)	1762 (0.05)	824 (100)

Section 3.3.7.2 showed that ^{67}Cu could be produced with high radiopurity using an enriched isotope target and electron energies from about 30–50 MeV. Small fractions of the other naturally occurring isotopes of zinc in the target will not produce significant deterioration of the radiopurity. It is significantly more challenging to produce ^{47}Sc with high radiopurity. The (γ, p) reaction cross-section is roughly equal for all four isotopes [259] and the interference of the other scandium isotopes is large. If an enriched ^{48}Ti target is used there is still the interference caused by the 83.6 d ^{46}Sc isotope produced by the ^{48}Ti(γ, pn)^{46}Sc reaction. Figure 21 shows the TENDL [259] cross-sections for the ^{48}Ti(γ, p)^{47}Sc and the ^{48}Ti(γ, pn)^{46}Sc reactions and the bremsstrahlung spectrum produced by a one-mA beam of 25 MeV electrons. The bremsstrahlung spectrum was calculated by FLUKA for a converter target of three one-mm discs of tantalum [219], each disc separated by one mm for water cooling. At 25 MeV there is very little overlap of the bremsstrahlung spectrum with the (γ, pn) cross-section and a significant overlap with the (γ, p) reaction.

FIG. 21 also shows a measurement of the experimental cross-section reported by Weise et al. [260] as a differential measurement at 90° and multiplied by 4π, assuming an isotropic angular distribution. This assumption seems adequate judging from previous experiments in this nuclear region [261]. The integrated cross-section, σ_{int} = 345 MeV-mb, essentially the same as the

integrated cross-section for the (γ, n) reaction that is given as σ_{int} = 398 MeV-mb by Belyshev et al. [262]. Belyshev et al. makes the argument that the cross-section should be closer to the value computed by the TALYS code that is about the same value as the TENDL results shown in Fig. 21. A value of σ_{int} = 109 MeV-mb is calculated by the TALYS code for the integrated cross-section, just over 30% of the experimental value. The experimental work and associated theory use isospin splitting to describe the observed high cross-sections of the (γ, p) reactions of titanium isotopes [263] and the TALYS code does not include that contribution according to Belyshev et al. [262].

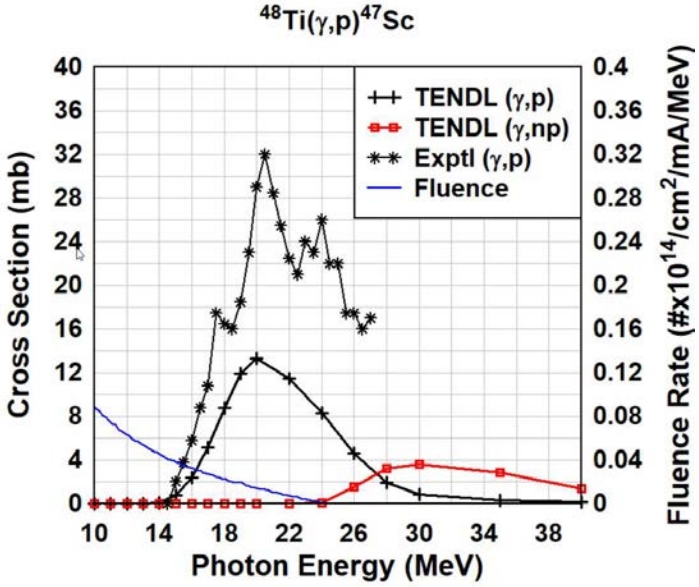

FIG. 21. The cross-section of ^{48}Ti(γ, p)^{47}Sc predicted by the TENDL [259] data base and experimental results by Weise [260]. The electron fluence for a 1 mA beam of 25 MeV electrons produced by a converter of three 1-mm sheets of tantalum is also shown.

There are greater challenges in development of the photonuclear production of ^{47}Sc at high yields than the development of ^{67}Cu. However, the higher cross-section and the favourable target characteristics of a metallic titanium target could enable the production of higher total activities even if required to use the low irradiation energy of 25 MeV. The photonuclear reaction appears to have several advantages over cyclotron produced reactions that are challenged by higher yields of ^{46}Sc [256, 258]. For details on experimental production of ^{67}Cu the reader is referred to [72, 256].

An advantage of producing ^{47}Sc from titanium is that it can relatively easily be chemically separated from the target material. Kolsky et al., [264] have already described the separation of either TiO_2 or titanium metal targets. Kolsky also described methods to recover the target material from either type of target. If an isotopically enriched ^{48}Ti target is used then there is tolerable residual activity in the titanium material from ^{46}Ti(γ,2n)^{44}Ti reactions, a recycling technology could be developed with reasonable effort.

3.3.6.4. Actinium-225 Production

Actinium-225 can be produced via the reaction ^{226}Ra(γ, n)^{225}Ra. The ^{225}Ra decays to ^{225}Ac with a half-life of 14.9 days. There is considerable clinical interest in the use of ^{225}Ac or one of its daughter products, ^{213}Bi, for targeted alpha therapies [265] but the supply is limited and the challenges of producing larger quantities with accelerators are substantial. Production with either a cyclotron via the ^{226}Ra(p, 2n)^{225}Ac reaction or an electron accelerator requires using a

radium target. ^{226}Ra is a highly radiotoxic element with an activity of 37 GBq/g (1 Ci/g) of alphas that are in secular equilibrium with four more alpha decays and one of the isotopes in the decay chain (^{222}Rn, $T_{1/2}$ = 3.825 d) is a noble gas. ^{222}Rn serves as gaseous carrier of the major dose contributing isotopes in the ^{226}Ra decay chain ultimately forming ^{210}Pb, which induces long lived contamination if ^{222}Rn is not contained. Even so, alpha decay induces helium formation that can build up sufficient pressure to damage a target envelope [266]. It has been suggested that the maximum mass that might be safely operated is one gram [267]. This leads to the requirement of hermetically sealed targets with optimized geometry to provide high yields of the reaction.

Radium is the heaviest alkaline metal from group 2 of the periodic table and is a highly reactive metal that also has poor physical, chemical and thermal properties for use as a target material. One gram of radium with a density of 5 g/cm^3 is only 0.2 cm^3 of target material. Diamond et al. [191] has proposed a conceptual design of a radium target and target chamber that should enable the use of the photonuclear reaction for producing reasonable yields of ^{225}Ac. The target shape has been optimized to use the maximum thickness still allowing acceptable heat removal, leading to a target disk size of 10 mm diameter and 2.56 mm thickness. Because of the poor thermal properties of radium and the intense radioactivity including an unshielded gamma field of about 9 mSv/h at one meter from a 37 GBq (one gram) source of ^{226}Ra, the source is further divided into two to four separate hermetically sealed targets to reduce the thermal load during irradiation and the activity per target at all stages of handling.

Figure 22. shows a concept of a radium target hermetically sealed with an aluminium shell. It uses two sections of high purity aluminium metal to encapsulate radium. The aluminium is ½-mm thick on both sides of the radium, sufficiently thick to withstand internal pressure from helium buildup with a high margin of safety. It is proposed to fuse the two aluminium sections using a cold weld under a rough vacuum so that the plates would collapse on to the target material when exposed to atmospheric pressure. High pressure cooling water would increase the contact pressure and aid in heat transfer to the cooling water.

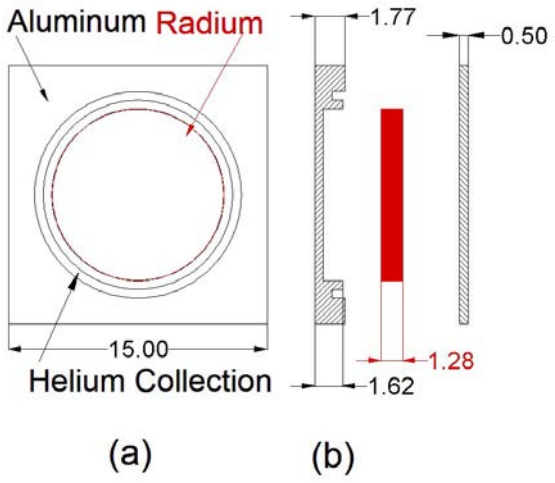

FIG. 22. Example of a high-powered radium target for electron irradiation with (a) top view of the target and (b) details of the three sections of the target assembly. Dimensions are in mm. (Reproduced from Ref. [191] with permission courtesy of [AIP Publishing]).

A converter target of three discs of 1 mm thick tantalum is about optimum to produce the bremsstrahlung photons used to produce the photonuclear reactions. The paper by Diamond et al. [191] describes target designs and a target holder to optimize the irradiation geometry for maximum yield. The FLUKA code [191] was used to assist in the design and to reproduce

experimental yield measurements of the production of $^{226}Ra(\gamma, n)^{225}Ra$ by Maslov et al. [158] to provide some confidence in theoretical cross-section data used in the FLUKA calculations.

There are a number of challenges associated with the development and production of suitable gram scale ^{226}Ra targets for commercial production of ^{225}Ac. Due to its radioactive nature, all operations will require a hot cell environment that greatly reduces the freedom of choice for methodologies usually employed in the manufacturing of stable targets. It also needs to be kept in mind that many physico-chemical properties of radium and its compounds are not well known due to obvious difficulties working with this element. For example, the melting temperature of radium metal accepted in literature today was only measured once by Marie Curie herself in 1910. Similarly, available water solubility data of common radium salts are almost 100 years old [268]. While these data may not be necessarily wrong, surprises will certainly appear since there is barely any experience working with gram amounts of radium and its compounds nowadays. The emanation of ^{222}Rn, the high dose from its daughters, alpha recoil and radiolysis makes ^{226}Ra one of the most difficult elements to work with. The rising interest in ^{225}Ac and the promising potential producing it via photonuclear transmutation might induce a renaissance of scientific research on radium and its compounds in future.

4. RADIOCHEMICAL SEPARATION

The radioisotope to be useful for its further applications, many times requires to be free from target material and other radionuclidic and chemical impurities. Minimizing the mass fraction of the target material relative to the desired radioisotope is especially necessary for formulation of radiopharmaceutical for patient use either for diagnostic or therapeutic purpose.

4.1. GENERAL CONSIDERATIONS

Radiochemical separation is the most common strategy to isolate produced radionuclides from bulk target material [269]. One of the main differences compared to cyclotron production of medical radionuclides verses photonuclear reactions is the possibility to efficiently use a large mass of the target material and higher electron beam powers. Typically for photonuclear reaction tens to hundreds of grams are used compared to cyclotron targets ranging from 100's of mg to several grams. This, however, may also require additional purification steps in order to achieve suitable product purity with regard to radiopharmaceutical applications.

In some cases, the desired isotope and the target material have very similar chemical behaviour. It is crucial to achieve a separation factor similar to the atomic ratio of the target material to that of the desired isotope. In other words, for multiple gram targets and produced product quantities in the nanogram range, separation factors of 10^8-10^{10} are typically required. Taking into account that the average separation factor per separation step is 10^3-10^5, several separation steps should be applied to satisfy this requirement.

Ideally, a suitable target for a specific photonuclear reaction needs to be monoisotopic to provide a product of highest isotopic purity. This often requires the usage of highly enriched targets (e.g., ^{100}Mo, ^{48}Ti, ^{68}Zn etc.). This requires a significant upfront investment to purchase the multiple gram target and demands for efficient target recovery strategies to make routine commercial production commercially viable. This needs to be accounted for in the chemistry design and the further operation of the generator (e.g., $^{99}Mo/^{99m}Tc$ generator produced via $^{100}Mo(\gamma, n)^{99}Mo$ reaction).

4.2. PHOTO NEUTRON PRODUCED ISOTOPES

In the case of (γ, xn) reactions, the final reaction product is isotopic with the target element making it practically impossible to chemically separate the product from the target material. In most cases, the specific activity will not be acceptable for radiopharmaceutical applications. The only potential application in radiopharmaceutical sciences is using the produced isotope as a parent isotope for the decay product or generator system (e.g., ^{100}Mo(γ, n)^{99}Mo→^{99m}Tc, ^{48}Ca(γ, n)^{47}Ca→^{47}Sc). In this case, the irradiated target with the parent radionuclide needs to be chemically isolated once or routinely from the decay product (daughter) before the daughter isotope can be used. The typical generator setup is to bind the parent isotope to a matrix and 'milk' the daughter isotope. This approach may not be applicable to photo production with the large mass of the parent isotope and target mixture as it would require a relatively large amount of solid phase (e.g., resin) or very selective systems with high K_d (distribution coefficient) values to retain this mixture for the time of generator operation. Alternatively, the inverse generator principle based on the opposite concept may be applied where the parent isotope stays in solution while the daughter product is retained on a solid support and subsequently eluted. Generators based on liquid–liquid extraction or precipitation may be applied as well.

4.3. PHOTO PROTON INDUCED ISOTOPES

In case of (γ, xp) reactions, the atomic number of the reaction product changes and thus can be chemically separated from the target material. In contrast to proton irradiation reactions of the form (p,xn), where the atomic number of the product is Z+1, radiochemical separation can be more challenging for photo proton reactions since higher Z target elements are preferably retained or extracted compared to lower Z product elements. Typically, several separation steps are applied as illustrated in Fig. 23. Similar separation concepts may apply to cyclotron produced isotopes as well.

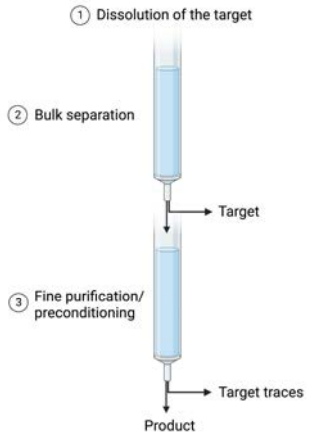

FIG. 23. Scheme of the radiochemical separation concept for (γ, p) produced radionuclides (Courtesy of G. Engudar V. Radchenko, TRIUMF).

4.3.1. Bulk separation

The first crude separation step aims to remove the bulk of the target material. Typically, this separation step provides mass reduction of the target material compared to the n.c.a product between 10^3–10^5. The preferable situation to minimize the use of resins and reagents is when the product is retained on the resin or extracted on a column while the target material shows no

affinity towards the stationary phase. However, in the case of photo proton reactions, this is more challenging to achieve as the target product with higher Z is preferentially retained. Separation is still possible but will require additional adsorbent mass and reagent volumes to achieve the required separation factors. Alternatively, precipitation, distillation/sublimation or liquid–liquid extraction can be applied during a first bulk separation step. However, this may result in problems with reproducibility and automation of the process. Another important factor is the product recovery and, preferably, direct product transfer from the crude separation to fine purification is preferred to minimize time and product losses. At the end of the bulk separation stage, the mass ratio of target to product material will still be in the order of 10^4–10^6.

4.3.2. Fine purification and preconditioning

The fine purification step is aiming to provide additional reduction of target mass in order to be suitable for radiopharmaceutical applications. Fine purification can be also combined with preconditioning of the final sample for radiolabelling and synthesis of radiopharmaceuticals. Final purification based on ion exchange or solid phase extraction chromatography is most efficient and suitable due to the possibility to achieve the highest separation factors and minimizing losses compared with other separation methods (e.g., precipitation, liquid–liquid extraction etc.). In the case of fine purification, there is usually no preference between sorption of target or product, because the difference in mass is not as significant as during the bulk separation step. However, sorption of the product may help to combine fine purification with pre-conditioning. Additional pre-conditioning steps may be applied to transfer the final product into a solution compatible (in terms of acidity, buffer etc.) with pharmaceutical synthesis (e.g., peptides, antibodies etc.). Column based separation procedures are preferred for compatibility with automation since it enables the use of a cartridge-based disposable setups required in radiopharmaceutical synthesis and clinical standards.

The radiochemical concepts and strategies given above can be used as a general guidance. Nevertheless, production of medical radionuclides via photonuclear reactions and their purification strategies are all unique in their own way and cannot be summarized with just one general approach. For example, material availability and handling peculiarities make it challenging to work with ^{226}Ra resulting in significant impact on target design. The cost of enriched ^{48}Ti of hundreds of grams can be unacceptably high. Yet, acceptable radionuclidic purity of ^{47}Sc can be achieved in the production via (γ, n) reactions on ^{nat}Ca. Therefore, each specific case in the production of medical radionuclides via photonuclear reactions needs to be treated individually and all details need to be considered.

To realize the full potential of photonuclear isotope production and to utilize most of the generated photons on the target, taking into account the challenges with obtaining large quantities of enriched isotopes, the possibility of irradiating multiple target stacks to maximize production efficiency becomes an attractive option to pursue in future.

4.4. SPECIFIC EXAMPLES

Most of the medical radioisotopes produced by the photonuclear process will be via the (γ, n) reaction followed by either β^- or positron decay to an isotope of a different Z value or via (γ, p) reactions. These will have many of the features of reactor produced isotopes that use the (n, p) reaction to produce a product of a different Z value than the target. The (n, p) reactions have a low cross-section, comparable to or lower than the (γ, p) reactions and the flux of high energy neutrons will generally be similar to the flux of bremsstrahlung photons so the irradiated product will have similar characteristics. Reference [270] is an IAEA TECDOC on reactor produced radioisotopes that includes both irradiation conditions and the radiochemistry used to

separate the product. Nearly 70% of the radioisotopes listed in Table 1 in Section 2 of this publication that have a different final Z value than the target nucleus, have also been produced via reactor based reactions, including ^{47}Sc and ^{67}Cu. Reference [270] contains one or several processing procedures for each of the isotopes listed. That document and the included references could be a useful starting point to help to establish separation procedures for many of the listed radioisotopes in Table 1. There have also been significant efforts to establish procedures for three of the radioisotopes featured in this publication.

The four isotopes featured in this document are at differing stages of development. ^{99}Mo has a well developed marketing and distribution scheme based on a fission produced, high specific activity product. The ^{99}Mo/^{99m}Tc generators in use are compact and convenient. New sources of ^{99}Mo produced by the photonuclear reaction need to include as much convenience as possible in the shipping and separation technology to gain acceptance in that market. Both ^{47}Sc and ^{67}Cu are isotopes with significant therapeutic potential with only limited supply. Cyclotron production utilizes the (p, 2p) reaction with low cross sections (10–20 mb) on the same target material as used for photonuclear production [270] and requires proton energies of 40–70 MeV what is above most medical cyclotrons can deliver. Photonuclear technology can increase the supply of ^{47}Sc and ^{67}Cu with high radioisotopic purity and become an independent supply pillar. ^{225}Ac has been available in limited quantity from several ^{229}Th sources but this route is not able to provide an ^{225}Ac supply required for clinical trials. Most other methods to produce larger quantities require the use of radium as a target or high energy (≥ 100 MeV) proton accelerators. Photonuclear production could become one of the preferred routes [191] since it may deliver ^{225}Ac of high radiopurity due to indirect formation from ^{225}Ra having a half-life of 14.9 days. The long half-life enables transportation of the irradiated target to a central processing location where ^{225}Ac is distributed to the users after repeated milking operations.

4.4.1. Separation of ^{99m}Tc from ^{99}Mo

Photonuclear production of ^{99}Mo is the most advanced technology for the potential production of relevant quantities of radioisotopes with electron accelerators. Section 3 provides an overview of facility design, target technology and important developments related to target handling and transport. The irradiated product is Low Specific Activity (LSA) ^{99}Mo of 50–300 GBq/g, while it is approximately 40 TBq/g for High Specific Activity (HSA) ^{99}Mo obtained from fission. LSA ^{99}Mo produced by neutron irradiation of ^{98}Mo was used for a number of years before the fission based supply became available. This required different separation techniques compared to generators that are in use nowadays. After several periods of significant shortages of the standard generator kits in the period from 2007 until 2010, interest was revived in these separation technologies. Dash [272] examined the various options in a detailed report with many references. Some of the important properties of a generator for LSA ^{99}Mo noted by Dash were:

- The physical or chemical techniques used should have high throughput capabilities;
- The separation process should be rapid to reduce the decay losses of ^{99m}Tc;
- The yield of ^{99m}Tc should be high;
- Human intervention should be minimal;
- Radioactive concentration of the ^{99m}Tc should be adequate to use with current kits;
- ^{99m}Tc should be obtained in a ready to use form, preferably in 0.9% NaCl and compatible with the existing freeze dried kits.

Table 1 in Dash [272] listed nine separate methods to separate ^{99m}Tc from ^{99}Mo, including physical routes such as sublimation, chemical routes such as solvent extraction using methyl ethyl ketone (MEK) and various column chromatography methods. Some of the processes are

not easily automated while a few have already been automated for routine use. Column chromatography using Al_2O_3 applied for HSA separation of ^{99m}Tc from ^{99}Mo is not practical for LSA material because of the low capacity to absorb molybdenum. A technique where ^{99m}Tc is adsorbed on the column and the molybdenum is rinsed from it has been developed as one of the more successful approaches. Dash [5] refers to this as the multicolumn selectivity inversion generator in which ^{99}Mo is stored in solution and passed through a chromatographic column (primary separation column, PSC) specific for ^{99m}Tc wherein ^{99m}Tc is selectively retained, stripped, and passed through a second guard column that retains any ^{99}Mo or other ^{99m}Tc interfering ions. ^{99m}Tc is then recovered in a small volume of eluate (0.9% NaCl) solution. NorthStar has developed this into an automated separation system called the RadioGenix™ technetium generator [273]. The process uses an ABEC (aqueous biphasic extraction chromatography) column for the primary separation and has been approved for nuclear pharmacy use by the U.S. Food and Drug Administration.

Jang et al. presented a similar approach using an activated carbon column to capture ^{99m}Tc [274]. They have developed a system called the Technetium Master Milker, TcMM, as an automated system based on this column. Wojdowska et al. [275] has reported on experiments with three different column materials that could be used to produce an automated separation device based on this approach.

The other method for which automated extraction modules have been developed is solvent extraction based on MEK. Martini et al. [276, 277] described the work to produce an automated module to separate ^{99m}Tc from ^{100}Mo after proton irradiation. This technology is equally applicable to photonuclear produced ^{99}Mo. Mang'era et al. described an automated MEK unit for extraction of ^{99m}Tc from LSA ^{99}Mo produced by photon irradiation of ^{100}Mo [278].

There are a number of methods to separate LSA ^{99}Mo from ^{99m}Tc and some have already been developed into automated processes. The basic features of the transfer of the irradiated product will be different. Fission based ^{99}Mo is transferred and stored on the shielded chromatographic column while it is possible that the LSA ^{99}Mo will be distributed in liquid form within an inverse generator.

4.4.2. Separation of ^{47}Sc

^{47}Sc is a β^- emitter with a half-life of 3.35 days which can be used for targeted radionuclide therapy. There is currently no clinical study ongoing, but it represents very high potential for the theranostic concept with its imaging analogue: ^{44}Sc ($T_{1/2}$ = 3.97 h) and ^{43}Sc ($T_{1/2}$ = 3.89 hours) for Positron Emission Tomography (PET). Yagi et al. presented experimental measurements of ^{47}Sc production yields from enriched $^{48}TiO_2$ targets including methods to separate ^{47}Sc from the titanium target [279].

The production of ^{47}Sc using photons represents one of the most efficient ways to produce this valuable radionuclide for therapy. For Ca as target material, there are two viable pathways that can be pursued to produce ^{47}Sc; either by using photons via ^{48}Ca(γ, n)^{47}Ca(β^-)^{47}Sc or using neutrons via ^{46}Ca(n, γ)^{47}Ca(β^-)^{47}Sc. In either case, a separation of ^{47}Sc after ingrowth from the decay of ^{47}Ca is required. In both cases a highly enriched Ca target is required, favouring the use of ^{48}Ca due to its higher natural abundance (^{48}Ca - 0.187% versus ^{46}Ca - 0.004%). It is needless to say that target recovery has to be performed to the best possible extent for further production cycles. Radiochemical Ca/Sc separations were reported by several groups [280-282] for processing proton irradiated Ca targets in ^{44}Sc production runs. The proposed separation strategies are based on solid phase extraction using DGA or UTEVA resins with additional cation exchange purification and precondition. A similar separation principle based on a tandem

of DGA and cation exchange columns for ^{47}Sc extraction from neutron irradiated ^{46}Ca was reported by Domnanich et al. [283]

Yet another production pathway is ^{48}Ti(γ, p)^{47}Sc. In this case, n.c.a. ^{47}Sc is produced directly from ^{48}Ti (natural abundance 73.72%) via the (γ, p) reaction. Several publications on purification techniques for fast neutron irradiated targets utilized separation concepts similar to the ones described above. Works of Kolsky et al., Bartos et al. and Loveless S. et al. [54, 264, 284] applied a combination of cation and anion exchange columns separating ^{47}Sc produced by (n,p) reactions on titanium. Kolsky [262] showed that ^{47}Sc separation from a metallic titanium target was less challenging than that from TiO_2. As noted in Section 3.3.6.3, metallic titanium would be the preferred choice as target for photonuclear production of ^{47}Sc since it withstands radiolytic cooling water attack during irradiation and has much better thermal performance compared to TiO_2 imperative at high power levels.

4.4.3. Separation of ^{67}Cu

Scientific literature has shown that ^{67}Cu can be separated from a zinc target by chemical [285] and thermal techniques [72]. As already described in Section 3.3.6.2, ANL performs ^{67}Cu extraction using sublimation of the metallic ^{68}Zn target. This strategy comes with the advantage of removing the majority of the target material without changing its chemical state, significantly simplifying target recycling. The second separation step involves chemical dissolution of the sublimation residue containing ^{67}Cu. While sublimation is an efficient way to perform the required task, there have been several other methods reported on the extraction of ^{67}Cu from a zinc target including procedures to recover the target material [75, 255, 286]. Most of these were developed for ^{67}Cu separations from fast neutron irradiated ^{67}Zn and the separation procedures remain identical.

4.4.4. Separation of ^{225}Ac

Previously reported publications describing the separation of ^{225}Ac from ^{226}Ra were based on the (p, 2n) reaction in a cyclotron. The advantage of photonuclear production over the one using protons is that ^{225}Ac is not produced directly, requiring multiple separations at different time intervals after ^{225}Ac accumulation from ^{225}Ra decay. This approach greatly improves the ^{225}Ac radioisotopic purity especially with regard to the content of ^{227}Ac. The radiochemical separation is based on cation exchange [160] or a combination of solid phase extractants using Ln/DGA and Sr resins as reported in [287]. It is necessary to note that most recent reports describe ^{225}Ac purification from relatively small masses of radium (μg to mg amounts) and for larger targets in the gram scale similar separation conditions may not be applicable in terms of columns capacities and process design.

4.4.5. Multiples recycle and buildup problems

The recycling of enriched target material after irradiation strongly depends on economic aspects of the radioisotope production cycle. While not common in practice, the recovery of enriched material might become increasingly important in the future considering the amount of material in use and its commercial value. This is an important consideration for photonuclear targets because they will typically be significantly larger than cyclotron targets. It is recommended to evaluate possible recovery strategies early for the enriched element in use and to develop a sustainable target material cycle from one production run to the next. Several aspects of that cycle have to be considered:

— Isotopic dilution and ingress of impurities from chemical processing;

During chemical or physical post-irradiation treatment the target material will come into contact with various chemicals and solid material that might possibly reduce the isotopic purity of the target material. High purity reagents and thoroughly cleaned surfaces of vessels in contact with the target material are to be used to minimize the effect. As an example, activities with ^{100}Mo require the use of Mo free steels to avoid possible isotopic dilution of the target material by natural molybdenum. Operations with enriched ^{68}Zn would, for example, require the use of powder free gloves, non-galvanized metals etc.

— Activation of target material by long lived isotopes of the same element;

Photon irradiation is inducing (γ, n) reactions on all isotopes present in the target material. Even with the highest enrichment grade, activation of the starting material by a long lived isotope of the same element is sometimes unavoidable. This fact invokes that the target material has to be treated as a radioactive substance after irradiation even if the separation from all other radio-elements is quantitative. Photonuclear production of ^{65}Zn ($T_{1/2}$ = 244 d) from (γ, n) reactions on residual ^{66}Zn will become a concern in the continuous production of ^{67}Cu from recycled enriched ^{68}Zn. Decay storage is an optional choice in some cases to circumvent that problem, but it will ultimately depend on the envisioned irradiation periodicity and half-life of the involved isotope.

— Material burnup due to nuclear transformation during irradiation;

Opposite to irradiation by thermal neutrons, photon irradiation induced (γ, n) and (γ, p) reactions on isotopes of the target element will shift the isotopic composition towards lower neutron numbers and result in target element depletion. Although only relevant for prolonged high power irradiations, this effect will require the addition of fresh material in order to compensate for burnup losses.

The above mentioned considerations do not take into account losses during material recovery and the incomplete separation from other radio-contaminants. Impurities that have similar chemical behaviour as the target element require special attention. For example, any W impurity in a ^{100}Mo target will result in the formation of radioactive Re, W and Ta isotopes upon irradiation. Measures as suggested above need to be undertaken in order to avoid interference from these impurities.

In summary, it is favourable to keep the target material as chemically and isotopically clean as possible. ICP-MS and/or ICP-AES analysis of the recovered enriched target material is strongly recommended for checks on isotopic composition, eventual metal impurities and quality control.

5. CONCLUSION

The photonuclear reaction method is becoming an emerging technology in the field of medical radioisotope production. This publication provides a general overview of the technology with greater details on four specific radioisotopes, ^{99}Mo, ^{47}Sc, ^{67}Cu, and ^{225}Ac. ^{99}Mo production has been under development for almost two decades and valuable operational experience was gained including production yields and target behaviour. NorthStar is building a new production facility that will eventually have eight high power electron accelerators for large scale production of ^{99}Mo. However, the technology can be used for a smaller scale market. A facility with a single 40 MeV electron accelerator capable of at least 40 kW can be used to produce in the order of 1500–2500 GBq ^{99}Mo from 12 grams of an enriched isotope target and 5 days irradiation at 25 kW. Processing and shipping time can be reduced to one to two days, reducing the decay losses between EOB and use. This is a clear advantage compared to fission based ^{99}Mo that typically requires six or more processing days. It is likely that a simplified water cooled system can be developed using hermetically encapsulated targets to avoid the technologically challenging development of a gas cooled system, such as being used by NorthStar.

^{67}Cu production is nearing both the quantity and radiopurity levels required to expand the use to larger clinical trials of the product. The radiopurity of the product appears to be as good as or better than other production modes. Typical treatments require from 4–10 GBq and production of up to 74 GBq per few days' irradiation is reported in Section 3.3.6. If the clinical trials prove the value of this isotope, then it may become necessary to build regional facilities dedicated to the production of ^{67}Cu and develop techniques to produce higher yields per irradiation.

It would be valuable if some research linacs could perform careful measurement of the (γ, p) cross-sections for ^{68}Zn and ^{48}Ti and of the (γ, n) cross-section for ^{226}Ra. This would assist development of economic models for the production of three important medical radioisotopes, ^{67}Cu, ^{47}Sc and ^{225}Ac.

^{47}Sc has also been identified as a good candidate for therapeutic use. There is the potential to produce significantly higher product yields per irradiation in the ^{48}Ti(γ, pn)^{46}Sc reaction than that can be produced for the ^{68}Zn(γ, p)^{67}Cu reaction, because its photonuclear cross-section is about twice that for ^{67}Cu production. Additionally, titanium metal targets can potentially be used at high electron beam power with direct water cooling. The competition from the ^{48}Ti(γ, pn)^{46}Sc reaction needs further investigation to identify the preferred irradiation energy that offers the best compromise between ^{47}Sc yield and interference from ^{46}Sc.

Photonuclear production of ^{225}Ra, decaying to ^{225}Ac, appears to be a preferred approach for the production of 10's to 100's of GBq of ^{225}Ac on a weekly basis. This is the least developed of the technologies that have been covered in this document, but the strong interest in ^{225}Ac for TAT should lead to increased R&D in this technology. The handling of GBq levels of a radium target is challenging and will likely require support from national laboratories having the required licensing, Highly Qualified Personnel (HQP), and supporting facilities such as specialized hot cells, that may not be available at most other settings. However, the long half-life of ^{225}Ra (14.9 d), decaying to ^{225}Ac (10 d) renders it possible to have the irradiation done at an accelerator facility and the irradiated target shipped to a laboratory with the required expertise. The long half-life of ^{225}Ac enables shipping of the product to many locations from a single processor. The per patient requirements for TAT's are much lower than the requirement for β^- emitting therapeutics, so 10's to 100's of GBq per week can service a large number of

patients and a single dedicated facility of about 20 kW and using 1 gr of target material should satisfy numerous clinical trials and early stage adaption in larger scale use.

Table 1 showed numerous other reactions that can lead to n.c.a. medical radioisotopes. Presently, little development of any of these is ongoing, but there are several that could be of significant interest. ^{68}Ga with a half-life of 68 min, decays by β^+ (89%) and is suitable for PET imaging. There are several methods of producing ^{68}Ga, including a generator that starts with ^{68}Ge with a half-life of 271 days. ^{68}Ge can be produced using the (γ, 2n) reaction on either an enriched isotope target of ^{70}Ge (isotopic abundance of 20.8%) or using natural germanium. All of the other products using a natural Ge target have much shorter half-life, except ^{71}Ge with a half-life of 11.4 d. It decays via electron capture with no gamma emission to a stable product and would be removed during the separation of the ^{68}Ga. A large (50–100 g) natural germanium target could be installed immediately downstream of the primary isotope production target, using its own cooling system. It would be irradiated by the substantial flux of bremsstrahlung that passes through the primary target and could be left in place for many months of irradiating the primary target (could be, e.g., either ^{68}Zn or ^{48}Ti). Such an arrangement should produce around 20–50 GBq of ^{68}Ge that could be used as a ^{68}Ga generator for many months after irradiation. Direct irradiation of a smaller but isotopically enriched target could produce significantly higher yields in a shorter time. Both options are worth pursuing.

^{123}I and ^{125}I produced by (γ, n) irradiation of gas targets of ^{124}Xe or ^{126}Xe are also interesting possibilities. These xenon isotopes make up only a small fraction of natural xenon but have been produced in gram quantities for use in the production of ^{125}I in reactor irradiations. ^{123}I is a good SPECT isotope with a short half-life of 13.2 h and it decays by electron capture with the production of one dominant 158 keV (83%) gamma ray. A gas cell, 10 cm long, containing one gram in 50 cm^3 of target volume would be equivalent to 0.02 g/cm^3 x 10 cm = 0.2 g/cm^2 or 0.04 radiation lengths. A rough calculation of the yield of ^{123}Xe is 50 GBq/kW for 1 h irradiation for a one radiation length target times 0.04 = 2.0 GBq/kW/h. This target thickness would absorb very little power from the beam so 10 to 20 kW of electron beam power could be used, leading to a yield as high as 40 GBq/h of ^{123}Xe.

The reaction is a two stage process, with the first stage producing ^{123}Xe (^{124}Xe(γ, n) ^{123}Xe), with a half-life of 2.0 h. After an irradiation of two to six hours, the gas could be transferred to a receiving cell, to decay for a similar time to ^{123}I. After sufficient ^{123}I ingrowth, xenon gas could be transferred back to the target cell and the receiving vessel would contain up to 5 GBq of ^{123}I with little contamination. This is the same process used to produce ^{125}I by neutron irradiation of ^{124}Xe. ^{125}I could be produced in the same manner with different times of irradiation and decay.

The cost of an electron accelerator should be comparable or somewhat higher than the cost of the modern high power, medium energy cyclotrons and the facility cost is expected to be similar. More shielding is required but that will be typically added as a high density shield surrounding the target area and the concrete shielding will be of comparable thickness. Some electron accelerators can produce multiple beams by splitting the beam with a fast pulsed magnet on a pulse by pulse basis. This would enable delivery to multiple target areas to produce several different isotopes or to multiple production lines of a single isotope. Electron accelerators have a history of highly stable operation with little maintenance required, based on the experience of the low energy accelerators used for numerous industrial applications in 24 h, 7 days per week operation.

Since this technology is still in the early stages of development, there is a serious shortage of HQP's needed to design new facilities and to operate them. There is a need to build at least one

facility for R&D on the technology, likely at a national laboratory, that could be used to develop the production of new isotopes and also become a source for training new HQP's. Both reactor and cyclotron based production of medical radioisotopes are mature fields and even there the development of new pathways requires a lot of effort. The photonuclear production of medical radioisotopes is an evolving field with the potential to provide useful quantities of the isotopes identified often with higher specific activity than can be achieved by either of the other processes. National and international support are a prerequisite to establish photonuclear production technology as a third pillar of medical isotope supply in the coming decades.

REFERENCES

[1] ZERKIN, V.V., PRITYCHENKO B., The experimental nuclear reaction data (EXFOR): Extended computer database and Web retrieval system, Nucl. Instrum. Methods. Phys. Res. A. **888** (2018) 31.

[2] WORLD NUCLEAR ASSOCIATION, Radioisotopes in Medicine (2021) https://www.world-nuclear.org/information-library/non-power-nuclear-applications/radioisotopes-research/radioisotopes-in-medicine.aspx.

[3] LIDSKY, L.M., LANZA, R., Method of producing molybdenum-99, Massatchussetts Institute of Technology, Cambridge, Mass., USA (1998).

[4] BENNETT, R.G., et al., A system of ^{99m}Tc production based on distributed electron accelerators and thermal separation, Nuclear Technology. **126** (1999) 102.

[5] CHADWICK, M.B., et al., Pauli-blocking in the quasideuteron model of photoabsorption, Phys. Rev. C. **44** (1991) 814.

[6] NATIONAL BUREAU OF STANDARDS, Photonuclear reactions, C13.44 NBS 118, US Govt. Print. Off, Washington, DC (1970).

[7] SPOHR, K.M., et al., Study of photo-proton reactions driven by bremsstrahlung radiation of high-intensity laser generated electrons, New Journal of Physics. **10** (2008) 43037.

[8] INTERNATIONAL ATOMIC ENERGY AGENCY, Handbook on photonuclear data for applications cross-sections and spectra, IAEA-TECDOC-1178, IAEA, Vienna (2000).

[9] ZUBER, S., et al., Iodine-125 seed brachytherapy for early stage prostate cancer: a single-institution review, Radiation Oncology. **10** (2015) 49.

[10] HERMAN, M., et al., EMPIRE: Nuclear reaction model code system for data evaluation, Nucl. Data Sheets, **108** (2007) 2655.

[11] KONING, A.J., HILAIRE S., DUIJVESTIJN, M.C., TALYS-1.0 International conference on nuclear data for science and technology, IAEA, Vienna (2007).

[12] BÖHLEN, T.T., et al., The FLUKA Code: Developments and challenges for high energy and medical applications, Nuclear Data Sheets. **120** (2014) 211.

[13] AKKERMANS, J.M., GRUPPELAAR, H., Analysis of continuum gamma-ray emission in precompound-decay reactions, Physics Letters B. **157** (1985) 95.

[14] BLANN, M., CHADWICK M.B., New precompound decay model: Angular distributions. Phys. Rev. C,. **57** (1998) 233.

[15] YOUNG, P.G., ARTHUR E.D., CHADWICK M.B., Comprehensive nuclear model calculations: Introduction to the theory and use of the GNASH code, los Alamos National Laboratory, los Alamos (1992).

[16] HAUSER, W., FESHBACH, H., The inelastic scattering of neutrons, Phys. Rev. **87** (1952) 366.

[17] CAPOTE, R., et al., RIPL – Reference input parameter library for calculation of nuclear reactions and nuclear data evaluations, Nuclear Data Sheets. **110** (2009) 3107.

[18] IWAMOTO, O., et al., The CCONE code system and its application to nuclear data evaluation for fission and other reactions, Nuclear Data Sheets. **131** (2016) 259.

[19] Cai, C.H., MEND: A program for calculating the complete set of nuclear data of medium-heavy nuclei in a medium-low energy region, Nuclear Science and Engineering. **153** (2006) 93.

[20] KAWANO, T., et al., IAEA Photonuclear Data Library 2019 (2019).

[21] Belyshev, S.S., et al., Photonuclear reactions on titanium isotopes, Physics of Atomic Nuclei. **78** (2015) 220.

[22] ALIEV, R.A., et al., Photonuclear production and radiochemical separation of medically relevant radionuclides: ^{67}Cu, J. Radioanal. Nucl. Chem. **321** (2019) 125.

[23] SHIN, J.W., A data-based photonuclear reaction model for GEANT4, Nucl. Instrum. Methods Phys. Res. B. **358** (2015) 194.

[24] QUINTIERI, L., et al., Quantification of the validity of simulations based on Geant4 and FLUKA for photo-nuclear interactions in the high energy range, EPJ Web of Conferences. **153** (2017) 06023.

[25] IWAMOTO, Y., et al., Benchmark study of the recent version of the PHITS code, J Nucl. Sci. Technol. **54** (2017) 617.

[26] WERNER, C.J., et al., MCNP Version 6.2 Release Notes. LA-UR-18-20808, Los Alamos, United States (2018).

[27] ALLISON, J., et al., Recent developments in Geant 4, Nucl. Instrum. Methods. Phys. Res. A. **835** (2016) 186.

[28] SATO, T., et al., Features of particle and heavy ion transport code system (PHITS) version 3.02, J. Nucl. Sci. Technol. **55** (2018) 684.

[29] SALVAT, F., The penelope code system. Specific features and recent improvements. Annals of Nuclear Energy. **82** (2015) 98.

[30] KAWRAKOW, I., et al., EGSnrcMP: the multi-platform environment for EGSnrc, NRC-INMS-2162, National Research Council of Canada, Ottawa (2006).

[31] BROWN, D.A., et al., ENDF/B-VIII.0: The 8th major release of the nuclear reaction data library with cielo-project cross sections, new standards and thermal scattering data, Nuclear Data Sheets. **148** (2018) 1.

[32] KONING, A.J., ROCHMAN, D., Modern Nuclear Data Evaluation with the TALYS Code System, Nuclear Data Sheets. **113** (2012) 2841.

[33] IWAMOTO, N., KOSAKO, K., MURATA, T., Photonuclear data file, J. Nucl. Sci. Technol. **60** (2016) 911.

[34] KAWANO, T., et al., IAEA Photonuclear Data Library 2019, Nuclear Data Sheets. **163** (2020) 109.

[35] KAZAKOV, A.G., EKATOVA, T.Y., BABENYA, J.S., Photonuclear production of medical radiometals: a review of experimental studies. J. Radioanal. Nucl. Chem. **328** (2021) 493.

[36] QUEERN, S.L., et al., Production of ^{15}O for Medical Applications via the ^{16}O(γ,n)^{15}O Reaction. J. Nucl. Med. **60** (2019) 424.

[37] MANABE, O., et al., ^{15}O-labeled water is the best myocardial blood flow tracer for precise MBF quantification. Ann. Nucl. Cardiol., **5** (2019) 69.

[38] MARUO, A., et al., Feasibility of quantifying myocardial blood flow with a shorter acquisition time using $_1OH_2O$ PET. Ann. Nucl. Cardiol., **2** (2016) 30.

[39] VARLAMOV, V.V., STEPANOV, M.E., Main channels of the decay of the giant dipole resonance in the ^{20,22}Ne nuclei and isospin splitting of the giant dipole resonance in the ^{22}Ne nucleus, Physics of Atomic Nuclei. **65** (2002) 49.

[40] DONNERHACK, A. SATTLER, E.L., The preparation of fluorine-18 with an electron linear accelerator for applications in medical and biological investigations, Int. J. Radiat. Res. **31** (1980) 279.

[41] BELYSHEV, S.S., et al., ^{18}F production in the ^{19}F(γ, n) reaction, Bull. Russ. Acad. Sci.: Phys. **77** (2013) 480.

[42] BRINKMAN, G.A., WYAND, A., Production of [^{18}F]fluoride from fluorocarbons by the ^{19}F(γ,n)^{18}F reaction, Int. J. Rad. Appl. Instr. A. **39** (1988) 1141.

[43] ALIEV, R.A., et al., Study of the possibility of the production and separation of the ^{18}F radioisotope at electron accelerators, Mosc. Univ. Phys. Bull. **69** (2014) 233.

[44] ALAUDDIN, M.M., Positron emission tomography (PET) imaging with ^{18}F-based radiotracers, Am. J. Nucl. Med. Mol. Imaging. **2** (2012) 55.

[45] TREGLIA, G., et al., Diagnostic performance of PET/CT with tracers other than ^{18}F-FDG in oncology: an evidence-based review. Clin. Transl. Oncol.. **16** (2014) 770.

[46] WEISE, G., et al., In vivo imaging of inflammation in the peripheral nervous system by ^{19}F MRI. Experimental Neurology. **229** (2011) 494.

[47] BRIX, P., et al., Relativmessung integrierter Wirkungsquerschnitte für den Kernphotoeffekt: Die Reaktion Ca^{44}(γ,p)K^{43}, Zeitschrift für Physik. **150** (1958) 461.

[48] ZARET, B.L., et al., Potassium-43 myocardial perfusion scanning for the noninvasive evaluation of patients with false-positive exercise tests, Circulation. **48** (1973) 1234.

[49] Martin, N.D., et al., Myocardial imaging using ^{43}K and the gamma camera, Radiology. **112** (1974) 446.

[50] Johnson, R.F., Rollo, F.D., An evaluation of ^{81}Rb and ^{43}K for imaging using the performance index technique, Physics in Medicine and Biology. **23** (1978) 761.

[51] STAROVOITOVA, V.N., COLE, P.L., GRIMM, T.L., Accelerator-based photoproduction of promising beta-emitters ^{67}Cu and ^{47}Sc, J. Radioanal. Nucl. Chem. **305** (2015) 127.

[52] RANE, S., HARRIS, J.T., STAROVOITOVA, V.N., ^{47}Ca production for ^{47}Ca/^{47}Sc generator system using electron linacs, Appl. Radiat. Isot., **97** (2015) 188.

[53] ROTSCH, D.A., et al., Electron linear accelerator production and purification of scandium-47 from titanium dioxide targets, Appl. Radiat. Isot. **131** (2018) 77.

[54] LOVELESS, C.S., et al., Photonuclear production, chemistry, and in vitro evaluation of the theranostic radionuclide ^{47}Sc, EJNMMI research. **9** (2019) 42.

[55] MAUSNER, L.F., STRAUB, R.F., SRIVASTAVA, S.C., Production and Use of Prospective Radionuclides for Radioimmunotherapy. in Radiolabeled Monoclonal Antibodies for Imaging and Therapy. Springer, Boston (1988).

[56] MÜLLER, C., et al., Scandium and terbium radionuclides for radiotheranostics: current state of development towards clinical application, the British Journal of Radiology. **91** (2018) 20180074.

[57] MÜLLER, C., et al., Promising prospects for ^{44}Sc-/^{47}Sc-based theragnostics: application of ^{47}Sc for radionuclide tumor therapy in mice. J. Nucl. Med. **55** (2014) 1658.

[58] DIKIY, N.P., et al., Electron linac production of Co-57 for gamma-chamber calibration. Voprosy Atomnoy Nauki i Tekhniki. **5** (2001) 200.

[59] Dikiy, N.P., et al., On production efficiency of medical & biophysicalisotopes using electron accelerator, Voprosy Atomnoy Nauki i Tekhniki. **3** (1999) 91.

[60] AJZATSKIJ, N.I., et al., Features of Cu-67 photonuclear production, Problems of Atomic Science and Technology. **3** (2008) 174.

[61] KAMNEV, A.A., Application of emission ^{57}Co Mössbauer spectroscopy in bioscience. J. Mol. Struct. **744** (2005) 161.

[62] ENGER, S.A., BEAULIEU, L., Modelling a Hypothetical ^{57}Co Source for Brachytherapy Application, Brachytherapy. **10** (2011) 33.

[63] ENGER, S.A., et al., Exploring ^{57}Co as a new isotope for brachytherapy applications. Medical Physics. **39** (2012) 2342.

[64] STAROVOITOVA, V.N., TCHELIDZE, L., WELLS, D.P., Production of medical radioisotopes with linear accelerators, Appl. Radiat. Isot. **85** (2014) 39.

[65] MA, Z., et al., Photonuclear production of medical isotopes ^{62,64}Cu using intense laser-plasma electron source, Matter and Radiation at Extremes. **4** (2019) 064401.

[66] LUO, W., Production of medical radioisotope ^{64}Cu by photoneutron reaction using ELI-NP γ-ray beam, Nuclear Science and Techniques. **27** (2016) 96.

[67] THIEP, T.D., et al., Activation method for measurement of bremsstrahlung photon flux produced by electron accelerator, Joint Institute for Nuclear Research, Radiochemical and Radioanalytical Letters. **2** (2005) 53.

[68] Anderson, C.J., Ferdani, R., Copper-64 radiopharmaceuticals for PET imaging of cancer: advances in preclinical and clinical research, Cancer Biother. Radiopharm.. **24** (2009) 379.

[69] SHOKEEN, M., ANDERSON, C.J., Molecular imaging of cancer with copper-64 radiopharmaceuticals and positron emission tomography (PET), Accounts of chemical research. **42** (2009) 832.

[70] GUTFILEN, B., SOUZA, S.A., VALENTINI, G., Copper-64: a real theranostic agent. Drug design, development and therapy. 12 (2018) 3235.

[71] BOSCHI, A., et al., The emerging role of copper-64 radiopharmaceuticals as cancer theranostics, Drug Discovery Today. **23** (2018) 1489.

[72] ROTSCH, D.A., et al. Production of medical isotopes with electron linacs. Proceedings of NAPAC 2016, Chicago (2016).

[73] AIZATSKY, N.I., et al., ^{99}Mo and ^{67}Cu isotope yields under production conditions of NSC kipt electron accelerator KUT-30, Problems of Atomic Science and Technology. **2** (2010) 140.

[74] ARJUN, G., et al., Production, separation and supply prospects of ^{67}Cu with the development of fast neutron sources and photonuclear technology, Radiochimica Acta. **106** (2018) 549.

[75] SMITH, N.A., BOWERS, D.L., EHST, D.A., The production, separation, and use of ^{67}Cu for radioimmunotherapy: A review. Appl. Radiat. Isot. **70** (2010) 2377.

[76] QAIM, S.M., SCHOLTEN, B., NEUMAIER, B., New developments in the production of theranostic pairs of radionuclides. J. Radioanal. Nucl. Chem. **318** (2018)1493.

[77] AKKOYUN, S., BAYRAM, T., KARA, S.O., Photonuclear reaction cross sections for gallium isotopes. Journal of Physics: Conference Series. **590** (2015) 012047.

[78] BARTOLD, S.P., et al., Procedure guideline for gallium scintigraphy in the evaluation of malignant disease, J Nucl Med. **38** (1997) 990.

[79] WEINER, R.E., The mechanism of ^{67}Ga localization in malignant disease, Nuclear Medicine and Biology. **23** (1996) 745.

[80] OTHMAN, M.F.B., et al., Re-assessing gallium-67 as a therapeutic radionuclide, Nuclear medicine and biology. **46** (2017) 12.

[81] CARLOS, P., et al., A study of the photoneutron contribution to the giant dipole resonance of nuclei in the $64 < A < 86$ mass region. Nuclear Physics A. **258** (1976) 365.

[82] McCARTHY, J.J., MORRISON, R.C., VANDER MOLEN, H.J., Systematic study of the photodisintegration of ^{70}Ge, ^{72}Ge, ^{74}Ge, and ^{76}Ge, Physical Review C. **11** (1975) 772.

[83] BANERJEE, S.R., POMPER, M.G., Clinical applications of Gallium-68. Appl. Radiat. Isot. **76** (2013) 2.

[84] JALILIAN, A.R., An overview on Ga-68 radiopharmaceuticals for positron emission tomography applications, Iranian Journal of Nuclear Medicine. **24** (2016) 1.

[85] INTERNATIONAL ATOMIC ENERGY AGENCY, Production of Long Lived Parent Radionuclides for Generators: ^{68}Ge, ^{82}Sr, ^{90}Sr and ^{188}W, Vienna (2010).

[86] GORYACHEV, A.M., ZALESNYY, G.N., The studying of the photoneutron reactions cross sections in the region of the giantdipole resonance in zinc, germanium, selenium, and strontiumisotopes, Voprosy Teoreticheskoy i Yadernoy Fiziki. **8** (1982) 121.

[87] KITATANI, F., et al., Measurement of ^{76}Se and ^{78}Se (γ, n) Cross Sections, J. Nucl. Sci. Technol. **48** (2011) 1017.

[88] BELOUSOV, A.V., et al., Simulation of ^{75}Se encapsulated sources for their potential use in brachytherapy, Mosc. Univ. Phys. Bull. **73** (2018) 339.

[89] RYSER, J.E., et al., Immunoscintigraphy with biosynthetically labeled ^{75}Se-antibodies I. Biodistribution of ^{75}Se-monoclonal antibodies and of free radionuclide, Int. J. Rad. Appl. Instr. B. **17** (1990) 487.

[90] MASLOV, O.D., DMITRIEV, S.N., Use of MT-25 microtron for scientific and applied investigations in Workshop on radioanalytical methods 'IAA 03', Seminar Radioanalyticke metody, Prague, (2013) 10.

[91] LAMBERT, F., et al., Production and purification of ^{77}Br suitable for labeling monoclonal antibodies used in tumor imaging, Radiochimica Acta. **65** (1994) 223.

[92] ASKIN, H.J., et al., ^{90,91}Zr photoproton spectra and the core-excitation model, Nuclear Physics A. **220** (1974) 241.

[93] O'DOHERTY, J., A review of 3D image-based dosimetry, technical considerations and emerging perspectives in ^{90}Y microsphere therapy, J. diagn. imaging ther. **2** (2015) 1.

[94] WU, T.J., et al., "Nanotechnologies for early diagnosis, in situ disease monitoring, and prevention", Nanotechnologies in Preventive and Regenerative Medicine, (Uskoković V., Uskoković, D.P., Eds), Illinois, Elsevier, (2018) 1-92.

[95] TONG, A.K.T., et al., Yttrium-90 hepatic radioembolization: clinical review and current techniques in interventional radiology and personalized dosimetry, the British journal of radiology. **89** (2016) 20150943.

[96] DALE, G.E., et al., Design and experimental activities supporting commercial U.S. electron accelerator production of Mo-99, AIP Conference Proceedings. **1525** (2013) 355.

[97] CHEMERISOV, S., et al. Development activities in support of accelerator production of ^{99}Mo production through the g/n reaction on ^{100}Mo, Transactions of the American Nuclear Society. **107** (2012) 68.

[98] AVAGYAN, R., et al., Photo-production of ^{99}Mo/^{99m}Tc with electron linear accelerator beam, Nuclear Medicine and Biology. **41** (2014) 705.

[99] NAKAI, K., et al., Feasibility studies towards future self-sufficient supply of the ^{99}Mo-^{99m}Tc isotopes with Japanese accelerators, Proc. Jpn. Acad. B: Phys. **90** (2014) 413.

[100] DIKY, N.P., DOVBNYA, A.N., UVAROV, V.L., The Fundamentals of ^{99m}Tc production cycle at electron accelerator, Problems of Atomic Science and Technology. **42** (2004) 168.

[101] INTERNATIONAL ATOMIC ENERGY AGENCY, Technetium-99m Radiopharmaceuticals: Status and Trends, IAEA Radioisotopes and Radiopharmaceuticals Series No. 1, Vienna (2010).

[102] DIKIY, N.P., et al., ^{196}Pd and Re isotope production in the field of mixed X,n radiation of electron accelerator, Voprosy Atomnoy Nauki i Tekhniki. **6** (2013) 196.

[103] STOPANI, K.A., "Photonuclear reactions on palladium isotopes", Institute of Nuclear Physics, (Skobeltsyn D.V., Ed.) Lomonosov Moscow State University (2016).

[104] RIVARD, M.J., A directional ^{103}Pd brachytherapy device: Dosimetric characterization and practical aspects for clinical use, Brachytherapy. **16** (2017) 421.

[105] UNNI, P.R., PILLAI, M.R.A., Production and radiochemical separation of rhodium-105 for radiopharmaceutical applications, Radiochimica Acta. **90** (2002) 363.

[106] JOHN, C.S., et al., Labeling of proteins with ^{105}Rh, Int. J. Rad. Appl. Instr. A. Appl. Radiat. Isot. **40** (1989) 701.

[107] ANDO, A., et al., Production of ^{105}Rh–EDTMP and its bone accumulation. Appl. Radiat. Isot. **52** (2000) 211.

[108] DALLAKYAN, R.K., Photonuclear production of ^{111}In on the linear electron accelerator, Armenian Journal of Physics. **6** (2013) 45.

[109] NIKIFOROV, V.I., UVAROV, V.L., A method for estimation of isotope yield in a thick target under photonuclear production, Nucl. Instrum. Methods. Phys. Res. B. **269** (2011) 3149.

[110] DANAGULYAN, A.S., et al., Formation of medical radioisotopes ^{111}In, ^{117m}Sn, ^{124}Sb, and ^{177}Lu in photonuclear reactions, Physics of Atomic Nuclei. **78** (2015) 447.

[111] LAHIRI, S., MAITI, M., GHOSH, K., Production and separation of ^{111}In: an important radionuclide in life sciences: A mini review. J. Radioanal. Nucl. Chem. **297** (2013) 309.

[112] ROCA, M., et al., Guidelines for the labelling of leucocytes with ^{111}In-oxine. Inflammation/Infection Taskgroup of the European Association of Nuclear Medicine, European journal of nuclear medicine and molecular imaging. **37** (2010) 835.

[113] JANSEN, D.R., An in vitro approach to evaluate and develop potential ^{117m}Sn-based bone-seeking radiopharmaceuticals, IOS Press, Rotterdam, 2010.

[114] BALJINNYAM, N., et al., Possibility of ^{117m}Sn production using high-energy electron bremsstrahlung, Joint Institute for Nuclear Research, Radiochemical and Radioanalytical Letters. E18-2007-164N, (2007).

[115] VUCINA, J., et al. Production of tin-117m and its applications in nuclear medicine, Proceedings of YUNSC 2004, Serbian Institute of Nuclear Sciences, (2005).

[116] BISHAYEE, A., et al., Marrow-sparing effects of ^{117m}Sn(4+)Diethylenetriaminepentaacetic acid for radionuclide therapy of bone cancer, J. Nucl. Med. **41**(2000) 2043.

[117] SRIVASTAVA, S.C., The role of electron-emitting radiopharmaceuticals in the palliative treatment of metastatic bone pain and for radiosynovectomy: applications of conversion electron emitter Tin-117m, Brazilian Archives of Biology and Technology. **50** (2007) 49.

[118] STEVENSON, N.R. Tin-117m: A new isotope and approach to radiosynoviorthesis and other therapies, HCNMC 2018, Texas (2018).

[119] PARK, H.M., ^{123}I: Almost a Designer Radioiodine for Thyroid Scanning, J. Nucl. Med. **43** (2002) 77.

[120] SCHWARZ, S.B., et al., Iodine-125 brachytherapy for brain tumours - a review, Radiation oncology. **7** (2012) 30.

[121] BELOV, A.G., et al., Integral cross sections of photonuclear reactions near the giant dipole resonance, Atomic Energy. **88** (2000) 408.

[122] HENSCHKE, U.K., LAWRENCE, D.C., Cesium-131 seeds for permanent implants, radiology. **85** (1965) 1117.

[123] MURPHY, M.K., et al., Evaluation of the new cesium-131 seed for use in low-energy x-ray brachytherapy, Medical Physics. **31** (2004) 1529.

[124] NICULAE, D. Molecular targeting with radioisotopes: Application of laser-driven isotopic production in seminar at ucirvine, Horia Hulubei National Institute for Physics and Nuclear Engineering, IFIN-HH, Romania (2016)

[125] Dikiy, N.P., et al., Photonuclear Production of Pm-149, Voprosy Atomnoy Nauki i Tekhniki. **6** (2015) 157.

[126] CARLOS, P., et al., The giant dipole resonance in the transition region for the neodymium isotopes, Nuclear Physics A. **172** (1971) 437.

[127] HU, F., et al., Pm-149 DOTA bombesin analogs for potential radiotherapy: In vivo comparison with Sm-153 and Lu-177 labeled DO3A-amide-βAla-BBN(7–14)NH2, Nuclear Medicine and Biology. **29** (2002) 423.

[128] GHEORGHE, I., et al., Absolute photoneutron cross sections of Sm isotopes, AIP Conference Proceedings. **1645** (2015) 327.

[129] WILKY, B.A., LOEB, D.M., Beyond palliation: Therapeutic applications of ^{153}Samarium-EDTMP, Clinical & experimental pharmacology. **3** (2013) 1000131.

[130] SHARMA, S., et al., Comparative therapeutic efficacy of ^{153}Sm-EDTMP and ^{177}Lu-EDTMP for bone pain palliation in patients with skeletal metastases: Patients' pain score analysis and personalized dosimetry, Frontiers in Medicine. **4** (2017).

[131] LEVIN, V.I., MALININ, A.B., TRONOVA, I.N., Production of radionuclides by photonuclear reactions Pt 1, Radiochemical and Radioanalytical Letters. **49** (1981) 111.

[132] NASKAR, N., LAHIRI, S., Theranostic terbium radioisotopes: Challenges in production for clinical application, Frontiers in Medicine. **8** (2021) 675014.

[133] MÜLLER, C., et al., Future prospects for SPECT imaging using the radiolanthanide terbium-155 – production and preclinical evaluation in tumor-bearing mice, Nuclear Medicine and Biology. **41** (2014) e58.

[134] BAYRAM, T., et al., Transition energy and half-life determinations of photonuclear reaction products of erbium nuclei, International Journal of Modern Physics E. **25** (2016) 1650107.

[135] KACHALOVA, D.I., New nuclear-physical data for photonuclear production of medical radionuclides ^{166}Ho,^{198,199}Au, Lomonosov Moscow State University (2020).

[136] KLAASSEN, N.J.M., et al., The various therapeutic applications of the medical isotope holmium-166: A narrative review, EJNMMI Radiopharmacy and Chemistry. **4** (2019) 19.

[137] VAGENA, E., STOULOS, S., Ytterbium (γ, n) average cross-sections data near to photodisintegration reaction threshold, The European Physical Journal A. **54** (2018) 153.

[138] DIKIY, N.P., et al., Photonuclear Production of Yb-175, Voprosy Atomnoy Nauki i Tekhniki. **6** (2017) 130.

[139] CHAKRABORTY, S., et al., Feasibility study for production of ^{175}Yb: A promising therapeutic radionuclide, Appl. Radiat. Isot. **57** (2002) 295.

[140] SAFARZADEH, L., et al., Production, radiolabeling and biodistribution studies of ^{175}Yb-DOTMP as bone pain palliation, Iranian Journal of Pharmaceutical Sciences. **8** (2012) 135.

[141] KAZAKOV, A.G., et al., Production of ^{177}Lu by hafnium irradiation using 55-MeV bremsstrahlung photons, J. Radioanal. Nucl. Chem. **317** (2018) 1469.

[142] TAPAS, D. SHARMILA, B., Theranostic Applications of Lutetium-177 in Radionuclide Therapy, Current Radiopharmaceuticals. **9** (2016) 94.

[143] BANERJEE, S., PILLAI, M.R.A., KNAPP, F.F., Lutetium-177 therapeutic radiopharmaceuticals: Linking chemistry, radiochemistry, and practical applications, Chemical Reviews. **115** (2015) 2934.

[144] SEKIMOTO, S., Examination of medical radionuclides production system using an electron accelerator, Annual Meeting of AESJ. Tohoku University, Japan (2016).

[145] JANG, J., UESAKA, M., YAMAMOTO. M., Development of a compact X-band electron linac for production of Mo-99/Tc-99m, IPAC2016. Busan, Korea (2016).

[146] LAMBERT, B., DE KLERK, J.M.H., Clinical applications of ^{188}Re-labelled radiopharmaceuticals for radionuclide therapy, Nuclear Medicine Communications. **27** (2006) 223.

[147] BOSCHI, A., et al., $^{188}W/^{188}Re$ Generator system and its therapeutic applications. Journal of Chemistry, **14** (2014).

[148] DOVBNYA, N.A., et al., Production of isotopes ^{184}Re, ^{186}Re and ^{188}Re at linear electron accelerators of NSC kipt, Probl. At. Sci. Technol. **309** (2001) 203.

[149] Vucina, J., Han, R., Production and therapeutic use of rhenium-186, 188-the future of radionuclides, Med Pregl. **56** (2003) 362.

[150] PHILLIPS, W.T., et al., Rhenium-186 liposomes as convection-enhanced nanoparticle brachytherapy for treatment of glioblastoma, Neuro-oncology. **14** (2012) 416.

[151] DYKIY, M.P., et al., Photonuclear production of $^{193m,195m}Pt$ and synthesis of radioactive cisplatin, J. Label. Compd. Radiopharm. **50** (2007) 480.

[152] WILMSEN, D., et al., 218: The doorway to high specific activity of ^{195m}Pt, Radiotherapy and Oncology. 110 (2014) S106.

[153] BODNAR, E.N., DIKIY, M.P., MEDVEDEVA, E.P., Photonuclear production and antitumor effect of radioactive cisplatin (^{195m}Pt), J. Radioanal. Nucl. Chem. 305 (2015) 133.

[154] HABS, D. KÖSTER, U., Production of medical radioisotopes with high specific activity in photonuclear reactions with γ-beams of high intensity and large brilliance, Applied Physics B. **103** (2011) 501.

[155] NARBUTT, J., BILEWICZ, A., Gamma emitting radiotracers ^{224}Ra, ^{212}Pb and ^{212}Bi from natural thorium, Appl. Radiat. Isot. 49 (1998) 89.

[156] ATCHER, R.W., FRIEDMAN, A.M., HINES, J.J., An improved generator for the production of ^{212}Pb and ^{212}Bi from ^{224}Ra, Int J Rad Appl Instrum A. **39** (1988) 283.

[157] Melville, G., Allen, B.J., Cyclotron and linac production of Ac-225, Appl. Radiat. Isot. **67** (2009) 549.

[158] MASLOV, O.D., SABEL'NIKOV, A.V., DMITRIEV, S.N., Preparation of ^{225}Ac by ^{226}Ra (γ, n) photonuclear reaction on an electron accelerator, MT-25 microtron, Radiochemistry. **48** (2006) 195.

[159] LUO, W., et al., Estimates for production of radioisotopes of medical interest at Extreme Light Infrastructure – Nuclear Physics facility, Applied Physics B. **122** (2016) 8.

[160] MELVILLE, G., et al., Production of Ac-225 for cancer therapy by photon-induced transmutation of Ra-226, Appl. Radiat. Isot. 65(2007) 1014.

[161] MELVILLE, G., FAN LIU, S., ALLEN, B.J., A theoretical model for the production of Ac-225 for cancer therapy by photon-induced transmutation of Ra-226, Appl. Radiat. Isot. **64** (2006) 979.

[162] KRATOCHWIL, C., et al., ^{225}Ac-PSMA-617 for PSMA-targeted α-radiation therapy of metastatic castration-resistant prostate cancer, J. Nucl. Med. **57** (2016) 1941.

[163] KRATOCHWIL, C., et al., Targeted α-therapy of metastatic castration-resistant prostate cancer with ^{225}Ac-PSMA-617: Dosimetry estimate and empiric dose finding, J. Nucl. Med. **58** (2017) 1624.

[164] CHEN, J., et al., Precise absolute gamma-ray and beta(-)-decay branching intensities in the decay of Cu-67. Physical Review C, **92** (2015).

[165] EL SIOUFI, A., ERDOS, P., STOLL, P., (g,np)-process in Mo-92 and Zn-66, Helvetica Physica Acta. **30** (1957) 264.

[166] HOVHANNISYAN, G.H., BAKHSHIYAN, T.M., DALLAKYAN, R.K., Photonuclear production of the medical isotope ^{67}Cu, Nucl. Instrum. Methods Phys. Res. B. **498** (2021) 48.

[167] REHER, D., et al., The decay of ^{47}Sc. Int. J. Rad. Appl. Instr. A. **37** (1986) 973.

[168] SHERWOOD, T.R., TURCHINETZ, W.E., Some photo-disintegration reactions in the titanium isotopes, Nuclear Physics. **29** (1962) 292.

[169] MAUSNER, L.F., et al., Radionuclide development at BNL for nuclear medicine therapy, Appl. Radiat. Isot. **49** (1998) 285.

[170] VANSANT, P.D., Medical isotope production of actinium 225 by linear accelerator photon irradiation of radium 226, Virginia Polytechnic Institute, Blacksburg (2013).

[171] DUFFIELD, R.B., SCHMITT, R.A., SHARP, R.A., Mass-yield distributions in the photofission of radium and other heavy elements, General Dynamics Corporation. 1958) 202.

[172] ZHAGROV, E.A., et al., Photofission cross section of Ra-226, Soviet Journal of Nuclear Physics. **13** (1971) 537.

[173] MARTIN, T.M., et al., Production of ^{99}Mo/^{99m}Tc via photoneutron reaction using natural molybdenum and enriched ^{100}Mo: Part 1, theoretical analysis, J. Radioanal. Nucl. Chem. **314** (2017) 1051.

[174] FULLER, E., HAYWARD, E., The Giant Resonance of the Nuclear Photoeffect. PM Endt and PB Smith, (1962) 113.

[175] BERMAN, B.L., FULTZ, S.C., Measurements of the giant dipole resonance with monoenergetic photons, Reviews of Modern Physics. **47** (1975) 713.

[176] AOKI, K., et al., High-energy photon beam production with laser-Compton backscattering, Nucl. Instrum. Methods Phys. Res. A. 516 (2004) 228.

[177] LI, D., et al., Experiment on photonuclear reaction induced by laser compton scattering gamma-ray, J. Nucl. Sci. Technol. 42 (2005) 259.

[178] EJIRI, H., et al., Resonant photonuclear reactions for isotope transmutation, Journal of the Physical Society of Japan. **80** (2011) 094202.

[179] INTERNATIONAL ATOMIC ENERGY AGENCY, Database of industrial irradiation facilities. Available from: https://nucleus.iaea.org/sites/diif/Pages/Interactive-Map.aspx.

[180] WANGLER, T.P., RF Linear Accelerators, 2nd Ed, Wiley & Co, Berlin (2008).

[181] OSTROUMOV, P.N., CONWAY, Z.A., KELLY, M.P., Superconducting electron linac concepts for molybdenum-99 production, United States, 2014.

[182] JENNINGS, R.E., The microtron, Contemporary Physics. **2** (1961) 277.

[183] VEKSLER, V.I., A new method of acceleration of relativistic particles, J. Phys. **9** (1945) 153.

[184] JONGEN, Y., et al., The Rhodotron, a new high-energy, high-power, CW electron accelerator, Nucl. Instrum. Methods Phys. Res. B. **89** (1994) 60.

[185] BERTRAND, S., et al. A new compact high-power e-beam accelerator for radioisotopes production: a first evaluation, IAEA Int. Sym. on Trends in Radiopharmaceuticals. Vienna (2019).

[186] IBA. Great milestone for NorthStar Medical Radioisotopes, LLC and Nuclear Medicine! 2021. Available from: https://www.iba-radiopharmasolutions.com/great-milestone-northstar-medical-radioisotopes-llc-and-nuclear-medicine.

[187] INTERNATIONAL ATOMIC ENERGY AGENCY, Radiological Safety Aspects of the Operation of Electron Linear Accelerators, Technical Reports Series No. 188, Vienna (1979).

[188] SÄTHERBERG A., ANDREO P., KARLSSON M., Bremsstrahlung production at 50 MeV in different target materials and configurations, Med Phys. **4** (1996) 495–503.

[189] KIRK B.L., Overview of Monte Carlo radiation transport codes, Radiation Measurements. **45** (2010) 1318–1322.

[190] NATIONAL COUNCIL ON RADIATION AND MEASUREMENTS, Radiation protection design guidelines for 01 to 100 MeV particle accelerator facilities, United States. (1977) 166.

[191] DIAMOND, W.T., ROSS, C.K., Actinium-225 production with an electron accelerator, Journal of Applied Physics. 129 (2021) 104901.

[192] CHEMERISOV, S., et al. Beamline design for high power radioisotope production facility. Mo-99 Topical Meeting (2016).

[193] CHEMERISOV, S., et al. Accelerator based production of Mo-99: Photonuclear approach. Mo-99 Topical Meeting (2018).

[194] WOLOSHUN, K., et al. LANL Engineering and Design support for an accelerator facility to produce ^{99}Mo from ^{100}Mo. Mo-99 Topical Meeting (2018).

[195] YOUKER, A.J., et al., Fission-produced ^{99}Mo without a nuclear reactor. J. Nucl. Med. **58** (2017) 514.

[196] YOUKER, A.J., et al. Overview: Argonne assistance in developing SHINE production of Mo-99. Mo-99 Topical Meeting (2014).

[197] ODEH, F.Y., et al. Advanced GeniV recators Grimm LBE converter design, American Nuclear Society ANS (2018).

[198] GRIMM, T.L., et al., Commercial Superconducting Electron Linac for Radioisotope Production, DE-SC0007520, Idaho State University, Michigan (2015).

[199] JOHNSON, R.P. KRAFFT, G.A., Energy-Recovery Linacs for Commercial Radioisotope Production - Phase I, DE-SC0013123, Muplus, Michigan (2015).

[200] GRIMM, T., Commercial Applications of Small SRF Accelerators, (2013 North American Particle Accelerator Conf.), California (2013).

[201] GRIMM, T., et al. High-Purity Actinium-225 Production from Radium-226 using a Superconducting Electron Linac, J. Med. Imaging Radiat. Sci. (2019).

[202] STAROVOITOVA, V.N., et al. Mo-99 Production Using a Superconducting Electron Linac, in 2014 Mo-99 Topical Meeting Niowave, Lansing MI (2014).

[203] GRIMM, T., et al. Niowave's Domestic Production of Mo-99 from LEU without a Nuclear Reactor, in 2016 Mo-99 Topical Meeting Niowave, Lansing, MI (2016).

[204] LYNCH, S.T., BALAZIK, M.F., ADAMS, A., U.S. Nuclear regulatory commission activities related to the establishment of Molybdenum-99 production in the United States, (2017 Mo-99 Topical Meeting on Molybdenum-99 Production Technology Development), Montreal (2017).

[205] MAMTIMIN, M., et al. High power liquid lead-bismuth targetry for intense fast neutron sources using a superconducting electron linac, (2018 High Power Targetry Workshop), Lansing, MI (2018).

[206] GRIMM, T.L., et al. Niowave's domestic production of Mo-99 and other fission fragments from LEU without a nuclear reactor (2018 Mo-99 Topical Meeting on Molybdenum-99 Production Technology Development), Knoxville, TN (2018).

[207] GRIMM, T.L., et al., Isotope production using a superconducting electron linac, in DOE-NP SBIR/STTR Exchange Meeting, Gaithersburg, MD (2014).

[208] ROTSCH, D., et al. Photonuclear production of high specific activity copper-67 and scandium-47, Nuclear Medicine and Biology. **S7** (2019) 72.

[209] MERRICK, M.J., et al., Imaging and dosimetric characteristics of ^{67}Cu, Physics in Medicine & Biology. 66 (2021) 035002.

[210] EHST, D.A., et al., Copper-67 production on electron linacs - Photonuclear technology development, AIP Conference Proceedings. **1509** (2012) 157.

[211] GOPALAKRISHNA, A., et al., Production, separation and supply prospects of ^{67}Cu with the development of fast neutron sources and photonuclear technology, Radiochimica Acta. **106** (2018) 549.

[212] SHERMAN, N.K., et al., Bremsstrahlung radiators and beam filters for 25-MeV cancer therapy, Medical Physics. **1** (1974) 185.

[213] NORDELL, B., BRAHME, A., Angular distribution and yield from bremsstrahlung targets (for radiation therapy), Physics in Medicine & Biology. **29** (1984) 797.

[214] TSECHANSKI, A., et al., Electron accelerator-based production of molybdenum-99: Bremsstrahlung and photoneutron generation from molybdenum vs. tungsten. Nucl. Instrum. Methods Phys. Res. B. **366** (2016) 124.

[215] GAO, Q., et al., Design and optimization of the target in electron linear accelerator, IPAC2013, Shanghai, (2013) 3663.

[216] PETWAL, V.C., et al., Bremsstrahlung converter for high power EB radiation processing facility, in APAC 2007, Indore, India (2007) 767.

[217] Tsechanski, A., et al., Converter optimization for photonuclear production of Mo-99. Nucl. Instrum. Methods Phys. Res. B. **461** (2019) 118.

[218] CHEMERISOV, S., et al., Results of the Six-day electron-accelerator irradiation of enriched Mo-100 targets for the production of Mo-99, ANL-19/61, Argonne National Lab, Argonne, IL (2019) 20.

[219] Ross, C.K., Fluka calculation, W.T. Diamond, Editor.

[220] FEDORCHENKO, D.V., TSECHANSKI, A., Photoneutronic aspects of the molybdenum-99 production by means of electron linear accelerators, Nucl. Instrum. Methods Phys. Res. B. **438** (2019) 6.

[221] DE JONG, M., Producing medical isotopes with electron linacs, in 2015 CAP Congress, University of Alberta (2015).

[222] DE JONG, M., Canadian isotope innovations, in IAEA Second Research Coordination Meeting on New Ways of Producing Tc-99m and Tc-99m Generators, Poland (2019).

[223] JANG, J., et al., Design and testing of a W-MoO_3 target system for electron linac production of ^{99}Mo/^{99m}Tc, Nucl. Instrum. Methods Phys. Res. A. 987 (2021) 164815.

[224] DABBS, J.W.T., Neutron cross section measurements at ORELA, International conference on nuclear cross sections for technology 1979, Oak Ridge National Lab, Knoxville, TN (1979).

[225] FULLWOOD, R.R., GAERTTNER, E.R., KRASSE, R., Qualitative effects of radiation damage on equipment and components at the RPI Linac, RPI-328-27, Particle Accelerator Conference, Washington (1965) 705.

[226] BERGER, M.J., et al., Stopping-Power & Range Tables for Electrons, Protons, and Helium Ions, in NIST Standard Reference Database 124, Gaithersburg (2017).

[227] EGORITI, L., et al., Material development towards a solid 100 kW electron-gamma converter for TRIUMF-ARIEL, Nucl. Instrum. Methods Phys. Res. B. **463** (2020) 232.

[228] GRIMM, T., ET al., Niowave's Domestic Production of Mo-99 and other Fission Fragments from LEU without a Nuclear Reactor, in NNSA Mo-99 Stakeholders Meeting, Chicago, IL (2019).

[229] CHEMERISOV, S., et al., Activities for the production of Mo-99 using high current electron linac, 10th International Topical Meeting on Nuclear Applications and Accelerators, Argonne National Laboratory, Lemont (2011).

[230] HELMES, T., KARCZ, P., DIX, J., Ensuring a stable supply of Mo-99 in the United States without the use of HEU, in International Conference on Nuclear Security: Sustaining and Strengthening Efforts (ICONS 2020), IAEA, Vienna (2020) 1.

[231] LILLARD, R.S., PILE, D.L., BUTT, D.P., The corrosion of materials in water irradiated by 800 MeV protons, J. Nucl. Mater. **278** (2000) 277.

[232] VIRGO, M., et al., Results of thermal test of metallic molybdenum disk target and fast-acting valve testing, ANL/NE-16/44, Argonne National Lab, Argonne, IL (2016).

[233] Makarashvili, V., et al. Monte Carlo Calculations for the LINAC Irradiations, 2014 Mo-99 Topical Meeting, Argonne National Lab, Argonne, IL (2014).

[234] Chemerisov, S., et al., Results of four one-day electron-accelerator irradiations of enriched Mo-100 targets for the production of Mo-99, ANL/NE-16/26, Argonne National Lab, Argonne, IL (2016).

[235] CADE, B.G., et al., Thermal design of a 100 kW electron to gamma converter at TRIUMF, Journal of Physics. **1067** (2018) 032023.

[236] SMITH, M.S.C., ARIEL Electron to Gamma Converter Design, University of Victoria (2013).

[237] STOLARSKI, T., NAKASONE, Y., YOSHIMOTO, S., "6 - Application of ANSYS to thermo-mechanics", Engineering Analysis with ANSYS Software, 2nd Ed, Butterworth-Heinemann, Oxford (2018) 283-374.

[238] VAGHEIAN, M., A Point Source High Power Converter Target to Produce Bremsstrahlung for Photonuclear Reactions, University of Berne, Berne (2021) 207.

[239] FEBVRE, M., Manufacturing and supply of a mercury cooled rotary uranium target for the GELINA accelerator facility of IRMM, (2009 1st Int. Conf. on Advc. in Nuc. Instrum, Measurement Methods and their App.), Marseille (2009).

[240] MONDELAERS, W., SCHILLEBEECKX, P., GELINA a neutron time-of-flight facility for high-resolution neutron data measurements, Notiziario Neutroni E Luce Di Sincrotrone. **11** (2006) 19.

[241] YLIMAKI, R.J., Scalable Continuous-Wave Ion Linac PET Radioisotope System, US Patent 10,714,225, 14 Jul. 2020, PN LAbs, Inc. Moseley, VA (US).

[242] LAVIE, E., et al., Method and system For Production of Radioisotopes, and Radioisotopes Produced Thereby, U.S. Patent Application 11/663,782, Dec. 2007.

[243] DIERCKX, M., et al., WEBEXPIR: Windowless target electron beam experimental irradiation, Journal of Nuclear Materials. **376** (2008) 302.

[244] WOLOSHUN, K.A., et al., Thermal Test on Target with Pressed Disks, LA-UR-16-22211, Los Alamos National Lab., Los Alamos, NM (2016).

[245] DE JONG, M., et al., "A New Paradigm for Mo-99/Tc-99m Supply", in 2017 Mo-99 Top. Mtg on Molybdenum-99 Prod. Tec. Dev. 2017. p. 1.

[246] LOWDEN, R.A., et al., Powder Metallurgy Fabrication of Molybdenum Accelerator Target Disks, ORNL/TM-2014/238, Oak Ridge National Lab, Oak Ridge, TN (2015).

[247] TKAC, P., et al. "Chemical Processing Activities for ^{99}Mo production by (γ,n) and (n,γ) reactions using enriched ^{100}Mo and ^{98}Mo targets", in 2015 Mo-99 Topical Meeting on Mo-99 Tec. Dev. Boston (2015).

[248] LOWDEN, R.A., LOWDEN, R.R., BRYAN. C., "Powder Metallurgy Fabrication of Molybdenum Target Materials and Assemblies", in Topical Mtg On Mo-99 Tech. Dev, Boston, (2015).

[249] LOWDEN, R.A., LOWDEN, R.R., BRYAN. C., "Powder Metallurgy Molybdenum Accelerator Target Materials and Assemblies", in Topical Mtg on Mo-99 Tech. Dev., St. Louis, Missouri (2016).

[250] LOWDEN, R.A., et al. "Fabrication of Molybdenum Target Materials Employing “Recycled” Powders", in Topical Mtg on Mo-99 Tech. Dev., Knoxville, TN (2018).

[251] ROTSCH, D.A., et al., "Purification of electron LINAC produced Scandium-47," in 16th Int.Workshop on Targetry and Target Chemistry, University of Wisconsin Madison, Wisconsin (2016).

[252] DALE, G.E., Los Alamos National Laboratory Support for Commercial U.S. Production of ^{99}Mo without the Use of Highly Enriched Uranium, LA-UR-16-21406, Los Alamos National Lab., Los Alamos, NM (2016).

[253] STAROVOITOVA, V., et al., Cu-67 Photonuclear Production, in AIP Conference Proceedings, American Institute of Physics. **1336** (2011) 502.

[254] AJZATSKIJ, N.I., et al., Comparison of Cu-67 production at cyclotron and electron accelerator, in 18th Int. Conf. on Cyclotrons and their App. (Cyclotrons 2007), INFN, Giardini-Naxos (2007).

[255] JOHNSN, A.M., et al., Reactor production of ^{64}Cu and ^{67}Cu using enriched zinc target material, J. Radioanal. Nucl. Chem. **305** (2015) 61.

[256] ALIEV, R.A., et al., Photonuclear production of medically relevant radionuclide ^{47}Sc, J. Radioanal. Nucl. Chem. **326** (2020) 1099.

[257] INAGAKI, M., et al., Production of ^{47}Sc, ^{67}Cu, ^{68}Ga, ^{105}Rh, ^{177}Lu, and ^{188}Re using electron linear accelerator, J. Radioanal. Nucl. Chem. **322** (2019) 1703.

[258] MAMTIMIN, M., HARMON, F., STAROVOITOVA, V.N., Sc-47 production from titanium targets using electron linacs, Appl. Radiat. Isot. **102** (2015) 1.

[259] KONING, A.J., et al., TENDL: Complete Nuclear Data Library for Innovative Nuclear Science and Technology, Nuclear Data Sheets. **155** (2019) 1.

[260] WEISE, J., et al., Research Report of Lab. of Nuc. Sci., Tohoku University (1978) 43.

[261] MITCHELL, O.M.M., MCNEILL, K.G., Yields and angular distributions of fast photoprotons. Canadian Journal of Physics. **41** (1963) 871.

[262] BELYSHEV, S.S., et al., Measuring the yields of photonuclear reactions in natural titanium at (Eγ)max ≈ 55 MeV, Bull. Russ. Acad. Sci.: Phys. **78** (2014) 1153.

[263] SUTTON, R., et al., A study of photoreactions in ^{48}Ti, Nuclear Physics A. **339** (1980): 125.

[264] KOLSKY, K.L., et al., Radiochemical purification of no-carrier-added scandium-47 for radioimmunotherapy, Appl. Radiat. Isot. **49** (1998) 1541.

[265] BRUCHERTSEIFER, F., et al., Targeted alpha therapy with bismuth-213 and actinium-225: Meeting future demand, J. Label. Compd. Radiopharm. **62** (2019) 794.

[266] INTERNATIONAL ATOMIC ENERGY AGENCY, Conditioning and Interim Storage of Spent Radium Sources, IAEA-TECDOC-886, IAEA, Vienna (1996).

[267] ROBERTSON, A., et al., Development of ^{22}Ac Radiopharmaceuticals: TRIUMF Perspectives and Experiences, Current Radiopharmaceuticals. **11** (2018) 156.

[268] WEIGEL, F., "Radium"', Gmelin Handbook of Inorganic and Organometallic Chemistry, 8th Ed., Springer: Berlin, Heidelberg (1977) 435.

[269] RADCHENKO, V., BAIMUKHANOVA, A., FILOSOFOV, D., Radiochemical aspects in modern radiopharmaceutical trends: a practical guide, Solvent Extraction and Ion Exchange. **39** (2021) 714.

[270] INTERNATIONAL ATOMIC ENERGY AGENCY, Manual for Reactor Produced Radioisotopes, IAEA-TECDOC-1340, IAEA, Vienna (2003).

[271] INTERNATIONAL ATOMIC ENERGY AGENCY, Nuclear Data for the Production of Therapeutic, Radionuclides Technical Reports Series 473, IAEA, Vienna (2012).

[272] DASH, A., KNAPP, F.F., PILLAI, M.R.A., ^{99}Mo/^{99m}Tc separation: An assessment of technology options, Nuclear Medicine and Biology. **40** (2013) 167.

[273] JOHNSON, N.B., STEIL B., TechneGen. NorthStar Medical Radioisotopes, No. 85420367 filed on 12th Sept 2011, Madison, WI. Available from: http://www.trademarkia.com/technegen-85420367.html.

[274] JANG, J., et al., "Photonuclear production of Mo-99/Tc-99m using molybdenum trioxide and activated carbon", in Topical Mtg on Mo-99 Prod. Tech.Dev, Montreal, QC, (2017).

[275] WOJDOWSKA, W., et al., Studies on the separation of 99mTc from large excess of molybdenum, Nuclear Medicine Review. **18** (2015) 65.

[276] MARTINI, P., et al., A solvent-extraction module for cyclotron production of high-purity technetium-99m, Appl. Radiat. Isot. **118** (2016) 302.

[277] MARTINI, P., et al., In-house cyclotron production of high-purity Tc-99m and Tc-99m radiopharmaceuticals, Appl. Radiat. Isot. **139** (2018) 325.

[278] MANG'ERA, K., et al., Processing and evaluation of linear accelerator-produced ^{99}Mo/^{99m}Tc in Canada, J. Radioanal. Nucl. Chem. **305** (2015) 79.

[279] YAGI, M., KONDO, K., Preparation of carrier-free ^{47}Sc by the ^{48}Ti (γ,p) reaction, Int. J. Radiat. Res. **28** (1977) 463.

[280] VAN DER MEULEN, N.P., et al., Cyclotron production of ^{44}Sc: From bench to bedside. Nuclear Medicine and Biology. **42** (2015) 745.

[281] ALLIOT, C., et al., Cyclotron production of high purity ^{44m,44}Sc with deuterons from $^{44}CaCO_3$ targets, Nuclear Medicine and Biology. **42** (2015) 524.

[282] HERNANDEZ, R., et al., ^{44}Sc: An attractive isotope for peptide-based PET imaging, Molecular Pharmaceutics. **11** (2014) 2954.

[283] DOMNANICH, K.A., et al., ^{47}Sc as useful β emitter for the radiotheragnostic paradigm: a comparative study of feasible production routes, EJNMMI Radiopharmacy and Chemistry. **2** (2017) 5.

[284] BARTOŚ, B., et al., New separation method of no-carrier-added ^{47}Sc from titanium targets, Radiochimica Acta. **100** (2012) 457.

[285] SUGO, Y., et al., Application of ^{67}Cu Produced by ^{68}Zn(n,n′p+d)^{67}Cu to Biodistribution Study in Tumor-Bearing Mice, J. Phys. Soc. Japan. **86** (2016) 023201.

[286] HASSANEIN, M.A., EL-SAID, H., EL-AMIR, M.A., Separation of carrier-free ^{64,67}Cu radionuclides from irradiated zinc targets using 6-tungstocerate(IV) gel matrix, J. Radioanal. Nucl. Chem. **269** (2006) 75.

[287] APOSTOLIDIS, C., et al., Cyclotron production of Ac-225 for targeted alpha therapy, Appl. Radiat. Isot. **62** (2005) 383.

ABBREVIATIONS

ABEC	Aqueous Biphasic Extraction Chromatography
ANL	Argonne National Laboratory
CLS Inc.	Canadian Light Source Incorporated
DGA	Diglycolamine
EOB	End of bombardment
FWHM	Full Width Half Maximum
GDR	Giant Dipole Resonance
GMP	Good manufacturing practice
HAS	High-specific activity
HQP	Highly qualified personnel
IBA	Industrial Beam Applications
ICP-AES	Inductively Coupled Plasma Atomic Emission Spectrometry
ICP-MS	Inductively Coupled Plasma Mass Spectrometry
KIPT	National Science Center “Kharkov Institute of Physics and Technology”, Ukraine
LANL	Los Alamos National Laboratories
LBE	Lead-Bismuth Eutectic
LEAF	Low-Energy Accelerator Facility, ANL
LEU	Low Enriched Uranium
Linac	Linear accelerator
LSA	Low-specific-activity
LWR	Light water reactor
MEK	Methyl ethyl ketone
NNSA	National Nuclear Security Administration
ORELA	Oak Ridge Electron Linear Accelerator
ORNL	Oak Ridge National Laboratory
PET	Positron Emission Tomography
PSC	Primary separation column
RAC	Radioactive concentration
RF	Radio-frequency
RIPL	Reference Input Parameter Library
SAMEER	Society for Applied Microwave Electronics Engineering and Research
SPECT	Single Photon Emission Tomography
TAT	Targeted alpha therapy

TRL	Technology Readiness Level
UTA	Uranium Target Assembly

CONTRIBUTORS TO DRAFTING & REVIEW

Arjan Koning	International Atomic Energy Agency, Austria
Aruna Korde	International Atomic Energy Agency, Austria
Dmytro Fedorchenko	Kharkov Institute of Physics and Technology, Ukraine
Hanna Skliarova	Belgian Nuclear Research Centre (SCK CEN), Belgium
Mark De Jong	Canadian Isotope Innovations Corporation, Canada
Melissa Denecke	International Atomic Energy Agency, Austria
Stephan Heinitz	Belgian Nuclear Research Centre (SCK CEN), Belgium
Sergey Chemerisov	Argonne National Laboratory, USA
Valeriia Starovoitova	International Atomic Energy Agency, Austria
Valery Radchenko	TRIUMF, Canada
Vitaly Khryachkov	Institute of Physics and Power Engineering, Russia
William Diamond	Atomic Energy of Canada, Canada

IAEA
International Atomic Energy Agency

No. 26

ORDERING LOCALLY

IAEA priced publications may be purchased from the sources listed below or from major local booksellers.

Orders for unpriced publications should be made directly to the IAEA. The contact details are given at the end of this list.

NORTH AMERICA

Bernan / Rowman & Littlefield

15250 NBN Way, Blue Ridge Summit, PA 17214, USA
Telephone: +1 800 462 6420 • Fax: +1 800 338 4550

Email: orders@rowman.com • Web site: www.rowman.com/bernan

REST OF WORLD

Please contact your preferred local supplier, or our lead distributor:

Eurospan Group

Gray's Inn House
127 Clerkenwell Road
London EC1R 5DB
United Kingdom

Trade orders and enquiries:

Telephone: +44 (0)176 760 4972 • Fax: +44 (0)176 760 1640
Email: eurospan@turpin-distribution.com

Individual orders:

www.eurospanbookstore.com/iaea

For further information:

Telephone: +44 (0)207 240 0856 • Fax: +44 (0)207 379 0609
Email: info@eurospangroup.com • Web site: www.eurospangroup.com

Orders for both priced and unpriced publications may be addressed directly to:

Marketing and Sales Unit
International Atomic Energy Agency
Vienna International Centre, PO Box 100, 1400 Vienna, Austria
Telephone: +43 1 2600 22529 or 22530 • Fax: +43 1 26007 22529
Email: sales.publications@iaea.org • Web site: www.iaea.org/publications

24-01327E

International Atomic Energy Agency
Vienna